REPORT DOCUMENTATION PAGE

Form Approved OMB NO. 0704-0188

1. REPORT DATE (DD-MM-YYYY)	2. REPORT TYPE	3. DATES COVERED (From - To)
10-02-2012	Final Report	19-May-2008 - 30-Nov-2011

4. TITLE AND SUBTITLE

COMPUTATIONALLY EFFICIENT MODELING OF HYDROCARBON OXIDATION CHEMISTRY AND FLAMES USING CONSTITUENTS AND SPECIES

5a. CONTRACT NUMBER
W911NF-08-1-0130

5b. GRANT NUMBER

5c. PROGRAM ELEMENT NUMBER
611102

6. AUTHORS
Josette Bellan

5d. PROJECT NUMBER

5e. TASK NUMBER

5f. WORK UNIT NUMBER

7. PERFORMING ORGANIZATION NAMES AND ADDRESSES
California Institute of Technology
Sponsored Research MC 201-15
California Institute of Technology
Pasadena, CA 91125 -

8. PERFORMING ORGANIZATION REPORT NUMBER

9. SPONSORING/MONITORING AGENCY NAME(S) AND ADDRESS(ES)
U.S. Army Research Office
P.O. Box 12211
Research Triangle Park, NC 27709-2211

10. SPONSOR/MONITOR'S ACRONYM(S)
ARO

11. SPONSOR/MONITOR'S REPORT NUMBER(S)
54125-EG.11

12. DISTRIBUTION AVAILIBILITY STATEMENT
Approved for Public Release; Distribution Unlimited

13. SUPPLEMENTARY NOTES
The views, opinions and/or findings contained in this report are those of the author(s) and should not contrued as an official Department of the Army position, policy or decision, unless so designated by other documentation.

14. ABSTRACT
This report describes a study performed under ARO sponsorship, addressing the investigation of a novel way to reduce complex and extensive oxidation reaction mechanisms for fuel mixtures containing hundreds of species to a much smaller number of progress variables, typically by a factor of ten. The study has also been extended to computing laminar flames. Because the results have been documented in several papers published in the refereed literature and manuscripts, this final report is in the form of an Executive Summary succinctly describing the results

15. SUBJECT TERMS
chemical kinetics mechanism reduction; laminar flame prediction

16. SECURITY CLASSIFICATION OF:			17. LIMITATION OF ABSTRACT	15. NUMBER OF PAGES	19a. NAME OF RESPONSIBLE PERSON
a. REPORT	b. ABSTRACT	c. THIS PAGE			Josette Bellan
UU	UU	UU	UU		19b. TELEPHONE NUMBER: 818-354-6959

Report Title

COMPUTATIONALLY EFFICIENT MODELING OF HYDROCARBON OXIDATION CHEMISTRY AND FLAMES USING CONSTITUENTS AND SPECIES

ABSTRACT

This report describes a study performed under ARO sponsorship, addressing the investigation of a novel way to reduce complex and extensive oxidation reaction mechanisms for fuel mixtures containing hundreds of species to a much smaller number of progress variables, typically by a factor of ten. The study has also been extended to computing laminar flames. Because the results have been documented in several papers published in the refereed literature and manuscripts, this final report is in the form of an Executive Summary succinctly describing the results and putting them in perspective with respect to existing oxidation mechanism reduction schemes and flame computations. The papers and manuscripts are individually listed as Appendices, and attached to this report.

Enter List of papers submitted or published that acknowledge ARO support from the start of the project to the date of this printing. List the papers, including journal references, in the following categories:

(a) Papers published in peer-reviewed journals (N/A for none)

Received	Paper
2012/02/10 15 10	Kenneth Harstad, Josette Bellan. A model of reduced kinetics for alkane oxidation using constituents and species: Proof of concept for n-heptane, Combustion and Flame, (08 2010): 0. doi: 10.1016/j.combustflame.2010.02.013
2010/10/04 08 3	K. Harstad, J. Bellan. A model of reduced oxidation kinetics using constituents and species: iso-octane and its mixtures with n-pentane, iso-hexane and n-heptane, Combustion and Flame, (03 2010): . doi:

TOTAL: 2

Number of Papers published in peer-reviewed journals:

(b) Papers published in non-peer-reviewed journals (N/A for none)

Received	Paper

TOTAL:

Number of Papers published in non peer-reviewed journals:

(c) Presentations

"Alkane Kinetics Reduction Consistent with Turbulence Modeling using Large Eddy Simulation", (K. G. Harstad and J. Bellan), AIAA-2010-1514, presented at the 48th Aerospace Sciences Meeting, Orlando, FL, January 4-7, 2010

"Computation of Laminar Premixed Flames Using Reduced Kinetics Based on Constituents and Species", (K. G. Harstad and J. Bellan), AIAA-2011-ID892667, presented at the 49th Aerospace Sciences Meeting, Orlando, FL, January 4-7, 2011; also paper 1E08 presented at the 7th US National Combustion meeting, Atlanta, GA., March 21-23, 2011

"Modeling of Steady Laminar Flames for One-dimensional Premixed Jets of Heptane/Air and Octane/Air Mixtures", (K. G. Harstad and J. Bellan), AIAA-2012-0340, presented at the 50th Aerospace Sciences Meeting, Nashville, TN, January 9-12, 2012

Number of Presentations: 3.00

Non Peer-Reviewed Conference Proceeding publications (other than abstracts):

Received		Paper
2012/02/10 14	9	K. G. Harstad, J. Bellan. Modeling of Steady Laminar Flames for One-dimensional Premixed Jets of Heptane/Air and Octane/Air Mixtures, Aerospace Sciences Meeting. 2012/01/09 03:00:00, . : ,
2012/02/10 13	8	J. Bellan, K. G. Harstad. Alkane Kinetics Reduction Consistent with Turbulence Modeling using Large Eddy Simulation, Aerospace Sciences Meeting. 2010/01/09 03:00:00, . : ,
2011/08/22 10	6	Kenneth G. Harstad, Josette Bellan. Computation of Laminar Premixed Flames Using Reduced Kinetics Based on Constituents and Species, Aerospace Sciences Meeting. 2011/01/04 03:00:00, . : ,

TOTAL: 3

Number of Non Peer-Reviewed Conference Proceeding publications (other than abstracts):

Peer-Reviewed Conference Proceeding publications (other than abstracts):

Received	Paper

TOTAL:

Number of Peer-Reviewed Conference Proceeding publications (other than abstracts):

(d) Manuscripts

Received		Paper
2011/08/22 14	5	Kenneth G. Harstad, Josette Bellan. A model of reduced oxidation kinetics using constituents and species: iso-octaneand its mixtures with n-pentane, iso-hexane and n-heptane, Combustion and Flame (03 2010)
2010/12/20 08	4	K. Harstad, J. Bellan. Computation of Laminar Premixed Flames Using Reduced Kinetics Based on Constituents and Species, (12 2010)
2010/03/31 14	2	K. Harstad, J. Bellan. A model of reduced oxidation kinetics using constituents and species: iso-octane and its mixtures with n-pentane, iso-hexane and n-heptane, (03 2010)
2010/03/31 14	1	K. Harstad, J. Bellan. A model of reduced kinetics for alkane oxidation using constituents and species: proof of concept for n-heptane , (03 2010)

TOTAL: 4

Number of Manuscripts:

Books

Received	Paper

TOTAL:

Patents Submitted

Patents Awarded

Awards

None.

Graduate Students

NAME	PERCENT_SUPPORTED

FTE Equivalent:
Total Number:

Names of Post Doctorates

NAME	PERCENT_SUPPORTED

FTE Equivalent:
Total Number:

Names of Faculty Supported

NAME	PERCENT_SUPPORTED

FTE Equivalent:
Total Number:

Names of Under Graduate students supported

NAME	PERCENT_SUPPORTED

FTE Equivalent:
Total Number:

Student Metrics

This section only applies to graduating undergraduates supported by this agreement in this reporting period

The number of undergraduates funded by this agreement who graduated during this period:	0.00
The number of undergraduates funded by this agreement who graduated during this period with a degree in science, mathematics, engineering, or technology fields:.....	0.00
The number of undergraduates funded by your agreement who graduated during this period and will continue to pursue a graduate or Ph.D. degree in science, mathematics, engineering, or technology fields:.....	0.00
Number of graduating undergraduates who achieved a 3.5 GPA to 4.0 (4.0 max scale):	0.00
Number of graduating undergraduates funded by a DoD funded Center of Excellence grant for Education, Research and Engineering:	0.00
The number of undergraduates funded by your agreement who graduated during this period and intend to work for the Department of Defense	0.00
The number of undergraduates funded by your agreement who graduated during this period and will receive scholarships or fellowships for further studies in science, mathematics, engineering or technology fields:	0.00

Names of Personnel receiving masters degrees

NAME

Total Number:

Names of personnel receiving PHDs

NAME
Total Number:

Names of other research staff

NAME	PERCENT SUPPORTED
Josette Belan	0.05
K. G. Harstad	0.35
FTE Equivalent:	**0.40**
Total Number:	**2**

Sub Contractors (DD882)

Inventions (DD882)

Scientific Progress

Described in the attachment.

Technology Transfer

FINAL REPORT

COMPUTATIONALLY EFFICIENT MODELING OF HYDROCARBON OXIDATION CHEMISTRY AND FLAMES USING CONSTITUENTS AND SPECIES

Josette Bellan
Mechanical Engineering Department
California Institute of Technology
Pasadena CA 91125

Abstract

This report describes a study performed under ARO sponsorship, addressing the investigation of a novel way to reduce complex and extensive oxidation reaction mechanisms for fuel mixtures containing hundreds of species to a much smaller number of progress variables, typically by a factor of ten. The study has also been extended to computing laminar flames. Because the results have been documented in several papers published in the refereed literature and manuscripts, this final report is in the form of an Executive Summary succinctly describing the results and putting them in perspective with respect to existing oxidation mechanism reduction schemes and flame computations. The papers and manuscripts are individually listed as Appendices, and attached to this report.

TABLE OF CONTENTS

EXECUTIVE SUMMARY

The highlights of the results from the manuscripts in Appendices 1-5 are here summarized.

The challenge of modeling turbulent reactive flows is so considerable that the activity has traditionally been decomposed into its two essential parts: kinetics and turbulence. Usually, modeling of chemical kinetics has proceeded on a separate path from that of turbulence which also includes canonical models for turbulence/reaction interaction. The only constraint to kinetic modeling was that it should be compact enough to be computationally efficient when included in a complex turbulent combustion code. However, there are definite advantages on approaching chemical kinetic modeling in a similar manner to turbulent flow modeling because if the concepts are similar, the hope is that the models will mesh better and the results will be easier to understand. This was the approach taken in this study. The spirit of the chemical kinetic modeling approach is that of Large Eddy Simulations (LES) in which kinematic-energy significant flow scales are computed and the others are modeled; in turbulence, the large flow scales constitute the former category and the small flow scales constitute the latter category. The chemical kinetics parallel is to obtain a model which only retains the thermodynamic-energy significant chemical scales as progress variables, and models the influence of the other scales. But the parallel approach between kinetics and turbulence was here extended even further. In turbulence modeling, a common methodology is to assess the behavior of the modeled scales by analyzing databases created using Direct Numerical Simulations (DNS) in which all flow scales are computed; indeed, current experimental diagnostics do not permit the same thoroughness of information as that obtained from DNS. The DNS data is analyzed in what is called an *a priori* study to inquire about the behavior of the small scales and propose mathematical forms which fit this behavior. The *a priori* study is followed by an *a posteriori* study where the proposed mathematical forms are inserted into the model to evaluate its performance when compared to the DNS database at the LES resolution.

A complete analogy between turbulence and kinetics was here made by observing that kinetic elemental or skeletal mechanisms can serve for reduced kinetics the role that DNS serves for LES, in which case reduced kinetic mechanisms can be viewed as the complement to LES in achieving the goal of accurate computationally-efficient turbulent reactive flow simulations. The analogy between reduced kinetic models and LES is not entirely surprising since each chemical species has a characteristic time scale and in the kinetic reduction it is desirable to compute only those entities (e.g. species, combination of species, radicals, combination of radicals, etc.) having essential characteristic time scales (to be defined) and model the kinetics of the remaining entities.

Thus, there were two important components to this study, namely the *a priori* analysis and the *a posteriori* evaluation. Whereas turbulence modeling benefits from decades of work using the DNS/LES concept which originated in atmospheric turbulence predictions in the 1960s, the present work is the first investigation to take this approach in kinetic reduction modeling. Therefore, it was first necessary to produce a categorization of scales analogous to the large and small scales of turbulence, then it was required to propose mathematical forms for the scales to

be modeled rather than computed as progress variables in the reduced kinetic model, and finally it was required to perform an *a posteriori* study in order to evaluate the chemical kinetic model versus the elemental or skeletal mechanism for those species predicted by the reduced model. The present model depicts a constant-volume situation, so as to be consistent with the requirement of a LES grid.

We have proposed such a categorization [1, 2] through the definition of a total constituent molar density which is a progress variable representing the heavy species kinetics, and through the partition of the light species set into a set of modeled quasi-steady species and a set of progress variable species. By definition, constituent radicals are those composing species with a carbon number larger than or equal to 3. These species are called 'heavy', and their complement in the ensemble of species is called 'light'. Constituents are obtained by mathematically breaking the heavy species into parts. Although sometimes lights and constituents, both of which are radicals, may have the same chemical formula, the difference between constituents and these light species is that the later are unbound to other chemical entities whereas the former are bound to other chemical entities, i.e. other constituents. The element compositions of the constituents are not linearly independent, but the constituents are linearly independent. Thus, the constituents are independent structural elements which have individual valence bond topologies; the constituents are not just based on atom counts. The total constituent molar density is the sum of the individual constituents' molar densities.

Thus, rather than following all species through their reaction coordinates, we follow a reduced set of reaction coordinates (i.e. progress variables); this reduced set is called a base. An extensive analysis of the LLNL databases [3] of elementary sets of reactions for a given fuel species revealed that a normalized temperature can be defined which serves as a similarity variable, θ. The variable which is self-similar versus θ is the molar density of the constituents divided by the product of the equivalence ratio and a reference nitrogen molar fraction which serves as a surrogate pressure. Both the *a priori* and *a posteriori* models, with numerous results, were described for n-heptane [1], for iso-octane, for mixtures of iso-octane and n-heptane (which are called Primary Reference Fuels) and for mixtures of iso-octane and n-pentane or of iso-octane and iso-hexane [2]. The reduced models were compared with the original elementary LLNL mechanisms [3]. Comparisons involved temperature, species molar densities, the constituent molar density and ignition times. The results were uniformly excellent except for the very large equivalence ratios (i.e. 4) where they were only very good. The deterioration in performance for these very rich flames was due to the multivalued aspects of the functions versus θ.

Specifically, we have shown that the molar density of the constituents divided by the product of the equivalence ratio and a reference nitrogen molar fraction plotted versus θ is invariant with pressure over the range 5-50 atm, with the equivalence ratio over the range [1/4, 4] range and with initial temperature values in the cold ignition regime, i.e. [600 K, 900 K]. For larger initial temperatures than 900 K and up to 1200 K to which the model has been tested, the self-similarity holds modulo the initial temperature value. Remarkably, this model is valid over a much larger equivalence ratio range than all other chemical kinetic reduced mechanisms presented in the literature that are typically developed in the [1/2, 2] range. As part of another research program,

recent simulation results describing the mixing of five species under supercritical pressure [4] show that the [1/2, 2] range captures an extremely limited range of locations in the flow field. An additional feature of the self-similarity parameter θ is that the molar densities of oxygen and water plotted versus θ display a quasi linear decreasing and quasi linear increasing behavior, respectively, over the entire range of parameters explored. The fact that these features prevail for not only single-fuel species but also mixtures of fuel-species, including mixtures of different percentages of n-heptane and iso-octane, is very encouraging for its extension to heavier hydrocarbons. In fact, our model is hierarchical by construct, meaning that it is naturally extendable to higher carbon-number hydrocarbons (a primary necessity for modeling heavier than iso-octane and ring hydrocarbons), thus having advantages in this respect over the capabilities of other models. The hierarchical aspect comes in because the progress variables are not necessarily species, but also include species 'constituents' defined very much like in group additivity theory [5]. The number of constituents in the global constituent may increase with increasing carbon number or with moving from straight-chain alkanes to ring hydrocarbons, but the self-similarity is expected to remain. An example of the increasing number of constituents has already been observed on going from n-heptane to iso-octane (13 versus 14), but the primary pillar of the method which is the self-similarity, still holds.

To give perspective to our model, the number of species progress variables in our model is 11, whereas reduced models in the scientific literature claiming good agreement with data have more than 50 progress variables. The saving in computational time using our model is very significant.

On consulting chemical physicists [6] in retrospect, there seems to be no surprise to our success. This is because the heavy species decompose very fast upon heating, and it is only what results from this decomposition that makes an impact on the reaction. We have taken advantage of this property to develop a compact, yet accurate chemical kinetic model.

Building on the success with chemical kinetics reduction, the next topic addressed has been that of laminar flame propagation. Compared to chemical kinetics prediction alone, flames have the additional complication of involving transport of species, momentum and energy. Therefore, accurate transport coefficients must be computed for the mixtures under consideration. For example, the species mass diffusion matrix is a square matrix having as many elements in each of the two directions as species and species-like progress variables. Each element of the matrix depends on the composition, temperature and pressure [7, 8]. The thermal diffusion factor matrix is involved in the computation of Soret and Dufour effects which may be important under high-pressure conditions [8]. The thermal conductivity must be computed for the entire mixture, with appropriate mixing rules accounting for the varying composition and temperature during the evolution of the flame. Although the flow is considered inviscid, according to [9] the viscosity plays a role in the computation of thermal conductivity, so it must be modeled. Additionally, a real-gas equation of state, having capability to perform well under high-pressure conditions, must also be constructed, with appropriate mixing rules [9]. Moreover, because of the partitioning of the species into constituents, quasi-steady lights and progress-variable lights, the governing equations required now recasting in a new form to respect this partition. This preliminary work for computing flame has been presented in [10] and applied to computing the

evolution of the temperature and species in a premixed flame, up to the flame location, using a computational method based on a large Peclet number. To assess the importance of species mass diffusion, computations were performed with and without species mass diffusion and the effect of species mass diffusion has been highlighted. Further, by changing the numerical method to a split-step type where there are many chemical steps within a diffusion numerical step, computations were carried out for premixed flames through the flame region [11]. Currently, this work is being enlarged to perform simulations for preparing a manuscript to be submitted for publication in a refereed journal. The next step will be the establishment of a methodology for computing counterflow flames within the constituent concept.

REFERENCES

[1] Harstad, K. G. and Bellan, J., A model of reduced kinetics for alkane oxidation using constituents and species: proof of concept for n-heptane, *Combustion and Flame*, 157, 1594-1609, 2010

[2] Harstad, K. G. and Bellan, J., A model of reduced oxidation kinetics using constituents and species: iso-octane and its mixtures with n-pentane, iso-hexane and n-heptane, *Combustion and Flame*, 157, 2184-2197, 2010

[3] Lawrence Livermore National Laboratory, http://www-cms.llnl.gov/combustion/combustion2.html.

[4] Masi, E.; Bellan, J; Harstad, K., Direct Numerical Simulation of High-Pressure Multispecies Turbulent Mixing in the Cold Ignition Regime, AIAA-2012- 0351, presented at the 50th Aerospace Sciences Meeting, Nashville, TN, January 9-12, 2012

[5] Benson, S. W., *Thermochemical Kinetics*, John Wiley & Sons, Inc., 1968

[6] Stephen Klippenstein (Argonne National Laboratory) and James Miller (Sandia National Laboratory), private communication, Atlanta, Ga., March 2011

[7] Harstad, K. and Bellan, J., High-Pressure Binary Mass-Diffusion Coefficients for Combustion Applications, *Ind. & Eng. Chem. Res.*, 43(2), 645-654, 2004

[8] Harstad, K. G. and Bellan, J., Mixing rules for multicomponent mixture mass diffusion coefficients and thermal diffusion factors, *Journal of Chemical Physics,* 120(12), 5664-5673, 2004

[9] R. C. Reid, J. M. Prausnitz, B. E. Poling, The Properties of Gases and Liquids, 4th edition, McGraw-Hill, NY, 1987.

[10] Harstad, K. G. and Bellan, J., Computation of Laminar Premixed Flames Using Reduced Kinetics Based on Constituents and Species, AIAA-2011-ID892667, presented at the 49th Aerospace Sciences Meeting, Orlando, FL, January 4-7, 2011; also paper 1E08 presented at the 7th US National Combustion meeting, Atlanta, GA., March 21-23, 2011

[11] Harstad, K. G. and Bellan, J., Modeling of Steady Laminar Flames for One-dimensional Premixed Jets of Heptane/Air and Octane/Air Mixtures", (K. G. Harstad and J. Bellan), AIAA-2012-0340, presented at the 50th Aerospace Sciences Meeting, Nashville, TN, January 9-12, 2012

APPENDIX 1

Combustion and Flame 157 (2010) 1594–1609

Contents lists available at ScienceDirect

Combustion and Flame

journal homepage: www.elsevier.com/locate/combustflame

A model of reduced kinetics for alkane oxidation using constituents and species: Proof of concept for n-heptane

Kenneth Harstad, Josette Bellan *

4800 Oak Grove Drive, M/S 125-109, Jet Propulsion Laboratory, California Institute of Technology, Pasadena, CA 91109-8099, United States

ARTICLE INFO

Article history:
Received 15 October 2009
Received in revised form 19 January 2010
Accepted 18 February 2010
Available online 11 March 2010

Keywords:
Reduced oxidation kinetics for n-heptane

ABSTRACT

A methodology for deriving a reduced kinetic mechanism for alkane oxidation is described and applied to n-heptane. The model is based on partitioning the species of the skeletal kinetic mechanism into lights, defined as those having a carbon number smaller than 3, and heavies, which are the complement in the species ensemble. For modeling purposes, the heavy species are mathematically decomposed into constituents, which are similar but not identical to groups in the group additivity theory. From analysis of the LLNL skeletal mechanism in conjunction with CHEMKIN II, it is shown that a similarity variable can be formed such that the appropriately scaled global constituent molar density exhibits a self-similar behavior over a very wide range of equivalence ratios, initial pressures and initial temperatures that is of interest for predicting n-heptane oxidation. Furthermore, the oxygen and water molar densities are shown to display a quasi-linear behavior with respect to the similarity variable. The light species ensemble is partitioned into quasi-steady and unsteady species. The concept is tested by using tabular information from the LLNL skeletal mechanism in conjunction with CHEMKIN II. The test reveals that the similarity concept is indeed justified and that the combustion temperature is well predicted, but that the ignition time is overpredicted. To palliate this deficiency, functional modeling is incorporated into our conceptual reduction. Due to the reduction process, models are also included for the global constituent molar density, the kinetics-induced enthalpy evolution of the heavy species, the contribution to the reaction rate of the unsteady lights from the heavies, the molar density evolution of oxygen and water, the mole fractions of the quasi-steady light species and the mean molar heat capacity of the heavy species. The model is compact in that there are only nine species-related progress variables. Results are presented comparing the performance of the model for predicting the temperature and species evolution with that of the skeletal mechanism. The model reproduces the ignition time over a wide range of equivalence ratios, initial pressure and initial temperature.

1. Introduction

The reduction of elementary or skeletal oxidation kinetics to a subgroup of tractable reactions for inclusion in turbulent combustion codes has been the subject of numerous studies. The skeletal mechanism is obtained from the elementary mechanism by removing from it reactions which are considered negligible for the intent of the specific study considered. As of now, there are many chemical reduction methodologies. A typical way of reducing chemical mechanisms is to represent it by a few significant (in quantitatively defined ways) chemical species and correspondingly perform a lumping of Arrhenius-type reactions. Examples of models that fall in this category are those of Müeller et al. [1], Bollig et al. [2], Sung et al. [3] and Li et al. [4]. Another method, called piecewise implementation of solution mapping (PRISM) [5], relies on the construction of a polynomial representation in a region of chemical composition space to approximate the chemical kinetics. This representation is stored for use during a numerical simulation, and the chemistry evolution for points within the composition space is computed by evaluating these polynomials instead of solving differential equations. If the evolution of chemistry is required outside of the domain where the polynomials are available, the methodology dynamically samples the region and constructs a new representation. *In situ* adaptive tabulation (ISAT) [6] is a method similar to PRISM, and also relies on tabulated polynomial fits to the chemical mechanism over a given time interval at various locations in the composition space. ISAT is based on a linear approximation, whereas PRISM represents a piecewise quadratic fit of the chemistry. The intrinsic low-dimensional manifold (ILDM) [7] method is based on the observation that in a chemically reactive mixture at fixed pressure, fixed total enthalpy and fixed atomic element composition, the path of reaction in the high-dimensional state space lies in low-dimensional manifolds in the vicinity of reaction attrac-

* Corresponding author. Fax: +1 818 393 6682.
E-mail address: Josette.Bellan@jpl.nasa.gov (J. Bellan).

0010-2180/$ - see front matter © 2010 The Combustion Institute. Published by Elsevier Inc. All rights reserved.
doi:10.1016/j.combustflame.2010.02.013

tors, far from the final equilibrium point; these manifolds are intrinsic, meaning that except for the degree of reduction, the reaction mechanism in terms of Arrhenius-type elementary reactions is the only source of information necessary to build the approximation. However, ILDM is not easily implementable in some situations. Particularly, it (i) has the drawback of becoming very difficult to handle with increasing number of C atoms in the fuel [8], and we note that heavy species (i.e. large number of C atoms) enter the composition of most practical fuels, and (ii) does not work at low temperatures, or very lean or rich mixture conditions, which are precisely the conditions where a very large number of pollutants are formed. The Computational Singular Perturbation (CSP) method of Lam and Goussis [9] introduces simplifications by distinguishing between the different time scales of the elementary reactions. The CSP method computerizes the choice of the important reactions, and therefore does not rely on intuition to retain the important slow reactions with respect to the fast ones. However, CSP reduces only the number of reactions, not the number of species [9]. That is, the number of differential equations to be solved in order to find the evolution of the mixture remains the same as in the detailed mechanism, and thus, although rigorous and accurate, CSP remains computationally expensive. Lumping procedures, both for reactions and for components have also been used [10,11] for mechanism reduction; the components are usually possible isomers of large hydrocarbons and in this procedure a large number of real components is lumped into a judiciously selected number of equivalent components. Thus, the lumped mechanisms of heavy species are represented by a limited number of equivalent reactions. The directed relation graph (DRG) reduction [12–16] is a more recent method in which the coupling among species is plotted in a graph which is then analyzed to identify unimportant species; these species are then removed from the mechanism. These few reduction methodologies only represent a subset of all procedures devised for the goal of obtaining a kinetic mechanism compact enough to be utilizable for turbulent reactive flow calculations and accurate enough to be reliable over a wide range of equivalence ratios, ϕ, initial pressures, p_0 (subscript 0 denotes the initial value), and initial temperatures, T_0. As none of the existing methodologies for mechanism reduction is considered the ultimate answer in the quest for compactness and reliability, the search for novel ideas in kinetic mechanism reduction continues. The study presented here is the result of such a search.

In this study, one of the main concerns was to devise a kinetic reduction procedure which is consistent with the Large Eddy Simulation (LES) concept, as LES has shown considerable promise in simulating turbulent flows and represents the state-of-the-art capability in such simulations. The primary idea in LES is that due to the computational infeasibility of routinely solving the governing equations for fully turbulent flows (i.e. high Reynolds number), one should spatially filter the equations thus removing the dynamic-energy unimportant small scales, leaving only the large scales to be resolved. The influence of the small scales is re-introduced in the equations through functional modeling, allowing the solution of the large scales, and thus of most of the dynamic energy. The dynamic scales of fluid mechanics have a parallel in chemical kinetics since each species has its own characteristic time and can be thought to be a scale of the problem. The dynamic energy of the flow has a parallel in the thermodynamic energy of the reaction; at this early stage of our reduction model, we are only interested in recovering the energetics of the reaction, the major species, and some of the species through which a reaction is monitored (e.g. OH). Therefore, the idea here is to explore whether it is possible to remove scales unimportant to the energetics, and functionally model them. The study focusses on the cold ignition regime for hydrocarbon oxidation.

In LES, the small scales are modeled by examining solutions obtained from Direct Numerical Simulation for incipient (i.e. low Reynolds number) turbulence, as these solutions contain small-scale behavior information. For chemical kinetics, the information that could be neglected is contained in the skeletal kinetic mechanism. Therefore, the idea is here that examination of the solutions from the skeletal mechanism should reveal the functional forms of the kinetic scales which could be neglected.

This paper is organized as follows: We first describe the basis leading to our conceptual model. Then, we present the model which, because it results from examination of the n-heptane kinetic mechanism [17], is directly intertwined with the quantitative aspects of n-heptane oxidation. The interest is in n-heptane because it is the simplest hydrocarbon exhibiting a negative temperature coefficient (NTC) behavior and is a reference fuel. Further, we assess the model by comparing it with the skeletal mechanism to identify modeling needs. The functional model is next presented, and results from it are critically examined for different aspects of the predictions. In a following section, we discuss the ensemble of the results to indicate the strategy for future work. Finally, a summary and conclusions are presented.

2. Conceptual model

The conceptual model seeks to represent the species, thought to be akin to vectors in a mathematical space, by a reduced base set. The species are partitioned into heavies (carbon number, $n \geqslant 3$) and lights (the remaining of the set). The heavies can be either radicals or stable species. The lights are oxygen, nitrogen, the final combustion products and light radicals/molecules (e.g. CH_3, CH_4, H_2O_2). The heavies are decomposed into constituents, as described below, while the lights remain part of the base.

2.1. Heavy species: the total constituent molar density as progress variable

The definition of constituents stems from the observations that (i) plots of the heats of combustion for alkanes and for alkenes having a C double bond at the molecular chain end have a linear variation with the C number, n and (ii) at fixed temperature T, the species molar heats at constant pressure, C_p, vary linearly with n. The implications are that (1) heats of combustion and C_p may be considered obtainable by summing those of constituent radicals CH_2, CH_3 and C_2H_3 that form these hydrocarbons and (2) for $n \geqslant 3$, species may be mathematically decomposed into constituent radicals. The mathematical decomposition is not meant to emulate a real reaction, such as pyrolysis. Each constituent molar density, N_k, is the sum, over all heavy species, of the count of the constituent in each heavy species multiplied by the molar density of that species. The element compositions of the constituents are not linearly independent, but the constituents are linearly independent. Basically, the constituents are independent structural elements which have valence bond topologies (see below); the constituents are not just based on atom counts.

The constituents are similar to the groups in group additivity theory [18,19], however, there are marked differences from it. In group additivity one accounts for interactions with adjacent groups, interactions with non-adjacent groups and for steric effects. In our 'constituents' concept we only account for interactions with adjacent groups and first order (compositional) effects. Also, our process is different from lumping because we are decomposing all heavy species and, as explained above, a constituent may span the entire species set of heavy species. The heavy species constituent radicals are defined as a set of entities (here, 13 of

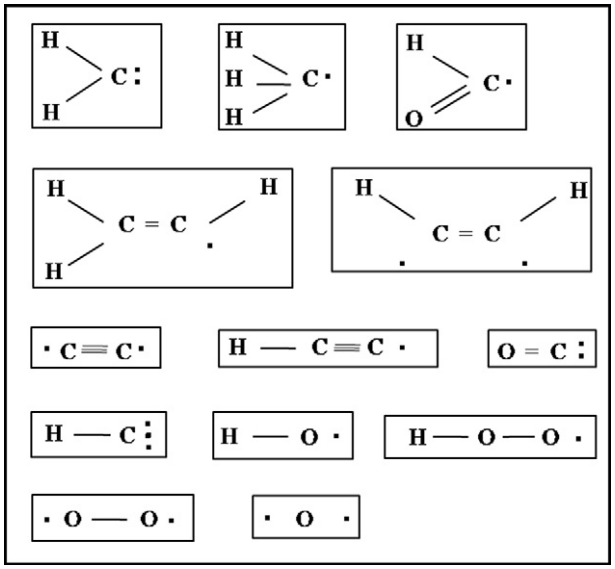

Fig. 1. Structure of the 13 constituents. First row, left to right: methylene, methyl, formyl. Second row, left to right: vinyl, vinylene. Third row, left to right: dicarbon, ethynyl, keto. Fourth row, left to right: methylidyne, hydroxyl, hydroperoxy. Fifth row, left to right: peroxy, atomic oxygen.

them: CH_2, CH_3, CH, C_2H_3, C_2H_2, C_2, HC_2, CO (keto), HCO, HO, HO_2, OO, O) from which any heavy species or radical may be constructed. The structural topology of the constituents is illustrated in Fig. 1. This mathematical decomposition is precise for the large majority of heavy species. If not precise, a particular constituent which is in the heavy species but not in our set of 13 constituents, is replaced by the closest constituent in the set. The total constituent molar density is

$$N_c \equiv \sum_{k=1}^{13} N_k \tag{1}$$

where the molar density of individual constituent k is N_k.

Each case computed is initialized at a specified p_0, T_0 and ϕ. Replacing the pressure variable p, we define a dimensionless molar density

$$N^* \equiv \frac{N_{N2}}{N_{ref}} \tag{2}$$

for N_2, where the reference N_2 molar density is $N_{ref} = 31.5\ \mathrm{mol/m^3}$ for dry air value at pressure $p_{ref} = 1$ bar and $T_{ref} = 298.15$ K. Thus, N^* acts as a convenient surrogate variable for p since the N^* value is essentially reaction rate invariant given that N_2 is inert and no NO_x mechanism is considered at this early stage of model development. That is, the partial pressure of N_2 is the overwhelming contribution to p; basically, the ratio of N^* to p_0 is nearly constant.

We seek to obtain a normalized variable θ such that at approximately the same value of θ, N_c has been consumed in the reaction for all initial conditions, except for rich situations. If such a variable can be obtained, one would hope to formulate the problem in more generic terms than if this variable could not be found. Beside the goal of achieving a normalization so that N_c decreases by 3 orders of magnitude at approximately same θ (except for rich situations), we also ask the question whether the normalization variable could additionally be a similarity variable such that all N_c versus θ curves nearly coincide. The advantage of self-similarity is that it reduces the dimensionality of the problem. Because of the complexity of hydrocarbon oxidation mechanisms, performing a general mathematical analysis to seek θ is unpractical, so the search for θ was performed by choosing a specific example, the n-heptane oxidation LLNL skeletal mechanism, and by exhaustively examining the database through curve fitting. The result of this very time-consuming empirical work, described in Section 3.1, was

$$\theta \equiv \frac{T - T_0}{T_r(\phi, N^*)} \tag{3}$$

$$T_r \equiv 2065 (N^*)^{0.06} w(\phi) \tag{4}$$

$$w(\phi) = \phi \frac{1.5 + 1.31\phi}{1 + 0.71\phi + 1.1\phi^2}. \tag{5}$$

As it will be shown in the following, the θ definition is such that indeed N_c decreases by three orders of magnitude (delving into higher order of magnitude decrease runs the risk of encountering round-off and truncation errors) from its initial value during stoichiometric combustion upon reaching $\theta \gtrsim 0.6$. The $\theta \simeq 0.6$ value was chosen to ensure that all θ values remain below unity for all test case calculations.

2.2. Light species: a modeled subset and a progress variable subset

According to the above procedure, light species are not subject to meaningful decomposition. Examination of runs made using the LLNL database in CHEMKIN II indicates that the light species should be categorized in two subsets: one which is modeled, and one which is computed subject to the heavy species model, as follows.

2.2.1. Quasi-steady light species

The species in the first subset are the radicals O, CH, CH_2, CH_3, HO, HCO, HO_2, HC_2, C_2H_3 which have a quasi-steady behavior (production and consumption rates are within 5% of each other during an overwhelming time of the reaction). Their mole fraction, X_i, is here modeled through mathematical fits as a function of the state variables (ϕ, N^*, T) and modeling parameters (here, only T_0). There are nine of these quasi-steady light species.

2.2.2. Progress variable light species

The species in the second subset are unsteady and require rate equations. This set consists of H_2O, CO_2, O_2, H, CO, H_2, CH_4, H_2O_2, C_2H_2, C_2H_4, CH_2O. The reaction rate of light species is conceptualized as

$$\mathscr{R}_i \equiv \left(\frac{dN_i}{dt}\right)_{reac} = \left.\frac{dN_i}{dt}\right|_{heavies} + \left.\frac{dN_i}{dt}\right|_{lights}, \tag{6}$$

where the first term expressing the contribution to the lights from of the heavy group must be modeled and second term in the right hand side has the same rates as in the LLNL skeletal mechanism. We make the ad-hoc assumption that to lowest order, through our reduction

$$\left.\frac{dN_i}{dt}\right|_{heavies} \to \sum_{k=1}^{13} N_k (KG_{i,k} - X_i KL_{i,k}) \tag{7}$$

where $KG_{i,k}$ and $KL_{i,k}$ represent gain and loss rates from the heavy constituent k to the light i. Examination of the skeletal mechanism result reveals that individual dominant constituents of molar density N_k are quasi-steady, which implies that there is a mole fraction XC_k such that $N_k \simeq N_c XC_k$, meaning that

$$\left.\frac{dN_i}{dt}\right|_{heavies} \to N_c \left(\sum_{k=1}^{13} XC_k KG_{i,k} - X_i \sum_{k=1}^{13} XC_k KL_{i,k} \right). \tag{8}$$

By defining $KG_i \equiv \sum_{k=1}^{13} XC_k KG_{i,k}$ and $KL_i \equiv \sum_{k=1}^{13} XC_k KL_{i,k}$, one obtains

$$\left.\frac{dN_i}{dt}\right|_{heavies} = N_c (KG_i - X_i KL_i), \tag{9}$$

where KG_i and KL_i are functions of (T_0, ϕ, N^*, T) and they must be modeled consistently with the heavy species model. There are eleven of these unsteady light species.

2.3. Model summary for species and computation of energetics

At this junction, the base set is composed of the total constituent radical molar density N_c and of the 11 molar densities of the light molecules or free radicals of the second light species subset. Thus, there are at this stage only 12 species-related progress variables. To use this model, one must first find a strategy for computing N_c; such a strategy will be shown next. To compute the 20 light species, one must model X_i of the first light species subset and compute the conventional light species reaction rates of the second light species subset. For the unsteady light species reaction rates, models of KG_i and KL_i are needed in functional form.

Computation of the temperature evolution in a reactive system requires knowledge of the species molar enthalpies and molar heat capacities. For species i, the molar enthalpy may be expressed as $h_i = h_i^0 + \tilde{h}_i(T)$ where h_i^0 is the heat of formation, $\tilde{h}_i$ is the sensible enthalpy and T is the temperature. The heat of formation is taken at the above reference conditions, giving $\tilde{h}_i = \int_{T_{ref}}^{T} C_{p,i}dT$ where $C_{p,i}$ is the molar constant-pressure heat capacity. Under the assumption that water remains in vapor state, a heat of combustion for species i is given by

$$h_i^c = h_i^0 - \sum_j w_{ji} h_j^0 \tag{10}$$

where w_{ji} is the number of species j in species i that produces the correct atom count, where the index j denotes the species set of air (O_2, N_2) and final combustion products (H_2O, CO_2). (This means that mathematically, we consider species i as being composed of air and final combustion product species.) Values of h_i^c and h_i^0 are provided in Table 1.

Considering the total enthalpy to be fixed, and consistent with the goal of only modeling the energetics resulting from the oxidation reaction, the temperature evolution is given by

Table 1
Thermodynamic properties of molecules and free radicals. h^0 and h^c (heats of formation and combustion, respectively), in kJ/mol; constants a^h and b^h for molar heat capacity in the form $C_p/R_u = a^h + b^h ln(T/T_{ref})$; $T_{ref} = 298.15$ K. "Mo" denotes "molecule". "Ra" denotes "radical".

Mo/Ra	h^0	h^c	a^h	b^h
H_2	0.0	241.5	3.282	0.400
O_2	0.0	0.0	3.476	0.5663
N_2	0.0	0.0	3.388	0.469
C	717	1111	2.50	0.0
H_2O	−241.5	0.0	3.688	1.217
CO_2	−393.5	0.0	4.690	1.390
N	473	473	2.50	0.0
H	218.0	339	2.50	0.0
HO	38	159	3.385	0.3637
HOO	10.5	131	4.150	1.307
O	249.2	249.2	2.536	0.0
CO	−110.5	283	3.426	0.4749
HCO	43.1	558	4.154	1.2875
CH_4	−74.6	802	3.797	4.305
CH_3	146	902	4.440	2.249
CH_2	390	1025	3.973	1.3015
CH	596	1110	3.220	0.7136
C_2H_3	300	1449	5.1	3.5
HC_2	566	1474	4.434	1.404
C_2	838[a]	1625	4.58	0.0
NO	90.3	90.3	3.533	0.4508
NO_2	33.2	33.2	4.691	1.151
H_2O_2	−136	106	5.269	1.880
HCOH	−109	526.5	4.27	2.546
C_2H_2	228	1257	5.368	2.294
C_2H_4	52.5	1323	5.383	4.676

[a] Alternate value of 832 from the CRC tables.

$$\left(\sum_{l\in heavies} C_{p,l}N_l + \sum_{i\in lights} C_{p,i}N_i\right)\frac{dT}{dt} = -\left(\sum_{l\in heavies} h_l\mathscr{R}_l + \sum_{i\in lights} h_i\mathscr{R}_i\right) \tag{11}$$

where R_u is the universal gas constant; this equation is general and holds for the skeletal mechanism. Equation (11) is an approximation of the energy equation in that it does not include the transient-p term, so as not to constrain the validity of the results to only low-p situations for which the perfect-gas equation of state (EOS) used in CHEMKIN is appropriate. CHEMKIN II contains two non-equivalent options for calculations of reaction rates: (1) providing T and the molar densities, a procedure which does not necessitate the use of the EOS, and (2) specifying p, additionally to T and the molar densities, a procedure which requires the utilization of the perfect-gas EOS. Since high-p combustion will necessitate the use of real-gas EOS, in our computations, we use option (1), so as to make our results independent of the EOS. The neglect of the p variation term in Eq. (11) is justified because (i) during the initial phase before ignition, the T variation is very small and the corresponding changes in p are also small, and (ii) during ignition, when the timewise p variation is significant, most of the T increase is due to the heat release from combustion. Neglect of the transient-p effects corresponds to slow and/or small changes in the mean local mass density (this is consistent with fixed total enthalpy results obtained using the LLNL skeletal model in CHEMKIN II; not shown), i.e. an approximately incompressible fluid.

For the reduced model, since the heavy species are not available, the sums over the heavy species must be replaced by functional forms which must be determined from numerical calculations with the LLNL skeletal mechanism. To this end, we define a mean heavy species molar heat capacity

$$C_{p,h} \equiv \frac{\left(\sum_{l\in heavies} C_{p,l}N_l\right)}{N_c}, \tag{12}$$

and a mean rate of enthalpy change (in units s^{-1})

$$K_h \equiv -\left(\sum_{l\in heavies} h_l\mathscr{R}_l\right)\frac{1}{R_u T_{ref} N_c}. \tag{13}$$

In Eqs. (12) and (13), N_c is used used for normalization purposes, which is consistent with Eq. (9) and the conceptual model described in Section 2.1. Replacing Eqs. (12) and (13) in Eq. (11) yields the temperature evolution equation

$$\left(N_c C_{p,h} + \sum_{i\in lights} C_{p,i}N_i\right)\frac{dT}{dt} = -\sum_{i\in lights} h_i\mathscr{R}_i + N_c(R_u T_{ref})K_h \tag{14}$$

in which, when using the reduced model, $N_c, C_{p,h}$ and K_h (all of which describe the heavy species set) are quantities not directly computable from the reduced model, and thus must be modeled as a function of (T_0, ϕ, N^*, T); additionally, one must obtain N_i using the model described in Section 2.2.2.

For the energetics, values of h^c are obtained from the literature and for each light species C_p is modeled as

$$\frac{C_p}{R_u} = a^h + b^h \ln\left(\frac{T}{T_{ref}}\right). \tag{15}$$

Values of a^h and b^h for the light molecules are given in Table 1 [20–23].

3. Results

The results are here presented from four perspectives. First, in Section 3.1 we examine the benefits of the reduction of the heavy species to N_c and of the normalization of the database using θ. The kinetic reduction from the skeletal mechanism to our model necessarily involves a loss of information which requires additional

modeling. Second, to separate the reduction concept from the necessary additional model, in Section 3.2 we evaluate the concept using an ideal model extracted from the skeletal kinetics. Third, in Section 3.3 we present the *a priori* study, which involves modeling of the information lost through the kinetic reduction by functional fits and comparing them to the skeletal mechanism derived functions. Finally, in Section 3.4, in an *a posteriori* study, we show the performance of the kinetic reduction using the functional fits.

3.1. Examination of the n-heptane skeletal mechanism using our concept

Fig. 2 shows $N_c/(\phi \times N^*)$ as a function of θ; the plots were obtained using the LLNL skeletal kinetics in CHEMKIN II. The similarity achieved with $N_c/(\phi \times N^*)$ and θ is notable despite small departures from the nominal curves. Even for as rich a mixture as $\phi = 2$, similarity holds, making this similarity valid in realms beyond those in advanced reduced schemes where the upper limit of the scheme validity is $\phi = 1.5$ [13], at most $\phi = 2.0$ [24] or exceptionally $\phi = 3$ [25]. At $\phi = 4$, the mixture is too rich for the reaction to obtain complete fuel burning, and as a result, the reaction termination induces the disparity from self-similarity at $\theta \simeq 0.24$.

The self-similar behavior can be understood as a reduction in dimensionality of the problem but should not be confused with the ILDM method [7] because that concept was developed for actual chemical species, whereas our findings are for N_c. Basically, N_c serves as a coarse-grained attractor compared to the attractors found through the ILDM. And neither is our model equivalent with lumping [10,11] because we are decomposing all heavy species rather than a selection of them, and because a constituent may span the entire species set of heavy species. The fact that N_c can embody the evolution of all heavy species is consistent with, and can be traced to, the fact that as T increases, the heavy species chemically decompose and no longer play a role; instead, the products of this decomposition determine the reaction evolution.

Once values of $\theta \simeq 0.6$ are achieved, the constituents have been nearly exhausted and the reaction may be considered to have reached completion. Thus, the normalization achieved through θ may be very useful because over the wide range of ϕ, p_0 and T_0, the reaction is completed at approximately the same θ value, as desired (see Section 2.1).

Plots of the molar densities of oxygen, N_{o2}, and of water, N_{h2o}, versus θ are illustrated in Fig. 3 over the same wide range of ϕ, p_0 and T_0 as in Fig. 2. Notably, both types of plots display a quasi-linearity. For H_2O, eventually, an asymptotic behavior is seen at $\theta \simeq 0.6$ indicative of the reaction having reached completion, consistent with the information from Fig. 2.

The above findings suggest that instead of computing N_c from a rate equation (i.e. as a progress variable), one may simply fit the $N_c/(\phi \times N^*)$ curves shown in Fig. 2; this fitting must be performed in the four parameter space (T_0, ϕ, N^*, T). That is, whereas the LLNL skeletal mechanism depends on more than the four variables we have chosen, the reduced model only depends on these four parameters; this fact is shown next in Section 3.2. Noteworthy, Fig. 2 shows that the accuracy of the $N_c/(\phi \times N^*)$ fits versus θ for $\theta \gtrsim 0.6$ is irrelevant, since either $N_c \simeq 0$ past this θ value or for very rich situations N_c is small well before $\theta \simeq 0.6$. Similarly, instead of considering O_2 and H_2O as progress variables, it seems reasonable to functionally fit the slope of the curves in Fig. 3 and use this fit in routine calculations to predict these two major species. Thus, this examination of our conceptual model for n-heptane using the LLNL skeletal kinetics in CHEMKIN II leads to further reducing the number of species-related process variables from 12 to 9. These 9 progress variables are the molar densities of the lights: CO_2, CO, H, H_2, CH_4, H_2O_2, C_2H_2, C_2H_4, CH_2O.

3.2. Assessment of the concept's predictive capabilities using an ideal model

Before launching into the task of performing functional fits for rates and X_i, we deemed it instructive to assess the predictive capability of the concept, independent of the functional fits, by utilizing ideal functional fits extracted from the LLNL skeletal mechanism using CHEMKIN II. These ideal functions were obtained in tabular form, every 5 °K, and served as input to our conceptual model. Examples of the results are portrayed in Fig. 4 for both N_c and T profiles; indeed, predicting the energetics and more particularly the ignition time, t_{ign}, is an important goal of the model.

Unsurprizingly according to Fig. 2, Fig. 4a shows that N_c is excellently predicted by our conceptual model. However, whereas the value of the combustion T is also excellently predicted, as shown in Fig. 4b, the predicted ignition time is longer than that of the skeletal mechanism, which epitomizes the missing information in the reduced kinetic model. The fact that the combustion T is well predicted for the largest t shown in Fig. 4b can be seen by mentally translating the $T(t)$ reduced mechanism curves to match the corresponding skeletal mechanism ignition time, to find that the translated curves coincide with those from the skeletal model. Experimentally, it is observed [26] that t_{ign} is an extremely sensitive quantity function of T_0 and even a 1°K change in T_0 makes approximately 10% change in t_{ign}.

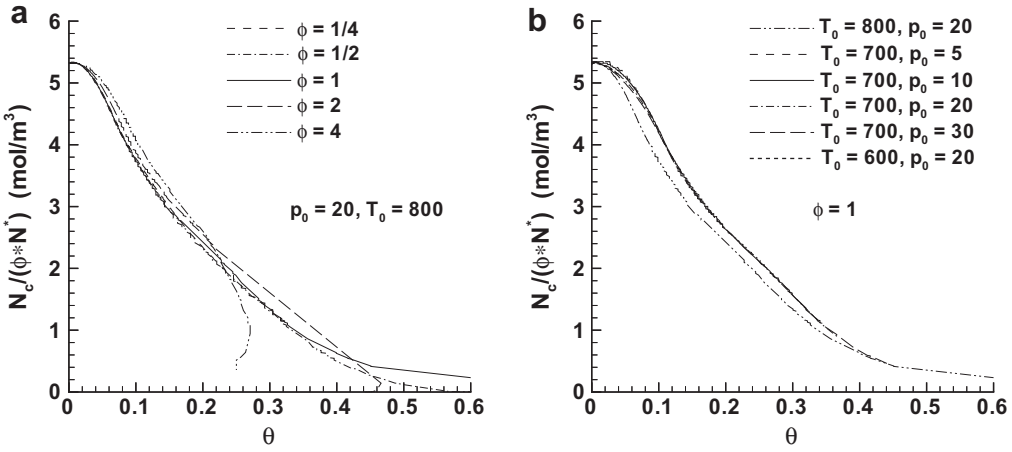

Fig. 2. Similarity plots of parameter $N_c/(\phi \times N^*)$ versus θ at (a) $p_0 = 20$ bar and (b) $\phi = 1$ using the LLNL skeletal mechanism in conjunction with CHEMKIN II. T_0 is in K.

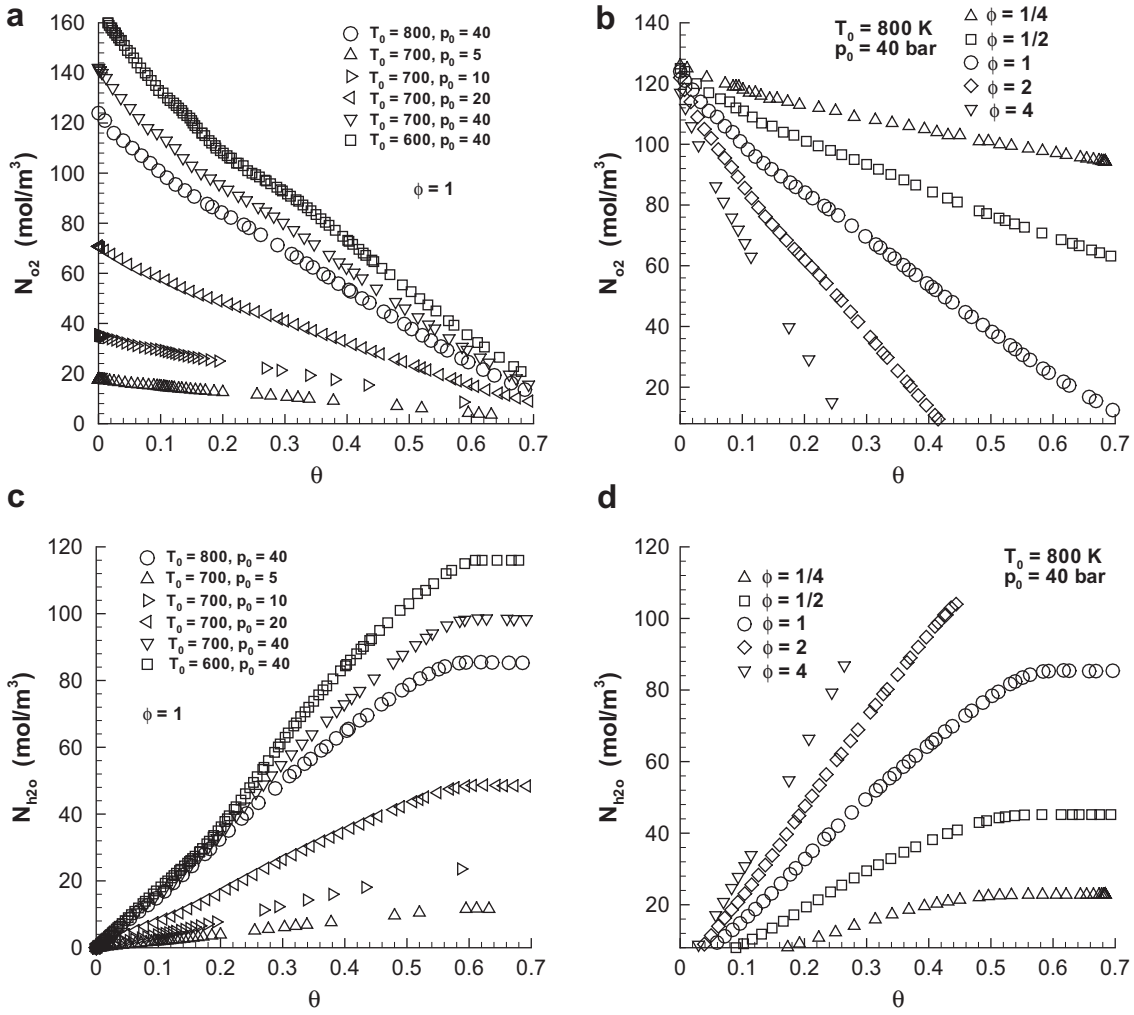

Fig. 3. Oxygen and water molar densities versus θ as extracted from the LLNL skeletal mechanism in conjunction with CHEMKIN II.

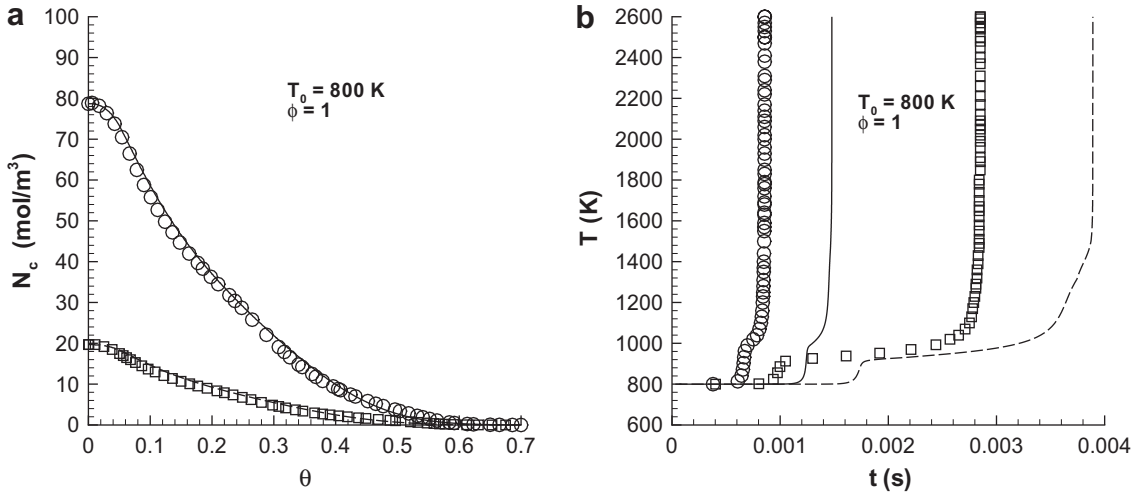

Fig. 4. Molar density of constituents (a) and temperature (b) obtained with our conceptual model and tabular information from the LLNL skeletal mechanism using CHEMKIN II. The symbols are from the LLNL skeletal mechanism in conjunction with CHEMKIN II (□□□ $p_0 = 10$ atm; ○○○ $p_0 = 40$ atm), and the lines are obtained using tabular information from the LLNL skeletal mechanism with CHEMKIN II in our conceptual model (- - - - $p_0 = 10$ atm; — $p_0 = 40$ atm).

Thus, the accurate prediction of t_{ign} is a very stringent test for a model. From the modeling viewpoint, this means that the neglected scales of the initial pre-ignition process must be reintroduced through very careful modeling. This modeling is described next.

3.3. Functional fits to emulate the LLNL skeletal mechanism

The functional fits necessary to complete the model fall into two categories: fits for the rates $K_h, KG_i, RL_i \equiv KL_i/KG_i$, for $N_c, C_{p,h}$ and for the X_i of the quasi-steady light species; and fits for the slopes of the unsteady quantities N_{o2}, and N_{h2o}.

3.3.1. Fits for the rate quantities and quasi-steady light species molar fractions

According to Eq. (14), to recover the value of T in the reduction scheme, the heavy species model should focus on an appropriate representation of $C_{p,h}$ and K_h. Plots (not shown) of $C_{p,h}$ at various p_0 values, calculated using the LLNL model over a wide range of ϕ, show that these curves exhibit a very modest variation over the range of strong N_c decay; moderate (i.e. up to 50%) variation occurs only after N_c values are very small to negligible. This indicates that the T recovery is primarily governed by K_h as far as heavy species modeling is concerned.

The model for K_h, KG_i, RL_i and X_i is constructed considering these quantities as functions of T or θ, with N^*, ϕ and T_0 being parameters. Quantities K_h, KG_i and X_i are split into a very low T region, i.e. $\theta \leqslant 10^{-2}$, termed the incubation region in which there are very slow changes; a low-rate portion corresponding to $10^{-2} \leqslant \theta \leqslant 0.2$ that exhibits a maximum, K_{mx}, and a minimum, K_{mn}; and a high $T, \theta \geqslant 0.2$, high-rate portion termed the fast-rate region in which a continuous increase is commonly observed. Conversely, RL_i first exhibits a minimum, and then a maximum. Thus, the functional fits are performed in three separate regions, with connection constraints between consecutive regions (the ultimate fits are piecewise continuous).

Curve fits for $\theta \geqslant 10^{-2}$ are generated utilizing either one of the two following methods. In the first method, one uses a cubic transformation, e.g. $KG_i(T)$ to $y(T)$, such that $y = -1$ at the maximum point and $y = 1$ at the minimum point. Then values of T at fixed y values are fitted in terms of parameters (T_0, ϕ, N^*); these values then generate the continuous curve $y(T)$ by interpolation of the discrete values. Specifically, the non-monotonic $10^{-2} \leqslant \theta \leqslant 0.2$ region behavior is captured by using a cubic functional mapping from $K(T)$ to $y(T)$ through the form

$$K(T) = \frac{1}{2}(K_{mx} + K_{mn}) + \frac{1}{4}(K_{mx} - K_{mn})(y^3 - 3y) \tag{16}$$

where $y(T) = -1$ at $T = T_{mx}$ which is the location of K_{mx} and $y(T) = 1$ at $T = T_{mn}$ which is the location of K_{mn}. In fact, the range of y is from slightly smaller than -2 at $T = T_s$ (i.e. temperature at which $K_c \equiv -d(\ln N_c)/dt > 0$) to $y \lesssim 1.8$. The values of K_{mx}, K_{mn}, T_{mx} and T_{mn} are fitted as polynomials in parameters $\ln(N^*), \ln(\phi)$ and $\ln(T_s/T_{ref})$. Temperature $T_s(T_0, N^*, \phi)$ is fitted as is T_n defined as the T value at which $y = 0$. Two different changes of variables are made from $y(T)$ to $y(z)$ depending on how T compares to T_n. For $T < T_n$, a variable $z \equiv (T_n - T)/(T_n - T_{mx})$ is defined, which means that $y = -1$ at $z = 1$. To achieve the mapping, we first generate (y, z) pairs which are functions of parameters $\ln(N^*), \ln(\phi)$ and $\ln(T_s/T_{ref})$. To match these pairs, a set of appropriate functions (e.g. polynomials $a + bz + cz^2 + \cdots$; power functions of type a^z; and combinations of the two functional forms) is chosen to produce the $y(z)$ mapping. For $T > T_n$, i.e. $y \geqslant 0$, a similar procedure is used for $y(z)$ where now $z \equiv (T - T_n)/(T_{mn} - T_n)$. Beyond $\theta \geqslant 0.2$, for the high-T region, $\ln(K)$ is fitted as a fifth order polynomial in θ^p where $p = 1$ for $\phi \leqslant 0.5$ and $p = (0.86 + 0.28\phi)/(0.74 + 0.52\phi)$ for $\phi > 0.5$. These polynomial coefficients are fitted in terms of $\ln(N^*), \ln(\phi)$ and $\ln(T_0/T_{ref})$.

In the second method, the T intervals before the maximum point, between maximum and minimum point and after minimum point are treated separately. Each of these intervals is divided into equal T slices, and logarithm values at slice boundaries are functionally fitted in terms of parameters (T_0, ϕ, N^*). The discrete set of these equally spaced functional forms is used to generate, by polynomial interpolation, the continuous function. This second method is also used sometimes for the high-rate region fits. The choice of the particular method for any i is determined by the overall results obtained in matching the input functions provided by CHEMKIN II using the LLNL database.

The need to introduce a model to capture t_{ign}, as explained in Section 3.2, as well as an extreme sensitivity of K_h on T_0 (e.g. $K_h \sim T_0^{21}$ for $\theta \simeq 10^{-3}$) meant that special care should be devoted to reproduce this dependency. Thus, we developed functional fits to the slopes dK_h/dT at T_0 and made corresponding adjustments to the rates at $\theta \lesssim 10^{-1}$. These turned out to be insufficient to reproduce t_{ign}, and an adjustment was introduced to the initial slope for K_h (for $\theta < 10^{-2}$) by using a multiplying factor determined by trial-and-error calculations, so as to best match the reduced model predictions compared to those of the skeletal mechanism.

This model was used for K_h, for the quasi-steady gain rates KG_i (where i stands for CO_2, H, CO, H_2, CH_4, H_2O_2, C_2H_2, C_2H_4, CH_2O), for the quasi-steady loss rate RL_i (where i stands for H and H_2, this rate being null for the other light species) and for the quasi-steady light species molar fractions X_i(O, CH, CH_2, CH_3, HO, HCO, HO_2, HC_2, C_2H_3).

Selected plots of K_h are presented in Fig. 5; KG_{h2} and KG_h are displayed in Fig. 6 and the ratio RL_i is correspondingly illustrated in Fig. 7 for $i = H$ and $i = H_2$. The rates K_h exhibit a variation by as much as seven orders of magnitude, and the task of developing curve fits over this extended regime in the four parameter space (T_0, ϕ, N^*, θ) is far from trivial. Despite the difficulty of developing accurate curve fits, the agreement between the fits and the LLNL skeletal mechanism in excellent to good over $p_0 \in [10, 40]$ bar, $T_0 \in [600, 800]$ K and $\phi \in [1/2, 4]$ and even extends to values as small as $\phi = 1/4$ (not shown). The same comments hold for KG and RL. Discrepancies between fits and the LLNL skeletal mechanism past $\theta \simeq 0.6$ are unimportant for the reduction concept since $N_c/N_{c,0} \ll O(1)$ past that station.

For the quasi-steady species, we chose to display N_o because of the high reactivity of the O radical and N_{oh} because the OH species is generally considered as indicative of the flame location. The quantities N_i were computed as $N_i = X_i N_L$ where $N_L = \sum_{i \in lights} N_i$; thus, the computation of N_o and N_{oh} is performed in conjunction with the calculated total light species molar density that includes the computation of the light unsteady species using the model of Section 2.2.2 for the interaction between heavy and light species. The results are presented in Fig. 8 and show that the agreement between fits and the skeletal mechanism is generally very good, including some extreme ϕ values in the lean regime, however, some exceptions occur in the very rich, $\phi = 4$, cases illustrated in Fig. 8e and f. It is apparent that for $\phi = 4$ the model cannot reproduce the multiple valued aspect of the skeletal mechanism that is due to the non-monotonic behavior of $T(t)$ for those cases. We attribute this lack of agreement of the reduced model with the skeletal mechanism to inaccuracies in the fits.

3.3.2. Fits for N_{o2} and N_{h2o}

Two quantities that constrain the evolution of N_{o2} and N_{h2o} are the initial value, N^i_{o2}, and the asymptotic value N^a_{h2o}. Thus, fits for N_{o2} and N_{h2o} were constructed as follows:

$$N_{o2}/N^i_{o2} \doteq \max(1.0 - A_{o2} \times \theta, 0.0), \tag{17}$$

$$N_{h2o}/N^a_{h2o} \doteq \min(1.0, A_{h2o} \times \theta), \tag{18}$$

and the slopes A_{o2} and A_{h2o} were fitted as

$$A_{o2} = C_{o2}(\phi, T_0) \times \phi \times (N^*)^{0.05}$$

$$A_{h2o} = C_{h2o}(\phi, T_0) \times (N^*)^{\varepsilon}$$

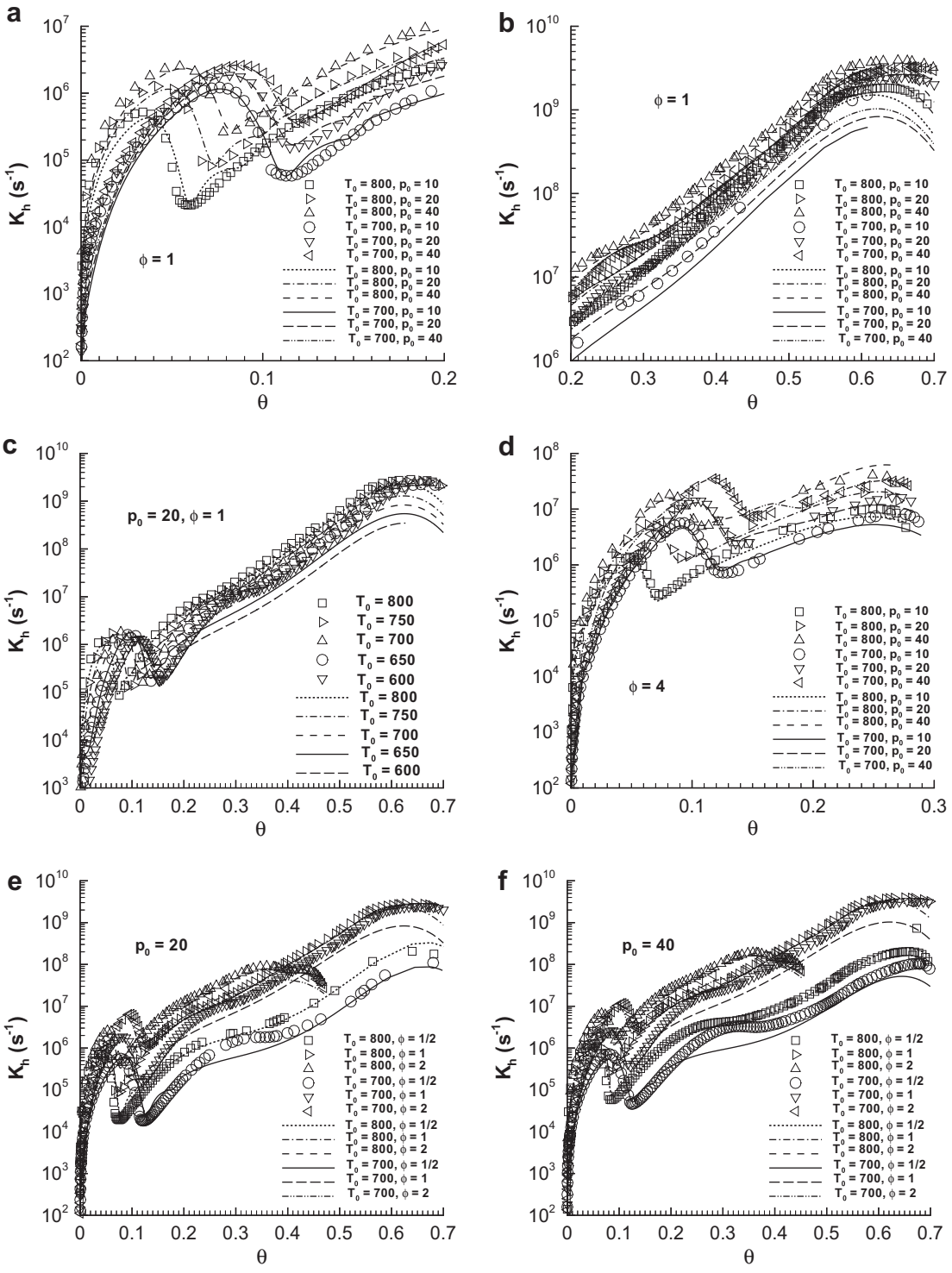

Fig. 5. K_h versus θ for different conditions. Symbols represent selected data from the LLNL runs; lines represent the corresponding fits. T_0 is in °K and p_0 is in bar.

where $\varepsilon(\phi) = 0.2 \times \phi \times \exp(-1.4\phi) \leqslant 0.0525$. To compute functions $C_{o2}(\phi, T_0)$ and $C_{h2o}(\phi, T_0)$, a set of ϕ values is first chosen. For a specified value in the set, $C_{o2}(\phi, T_0)$ and $C_{h2o}(\phi, T_0)$ are fitted as a polynomial function (up to quadratic) of T_0/T_{ref}. To obtain values for arbitrary ϕ, an interpolation is performed over ϕ using C_{o2} and C_{h2o} values at the specified ϕ values in the chosen set.

Fig. 9 shows an example of the obtained fits versus the LLNL skeletal mechanism. The agreement ranges from excellent to good and is typical of that obtained over a wide range of (T_0, ϕ, N^*).

3.4. Model predictions

The model predictions consist of the timewise temperature evolution $T(t)$, t_{ign} as extracted from the $T(t)$ profile, and the timewise evolution of the unsteady light species with the exception of O_2 and H_2O which are modeled as shown in Section 3.3.2.

3.4.1. Temperature profiles

Displayed in Fig. 10 are the reduced model predictions compared to those of the skeletal mechanism, spanning a wide range

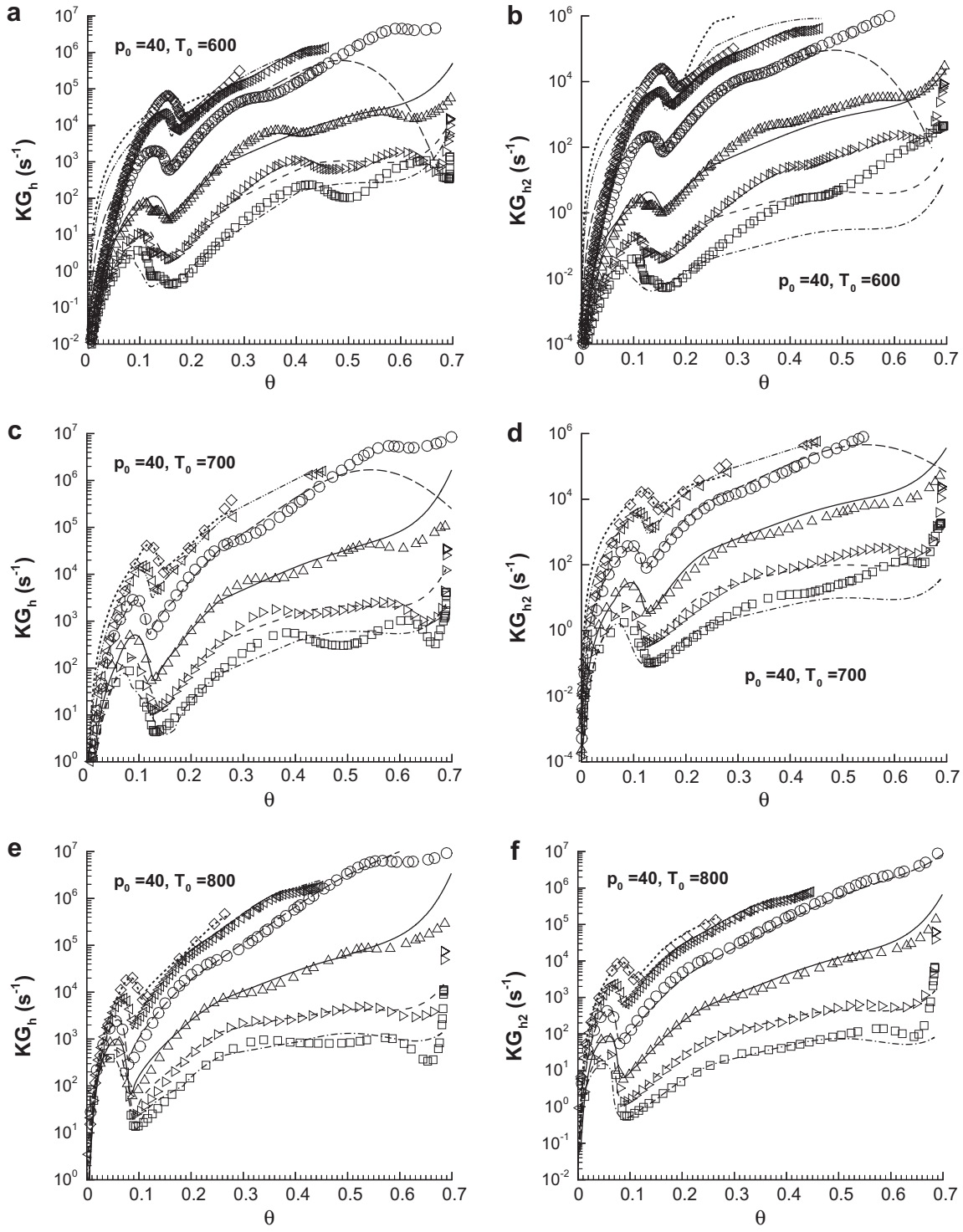

Fig. 6. KG_h and KG_{h2} versus θ for $p_0 = 40$ bar at different T_0 and ϕ. Symbols represent selected data from the LLNL skeletal mechanism; lines represent the corresponding fits: ◇ and $\cdots$ $\phi = 4$; ◁ and $- \cdot \cdot - \phi = 2$; ○ and $- - \phi = 1$; △ and —— $\phi = 1/2$; ▷ and $- - - \phi = 1/3$; □ and $- \cdot - \phi = 1/4$.

of ϕ values and two values of each T_0 and p_0. Although t_{ign} is well predicted for all cases, the ultimate combustion temperature is not well predicted at very lean conditions ($\phi = 1/4$) or relatively low pressure (i.e. $p_0 = 10$ bar). These inaccurate predictions of the reduced model are attributed to lack of accuracy of the mathematical curve fits and indicate, together with the conclusions for O and OH predictions at $\phi = 4$, that perhaps a better strategy than fitting would be to use the ideal model discussed in Section 3.2. As highlighted in Section 3.2, the reduced kinetics with the ideal model predicts T very well; the comparison with the skeletal mechanism showed that only the ignition time was not well predicted. On the favorable side for the results of Fig. 10, at the high temperature conditions representative of diesel, gas turbine and HCCI engines, the model performs very well; the same holds for the very rich conditions (e.g. $\phi = 4$) at which soot forms.

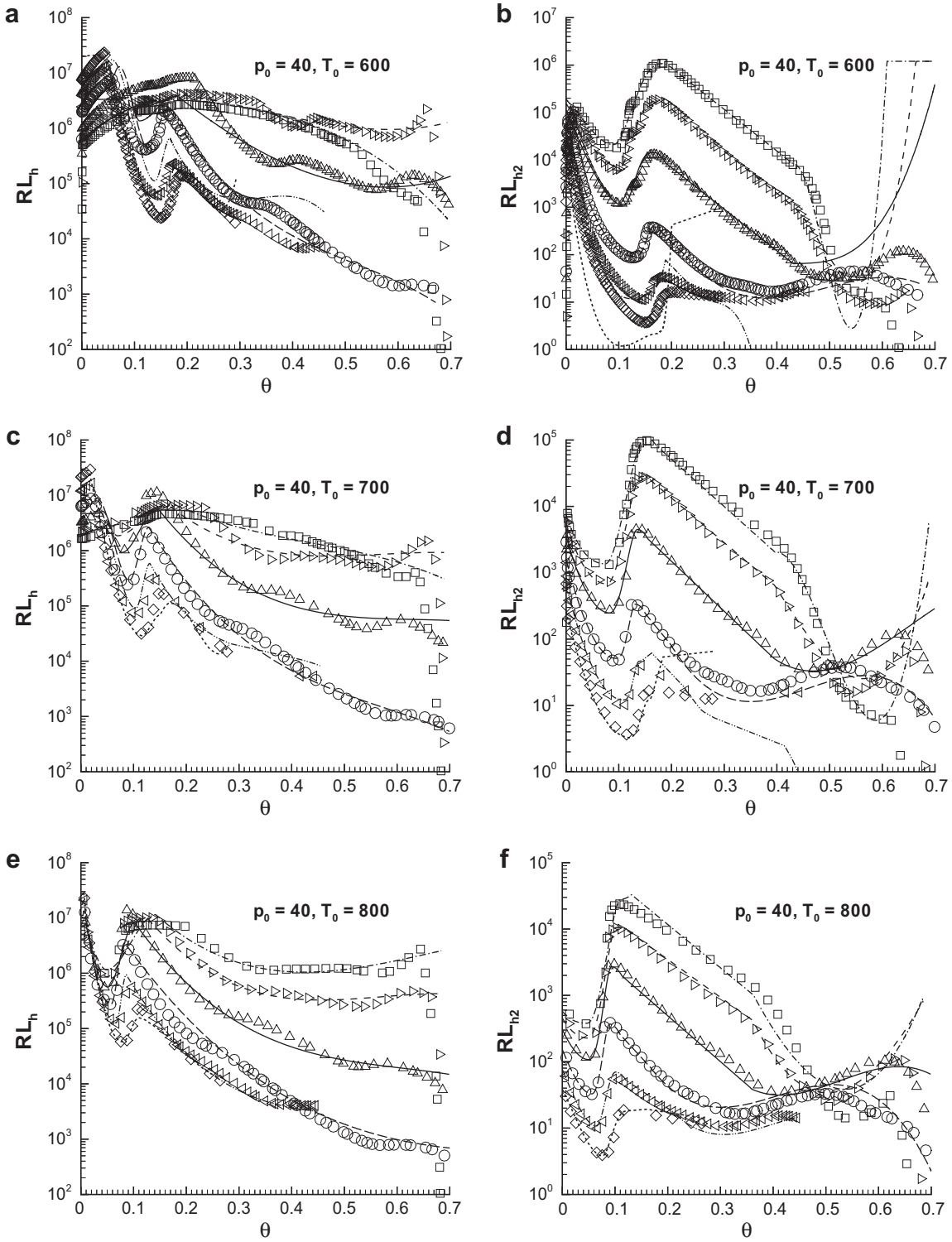

Fig. 7. RL_h and RL_{h2} versus θ for $p_0 = 40$ bar at different T_0 and ϕ. Symbols represent selected data from the LLNL skeletal mechanism; lines represent the corresponding fits: ◇ and · · · · $\phi = 4$; ◁ and — ·· — $\phi = 2$; ○ and —— $\phi = 1$; △ and —— $\phi = 1/2$; ▷ and – – – $\phi = 1/3$; □ and — · — $\phi = 1/4$.

3.4.2. Ignition times

The success of the adjusted initial K_h slopes instrumental in predicting t_{ign} is shown in Fig. 11. Noteworthy, the ordinate axis is the typical logarithmic one [27] for Fig. 11a and b, but it is here linear for Fig. 11c, so deviations between reduced model and skeletal mechanism observed in Fig. 11c are indeed logarithmically very small. The predictions in Fig. 11 are excellent over a wide range of T_0 including as low a temperature as 600 K, over a range of ϕ including mixtures as rich as $\phi = 4$, and as lean as $\phi = 1/3$ and p_0 from 10 to 40 bar.

3.4.3. Predicted unsteady species

The prediction of several unsteady light species is illustrated in Figs. 12 and 13. These results are obtained from solving Eq. (6) with

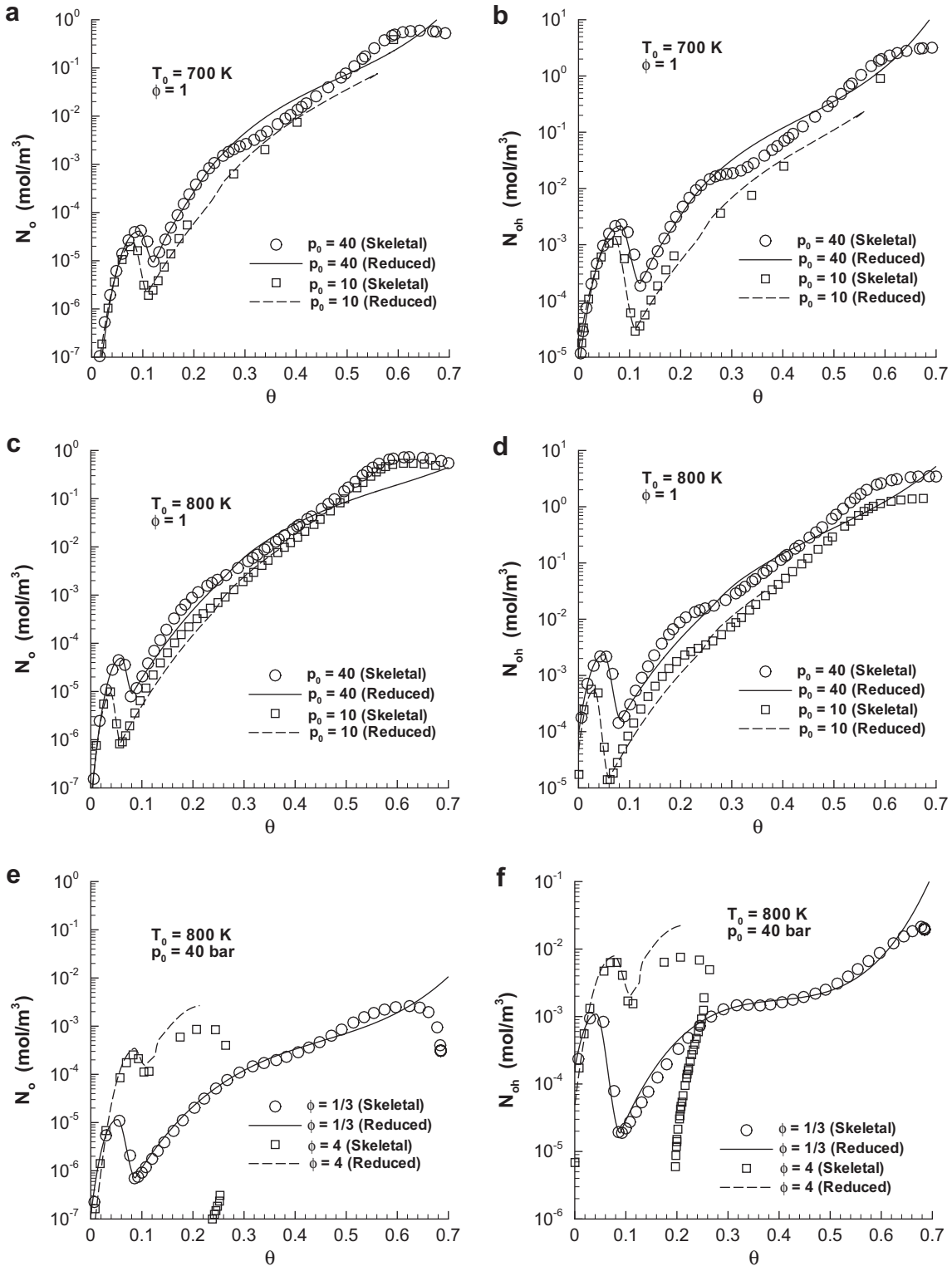

Fig. 8. Modeling results for the quasi-steady molar densities N_o and N_{oh} and comparison with those of the skeletal mechanism at various T_0, p_0 and ϕ conditions.

the modeled $\mathscr{R}_i$. The $N_i(\theta)$ is computed from $N_i(t)$ and $T(t)$, which allows computing $\theta(t)$.

We chose to display N_h and N_{h2} because they both depend on the *KG* and *RL* fits, and thus they provide a stringent test of the model given the possibility of additive error. N_{co} is chosen since CO is one important product of incomplete combustion. N_{ch4} is selected as a representative intermediary in the oxidation process. As discussed above, only prediction up to $\theta \simeq 0.6$ should be considered, as past that station the reaction is practically finished since $N_c \simeq 0$ according to Fig. 2.

Generally, the agreement between the reduced model and the skeletal mechanism is good, including at $p_0 = 10$ bar for which the combustion temperature was not well predicted. The lean region (as lean as $\phi = 1/3$) is much better reproduced by the model than the rich region for which exceptions from the good predictions occur at $\phi = 4$ for all $N_h,\ N_{h2},\ N_{co}$ and N_{ch4} as the multivalued

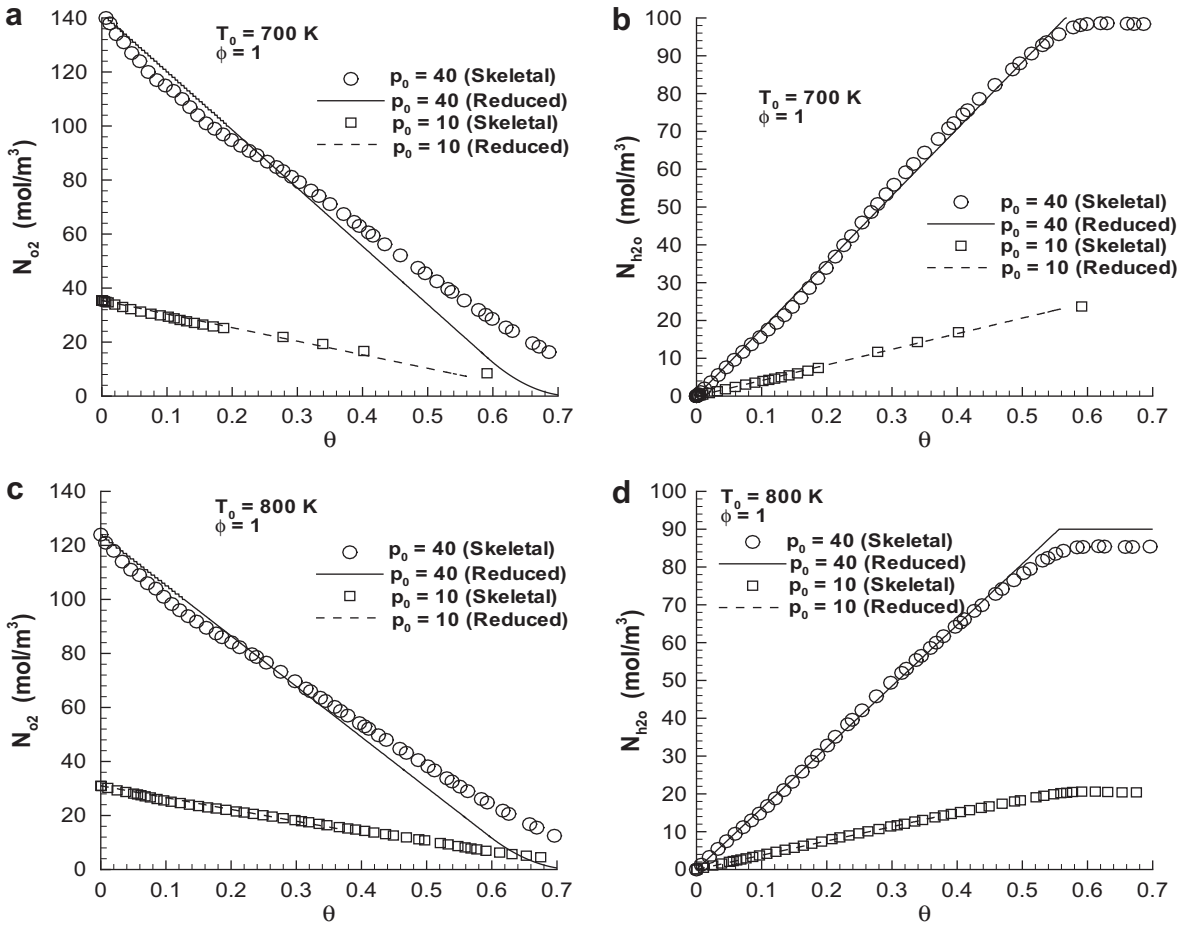

Fig. 9. N_{o2} and N_{h2o} versus θ at fixed $p_0 = 10$ and 40 bar for $\phi = 1$ and $T_0 = 700$ and 800 K.

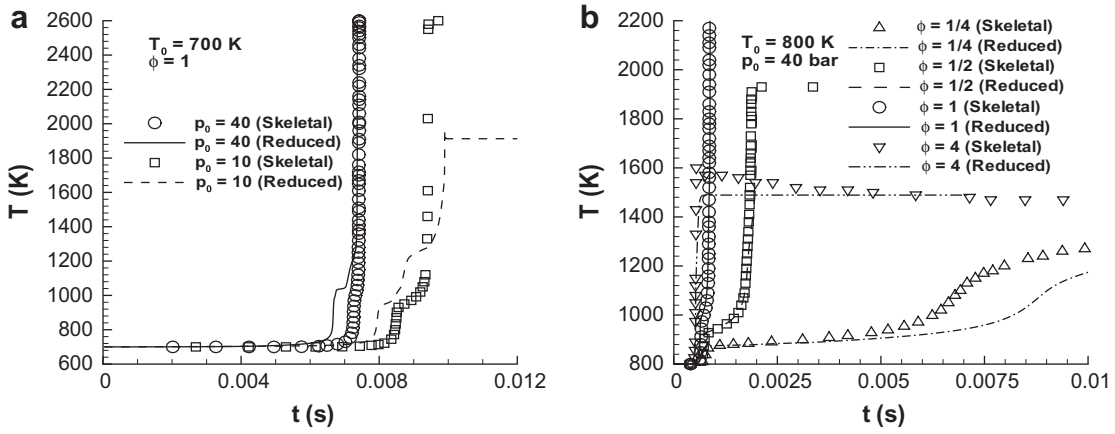

Fig. 10. $T(t)$ as predicted by the reduced model compared to the LLNL skeletal mechanism predictions for a variety of conditions.

region is not captured in Fig. 12e and f, or Fig. 13e and f. The inaccuracies at $\phi = 4$ are conjectured to rise from the imperfect curve fits and indicate again that the ideal model instead of the fits should be considered in the future. Also, the results seem to be slightly more accurate with increasing T_0.

4. Discussion

The goal of the presented kinetic reduction was to pragmatically reduce the skeletal n-heptane mechanism to the smallest possible set of progress variables that still accounts for the multiple time scales occurring in the NTC regime which cannot be reproduced by a one-step reaction. While current advanced kinetic reduction schemes having $O(50)$ species-related progress variables (e.g. [28]) have been proposed for the typical range $\phi = [0.5, 1.0, 1.5]$, compact reduced n-heptane kinetic schemes are already available in the literature, but they also have only been illustrated for a reduced ϕ range. For example, Pitsch and Peters [29] constructed a reduced n-heptane kinetics scheme for 16 species as progress variables but for $\phi = [0.5, 1.0, 2.0]$ which is a range much narrower than that used

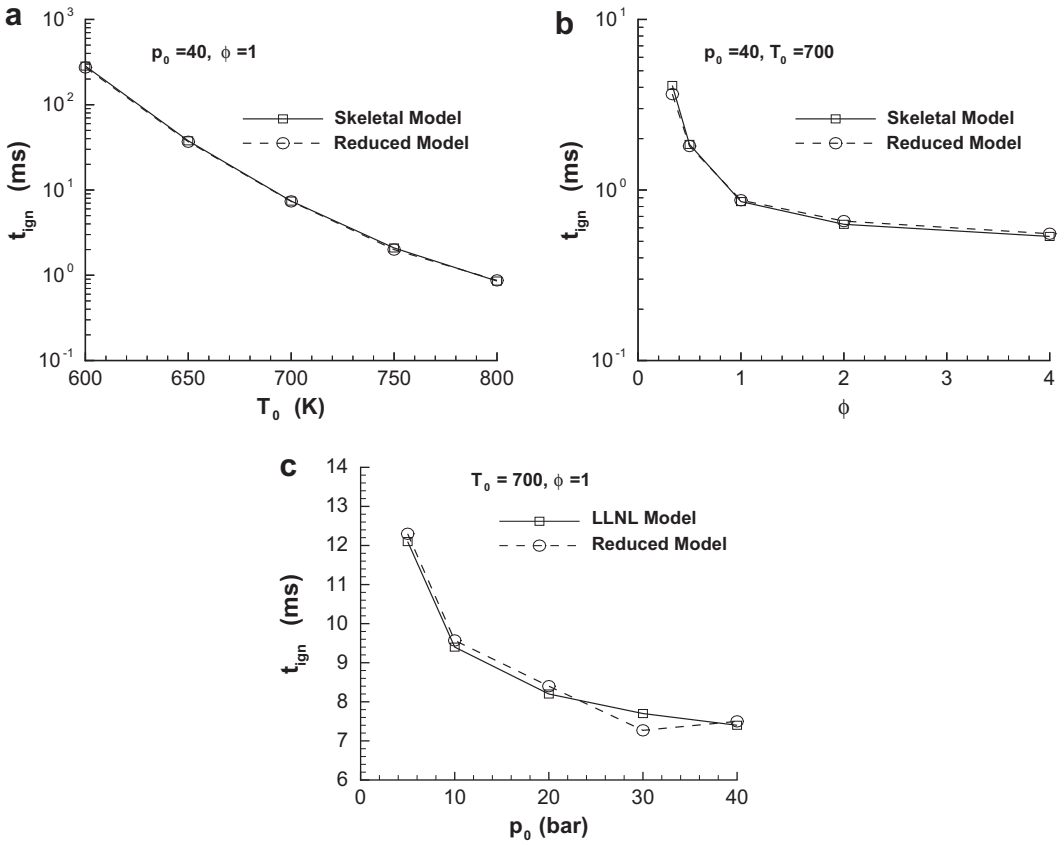

Fig. 11. t_{ign} as function of T_0, ϕ and p_0. Where not indicated on the plots, T_0 is in °K and p_0 is in bar.

in the present study, and Montgomery et al. [30] utilized in their reduced n-heptane mechanism from 28 to 37 progress variable species to simulate the ignition delay for $\phi = 1$. Our model only needs 9 progress variables, extends to a much wider ϕ range than the previous reduced schemes and predicts t_{ign} very well; although the success in predicting some species for very rich cases, such as $\phi = 4$, is less than desired and the combustion temperature is not well predicted over the entire parametric range. This lack of complete success is attributed to the imperfect mathematical fits over a very wide parametric range involving the four variables (T_0, ϕ, N^*, T). To improve the predictions, two avenues are possible for the future. The first possibility would be to improve the accuracy of the functional fits. The second possibility would be to use the ideal model extracted for our concept from the LLNL mechanism using CHEMKIN II. The inclination at this point would be to take the second avenue both because of accuracy and because the ideal model would be very efficient since it would only have to be read in once at the beginning of the computation.

5. Summary and conclusions

A kinetic reduction model has been developed that is based on the concept of constituents representing the evolution of all heavy species, and on light species representing the complementary chemistry to that of heavy species. The constituents are found through a mathematical decomposition of the heavy species and their global molar density is quasi-steady. The fact that the constituents rather than the heavy species are important can be directly traced to the fact that the heavy species decompose and it is the reaction of these products of decomposition that matters for the energetics. The light species fall into two categories: quasi-steady, for which no differential equation must be solved, and unsteady light species which are progress variables. A thorough examination of the LLNL skeletal mechanism for n-heptane revealed that it is possible to empirically define a similarity variable which is function of the initial temperature, initial pressure and equivalence ratio, and for which a scaled total constituent molar density exhibits a self-similar behavior across initial temperatures in the cold ignition regime, initial pressures and equivalence ratios. The significance of this finding is that there is a reduction in the dimensionality of the problem and that the total constituent molar density could be fitted as a function of the representative thermodynamic variables. Thus, just like in ILDM, we found a lower-dimensional manifold which is, however, different from that found in ILDM because it is of a more coarse-grained nature. Further examination of the skeletal mechanism revealed that the molar density of oxygen and that of water displayed a quasi-linear variation with the similarity variable over the entire range of parameters surveyed. The suggestion was that the molar densities of these two unsteady light species could be functionally modeled rather than computed from differential equations. The equation determining the temperature evolution was cast in the form corresponding to the global-constituent concept, thus identifying the quantities which must be mathematically fitted.

The concept was tested by using the LLNL skeletal mechanism in conjunction with CHEMKIN II. That is, instead of a model consisting of functional fits, we used an ideal model represented by tables extracted from the LLNL skeletal mechanism in the form needed in our conceptual model. Our conceptual model was found to be sound, but the ignition time it predicted was too long compared to the template. The meaning of this discrepancy is that the neglect of the chemical processes during the initial time of very small temperature changes results in the overprediction of the ignition time. The situation is equivalent to turbulent modeling

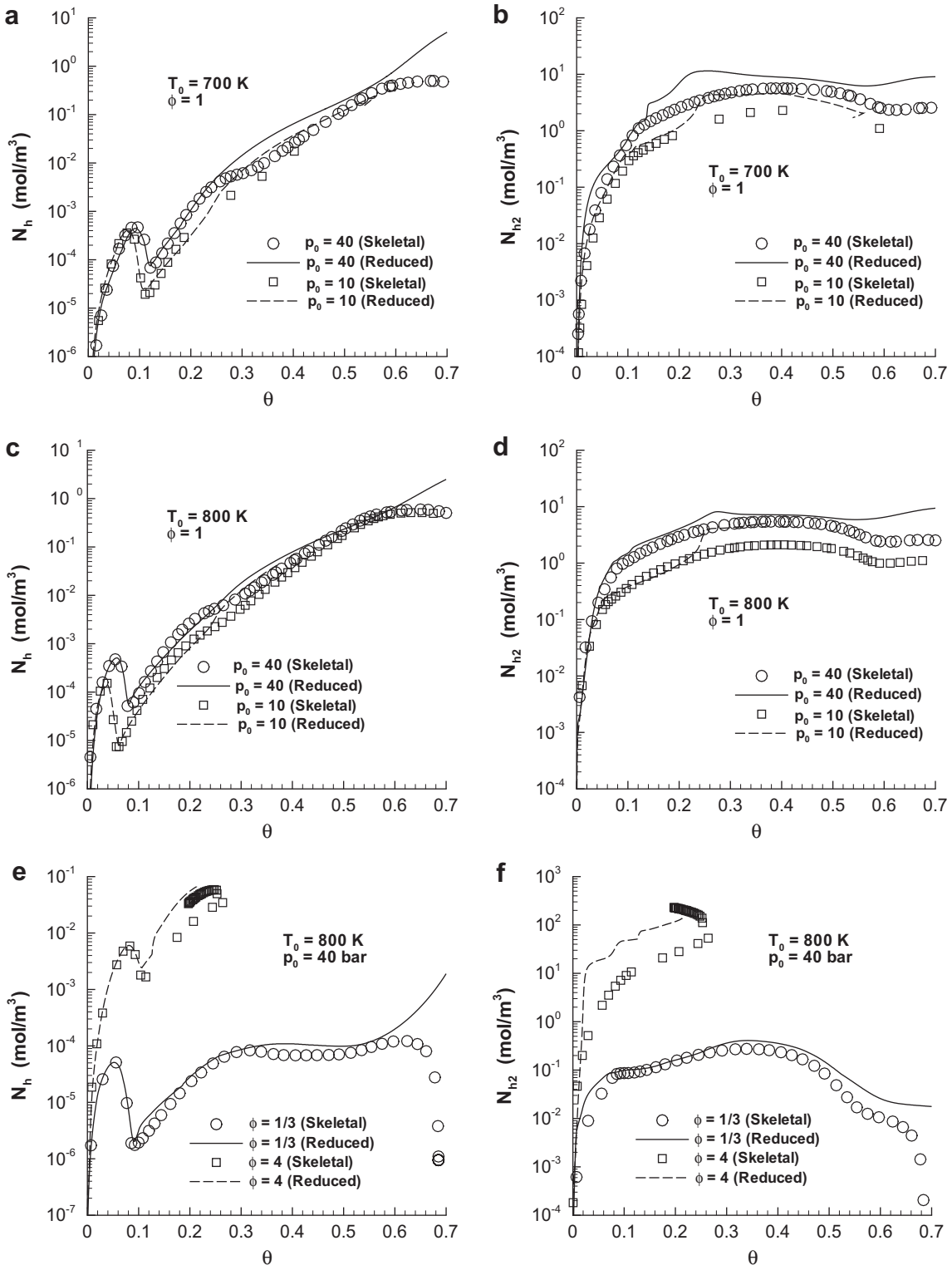

Fig. 12. Predictions of the reduced model for N_h and N_{h2} compared to those of the skeletal mechanism at various T_0, p_0 and ϕ conditions.

using the Large Eddy Simulation (LES) concept in which the spatial filtering of scales results in the need to re-introduce the effect of these small scales through models. Following the LES modeling philosophy, a small-scale model was developed and implemented at temperatures very close (1–2 °K) to the initial temperature, to be used with the conceptual model.

Moreover, also paralleling the LES concept, fits in functional form were developed for the sensible enthalpy production due to the constituents' reaction, for the quasi-steady light species mole fractions and for the reaction rate of the unsteady light species. The reaction rate of each unsteady light species was decomposed into contributions from the lights that were directly taken from the LLNL skeletal mechanism, and contributions from the heavy species that were modeled. The heavy species rate contribution was further categorized into a gain rate and a loss rate, which were individually modeled. The modeling effort was by no means trivial

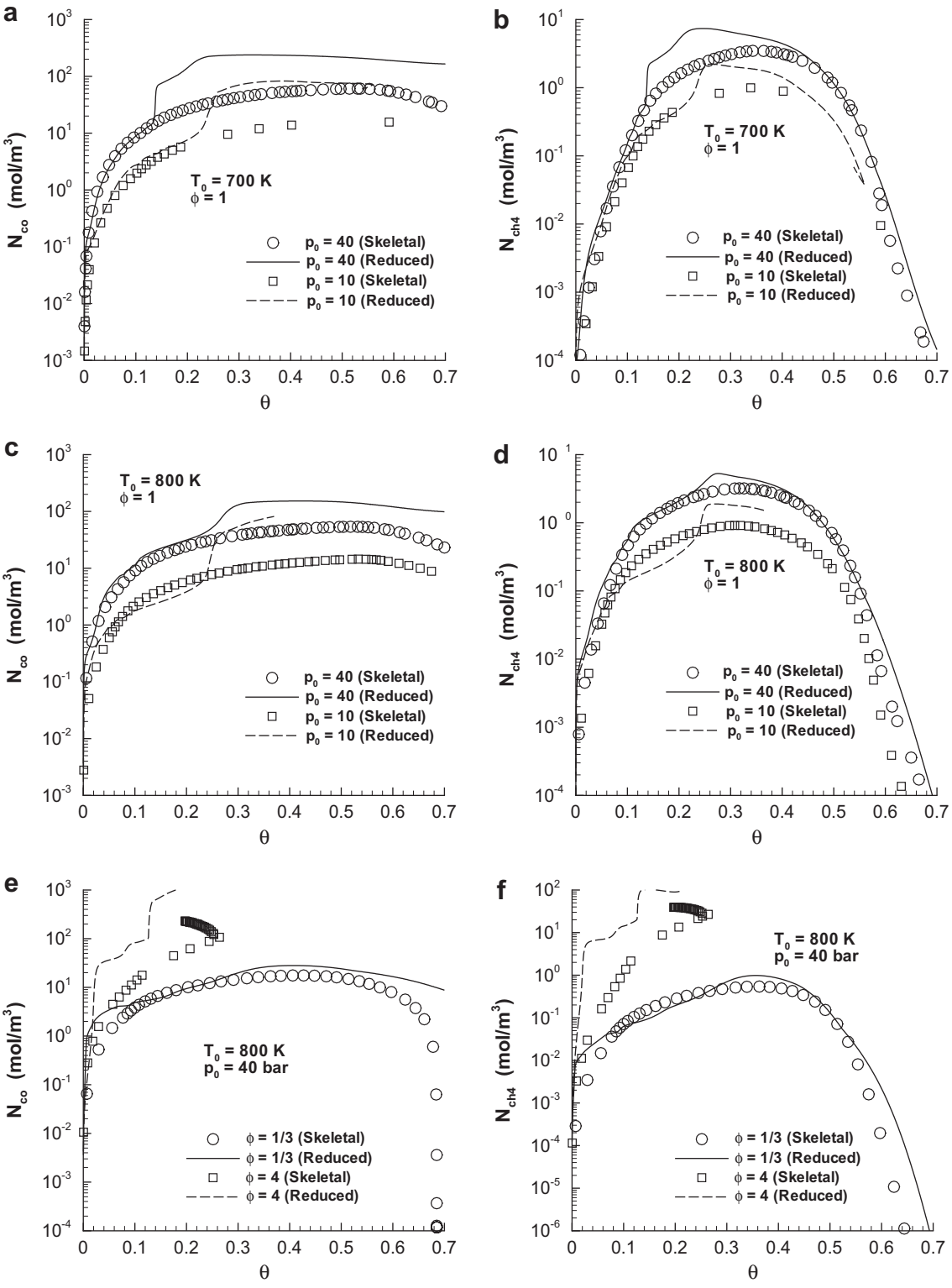

Fig. 13. Predictions of the reduced model for N_{co} and N_{ch4} compared to those of the skeletal mechanism at various T_0, p_0 and ϕ conditions.

as the rates and molar fractions varied by as much as seven orders of magnitude and this variation needed to be captured in the four parameter space of the initial pressure, the initial temperature, the equivalence ratio and the temperature.

The consequence of providing functional fits over a wide range of equivalence ratios encompassing mixtures as rich as $\phi = 4$ and as lean as $\phi = 1/4$ was that generally the fits were good to excellent, but sparse regions of only fair results could also be identified. The ignition times were excellently to very well reproduced by the model, and so were some major species (e.g. O_2 and H_2 O). Other major species (e.g. CO) and OH, which is an indicator of the flame location, were generally well reproduced with the exception of very rich situations (i.e. $\phi = 4$). The value of the final combustion temperature was generally but not always well predicted. To

improve the quality of the predictions where lacks were identified, it was suggested to use in the future the ideal model provided by the tables extracted from the LLNL mechanism using CHEMKIN II.

Finally, since results for most reduction schemes are presented in a much more restricted ϕ region than the $\phi \in [1/4, 4]$ considered here, it is difficult to directly evaluate our model with respect to other models. It is understood that for any given model, predictions will improve if a less ambitious validity regime is considered.

Acknowledgments

This study was conducted at the California Institute of Technology, Jet Propulsion Laboratory (JPL), and was sponsored by the Army Research Office, with Dr. Ralph Anthenien as Program Manager. Ms. Elly Ponce of JPL is thanked for the drawing of Fig. 1.

References

[1] U.C. Müeller, N. Peters, A. Liñan, Proc. Combust. Inst. 24 (1992) 777–784.
[2] M. Bollig, H. Pitsch, J.C. Hewson, K. Sheshadri, Proc. Combust. Inst. 26 (1997) 729–737.
[3] C.J. Sung, C.K. Law, J.-Y. Chen, Proc. Combust. Inst. 27 (1998) 295–304.
[4] S.C. Li, B. Varatharajan, F.A. Williams, AIAA J. 39 (12) (2001) 2351–2356.
[5] J.B. Bell, N.J. Brown, M.S. Day, M. Frenklach, J.F. Grcar, R.M. Propp, S.R. Tonse, Proc. Combust. Inst. 28 (2000) 107–113.
[6] S.B. Pope, Combust. Theory Model. 1 (1997) 41–63.
[7] U. Maas, S.B. Pope, Combust. Flame 88 (3–4) (1992) 239–264.
[8] C. Correa, H. Niemann, B. Schramm, J. Warnatz, Proc. Combust. Inst. 28 (2000) 1607–1614.
[9] S.H. Lam, D.A. Goussis, Int. J. Chem. Kinet. 26 (1994) 461–486.
[10] E. Ranzi, T. Faravelli, P. Gaffuri, A. Sogaro, Combust. Flame 102 (1995) 179–192.
[11] E. Ranzi, M. Dente, A. Goldaniga, G. Bozzano, T. Faravelli, Prog. Energy Combust. Sci. 27 (2001) 99–139.
[12] T.F. Lu, C.K. Law, Proc. Combust. Inst. 30 (2005) 1333–1341.
[13] T.F. Lu, C.K. Law, Combust. Flame 144 (2006) 24–36.
[14] T.F. Lu, C.K. Law, Combust. Flame 146 (2006) 472–483.
[15] X.L. Zheng, T.F. Lu, C.K. Law, Proc. Combust. Inst. 31 (2007) 367–375.
[16] P. Pépiot-Desjardins, H. Pitsch, Combust. Flame 154 (2008) 67–81.
[17] Lawrence Livermore National Laboratory, <http://www-cms.llnl.gov/combustion/combustion2.html>.
[18] S.W. Benson, Thermochemical Kinetics, John Wiley & Sons, Inc., 1968.
[19] R.C. Reid, J.M. Prausnitz, B.E. Poling, The Properties of Gases and Liquids, 4th ed., McGraw-Hill Book Co., 1987. Chapter 6.
[20] National Institute of Standards and Technology, Chemistry WebBook; <http://webbook.nist.gov/chemistry/>.
[21] D.R. Lide (Ed.-in-Chief), CRC Handbook of Chemistry and Physics, 86th ed., CRC Press, Boca Raton, FL, 2005 (internet edition).
[22] Gas Research Institute, <http://www.me.berkeley.edu/gri-mech/>.
[23] NASA Glenn Research Center, <http://cea.grc.nasa.gov/>.
[24] N. Peters, G. Paczko, R. Seiser, K. Sheshadri, Combust. Flame 128 (2002) 38–59.
[25] V.I. Babushok, W. Tsang, J. Propul. Power 20 (3) (2004) 403–414.
[26] R. Hanson, private communication, September 16, 2009.
[27] H.J. Curran, P. Gaffuri, W.J. Pitz, C.K. Westbrook, Combust. Flame 114 (1998) 149–177.
[28] T.F. Lu, C.K. Law, strategies for mechanism reduction for large hydrocarbons: n-Heptane, paper #C21, presented at the 5th US Combustion Meeting, March 25–28, 2007, San Diego, CA, 2007.
[29] H. Pitsch, N. Peters, SAE paper 98-2464, 1998.
[30] C.J. Montgomery, M.A. Cremer, J-Y Chen, C.K. Westbrook, L.Q. Maurice, J. Propul. Power 18 (1) (2002) 192–198.

APPENDIX 2

Combustion and Flame 157 (2010) 2184–2197

Contents lists available at ScienceDirect

Combustion and Flame

journal homepage: www.elsevier.com/locate/combustflame

A model of reduced oxidation kinetics using constituents and species: Iso-octane and its mixtures with *n*-pentane, iso-hexane and *n*-heptane

Kenneth Harstad, Josette Bellan *

California Institute of Technology, Jet Propulsion Laboratory, 4800 Oak Grove Drive, M/S 125-109, Pasadena, CA 91109-8099, United States

ARTICLE INFO

Article history:
Received 26 March 2010
Received in revised form 12 May 2010
Accepted 18 June 2010

Keywords:
Reduced oxidation kinetics for iso-octane
Iso-octane mixtures

ABSTRACT

A previously described methodology for deriving a reduced kinetic mechanism for alkane oxidation and tested for *n*-heptane is here shown to be valid, in a slightly modified version, for iso-octane and its mixtures with *n*-pentane, iso-hexane and *n*-heptane. The model is still based on partitioning the species into lights, defined as those having a carbon number smaller than 3, and heavies, which are the complement in the species ensemble, and mathematically decomposing the heavy species into constituents which are radicals. For the same similarity variable found from examining the *n*-heptane LLNL mechanism in conjunction with CHEMKIN II, the appropriately scaled total constituent molar density still exhibits a self-similar behavior over a very wide range of equivalence ratios, initial pressures and initial temperatures in the cold ignition regime. When extended to larger initial temperatures than for cold ignition, the self-similar behavior becomes initial temperature dependent, which indicates that rather than using functional fits for the enthalpy generation due to the heavy species' oxidation, an ideal model based on tabular information extracted from the complete LLNL kinetics should be used instead. Similarly to *n*-heptane, the oxygen and water molar densities are shown to display a quasi-linear behavior with respect to the similarity variable, but here their slope variation is no longer fitted and instead, their rate equations are used with the ideal model to calculate them. As in the original model, the light species ensemble is partitioned into quasi-steady and unsteady species; the quasi-steady light species mole fractions are computed using the ideal model and the unsteady species are calculated as progress variables using rates extracted from the ideal model. Results are presented comparing the performance of the model with that of the LLNL mechanism using CHEMKIN II. The model reproduces excellently the temperature and species evolution versus time or versus the similarity variable, with the exception of very rich mixtures, where the predictions are still very good but the multivalued aspect of these functions at the end of oxidation is not captured in the reduction. The ignition time is predicted within percentages of the LLNL values over a wide range of equivalence ratios, initial pressures and initial temperatures.

1. Introduction

Chemical kinetics simplification has generally followed several approaches. Examples are the approach where the elementary mechanism is reduced in a specified form which persists during an entire computation (e.g. Müeller et al. [1], Bollig et al. [2], Sung et al. [3] and Li et al. [4]), or where tabulations storing the change in the state vector over a time interval for later utilization (e.g. (PRISM) [5], (ISAT) [6]) are produced, or where the simplification in rate path description according to an intrinsic low-dimensional manifold ((ILDM) [7]) is performed. Kinetics reduction either through automatic reaction and species elimination [8] or through optimally reduced kinetic models [9] has also been proposed. Considering the importance of accurately predicting the ignition time and the fact that it is a very sensitive function of the initial temperature [10], the goal of most approaches has been its accurate prediction, although reproducing the temperature and species evolution is also important, particularly when pollutants are of interest.

This study presents results of a model which is in the framework of both kinetic reduction and storage of information for later utilization, and proposes a relatively compact yet accurate model. This model is based on the kinetic reduction proposed by Harstad and Bellan [11] through constituents and species; this reduction has been so far tested only for *n*-heptane. Although the present model adopts the same viewpoint and shows that the similarity variable found for *n*-heptane holds for iso-octane and its mixtures with *n*-pentane, iso-hexane or *n*-heptane, the extension of the previous model to higher initial temperatures than in the cold ignition

* Corresponding author. Fax: +1 818 393 6682.
E-mail address: Josette.Bellan@jpl.nasa.gov (J. Bellan).

0010-2180/$ - see front matter © 2010 The Combustion Institute. Published by Elsevier Inc. All rights reserved.
doi:10.1016/j.combustflame.2010.06.010

regime warrants some slight revisions. The model and its revisions are described in Section 2. Following the model exposition, is a presentation in Section 3 of the predictions from the reduced model which are compared for iso-octane and Primary Reference Fuels (PRFs), i.e. mixtures of iso-octane and *n*-heptane, to the corresponding full LLNL mechanism [12] in conjunction with CHEMKIN II. Finally, in Section 4 a summary is offered and conclusions dwell on the impact of this modeling approach.

2. Conceptual model

2.1. Summary of the n-heptane model

In the conceptual model of Harstad and Bellan [11], the species are partitioned into heavies (carbon number, $n \geqslant 3$) and lights (the remaining of the set). The model was developed using the LLNL skeletal mechanism (160 species and 1540 reactions). The heavies can be either radicals or stable species. The lights are oxygen, nitrogen, the final combustion products and light radicals/molecules (e.g. CH_3, CH_4, H_2O_2). The heavies are not treated as a species set, but as a set of base constituent radicals which correspond to radicals from group additivity theory [13]. Although sometimes lights and constituents, both of which are radicals, may have the same chemical formula, the difference between constituents and these light species is that the later are unbound to other chemical entities, whereas the former are bound to other chemical entities, i.e. other constituents. For each constituent k, its molar density, N_k, is the sum, over all heavy species, of the count of the constituent in each heavy species multiplied by the molar density of that species. The element compositions of the constituents are not linearly independent, but the constituents are linearly independent. Thus, the constituents are independent structural elements which have individual valence bond topologies; the constituents are not just based on atom counts.

For each heavy species, and thus for the entire set of heavy species, there is a unique and complete set of constituents. The subset of constituents that have a very small contribution to the total constituent count having molar density N_c, is replaced by the complementary subset of constituents already accounted for in N_c. The rule for replacement is that each constituent having a small contribution to N_c is replaced by one having, first, close valence structure and second, close composition to the constituent neglected. After this replacement, one obtains an optimal N_k set. For *n*-heptane, the following thirteen constituents, CH_2, CH_3, CH, C_2H_3, C_2H_2, C_2, HC_2, CO (keto), HCO, HO, HO_2, OO, O, constitute the optimal constituent set and

$$N_c \equiv \sum_{k=1}^{13} N_k. \tag{1}$$

Furthermore, the pressure variable p, was replaced by a dimensionless molar density

$$N^* \equiv \frac{N_{n2}}{N_{ref}}, \tag{2}$$

for N_2, where the reference N_2 molar density is $N_{ref} = 31.5\ \mathrm{mol/m^3}$ for dry air value at pressure $p_{ref} = 1$ bar and $T_{ref} = 298.15$ K. Indeed, for oxidation in air, N_2 is the dominant species and thus N^* is a surrogate variable for p. The N^* value is reaction-rate invariant since no NO_x mechanism is considered at this early stage of model development and N_2 is inert.

With the goal of obtaining a normalized variable θ such that at approximately the same value of θ, N_c has been consumed in the reaction for all initial conditions (except for rich situations), the LLNL skeletal mechanism was exhaustively examined to propose

$$\theta \equiv \frac{T - T_0}{T_r(\phi, N^*)}, \tag{3}$$

$$T_r \equiv 2065 (N^*)^{0.06} w(\phi), \tag{4}$$

$$w(\phi) = \phi \frac{1.5 + 1.31\phi}{1 + 0.71\phi + 1.1\phi^2}, \tag{5}$$

as the result of the search, where T is the temperature, T_0 is the initial temperature (subscript 0 denotes the initial condition) and ϕ is the equivalence ratio. It was shown by Harstad and Bellan [11] that indeed N_c decreases by three orders of magnitude upon reaching $\theta \gtrsim 0.6$, which ensures that all θ values remain below unity for all calculations. Moreover, for a wide range of p_0, T_0 in the range [600,900] relevant to the cold ignition regime, and $\phi \in [1/4, 4]$, all curves $N_c/(\phi \times N^*)$ as a function of θ nearly coincided, showing a self-similar behavior. This self-similar behavior was exploited in that mathematical fits of this curve replaced the otherwise needed computations for $N_c(\theta)$.

The light species were categorized into a quasi-steady subset comprising the O, CH, CH_2, CH_3, HO, HCO, HO_2, HC_2, C_2H_3 radicals. The radicals' mole fractions, X_i, were fitted as functions of the state variables (ϕ, N^*, T) and the modeling parameter T_0. The complementary subset to the quasi-steady species was that of the unsteady species consisting of H_2O, CO_2, O_2, H, CO, H_2, CH_4, H_2O_2, C_2H_2, C_2H_4, CH_2O. Because the LLNL skeletal mechanism showed that the mole fractions of O_2 and H_2O were quasi-linear functions of θ in the wide range of (p_0, ϕ, T_0) here investigated, the approach was to functionally fit the slope of these two mole fractions versus θ, so that the only remaining species progress variables were CO_2, H, CO, H_2, CH_4, H_2O_2, C_2 H_2, C_2H_4, CH_2O. The reaction rates of unsteady light species were conceptualized as

$$\mathscr{R}_i \equiv \left(\frac{dN_i}{dt}\right)_{reac} = \left.\frac{dN_i}{dt}\right|_{heavies} + \left.\frac{dN_i}{dt}\right|_{lights}, \tag{6}$$

where the first term expressing the contribution to the lights from the heavy group was modeled and the second term in the right hand side used the same rates as in the LLNL skeletal mechanism. Further, for the first term,

$$\left.\frac{dN_i}{dt}\right|_{heavies} = N_c(KG_i - X_i KL_i), \tag{7}$$

where KG_i and KL_i are functions of (T_0, ϕ, N^*, T) that were modeled consistently with the heavy species model.

Finally, the temperature evolution was computed from

$$\left(N_c C_{p,h} + \sum_{i \in lights} C_{p,i} N_i\right) \frac{dT}{dt} = -\sum_{i \in lights} h_i \mathscr{R}_i + N_c (R_u T_{ref}) K_h, \tag{8}$$

in which R_u is the universal gas constant and

$$C_{p,h} \equiv \frac{\left(\sum_{l \in heavies} C_{p,l} N_l\right)}{N_c}, \tag{9}$$

$$K_h \equiv -\left(\sum_{l \in heavies} h_l \mathscr{R}_l\right) \frac{1}{R_u T_{ref} N_c}, \tag{10}$$

were mathematically modeled as a function of (T_0, ϕ, N^*, T). For each light species C_p was modeled as

$$\frac{C_p}{R_u} = a^h + b^h \ln\left(\frac{T}{T_{ref}}\right) \tag{11}$$

and values for a^h and b^h were provided in [11].

Thus, the model required functional fits for the molar density N_c, molar density slopes for O_2 and H_2O, X_i of the quasi-steady light species, KG_i and $RL_i \equiv KL_i/KG_i$ for the unsteady light species, and K_h, all as functions of θ in the parametric space (T_0, ϕ, N^*, T).

2.2. Application of the n-heptane conceptual model to iso-octane and its mixtures

When applying the above described conceptual model to another alkane than *n*-heptane, the first question which must be asked is whether the number and list of constituents, particularly the optimal set of constituents, remains the same as for *n*-heptane. Examination of the LLNL full mechanism for iso-octane (857 species and 3606 reactions) revealed that there is an additional constituent, the carbon atom C, which must be included in the optimal set because its molar density was found to be significant, so that now

$$N_c \equiv \sum_{k=1}^{14} N_k. \tag{12}$$

We show in Sections 2.2.1 and 2.2.3 that by adopting the definition of Eq. (12), we can accommodate not only iso-octane, but also mixtures of iso-octane with *n*-pentane, iso-hexane, and *n*-heptane, that θ as defined by Eq. (3) remains a similarity variable but now for N_c as defined by Eq. (12), and that the molar densities of O_2 and H_2O also display a quasi-linear variation with θ (for $\phi = 2$ and 4 the N_{h2o} quasi-linearity only holds up to its maximum value), just like for *n*-heptane.

The model of Section 2.1 was tested in [11] for *n*-heptane in the T_0 range relevant to cold ignition, but it is obviously desirable to extend this model, if possible, to the higher value T_0 regime. In Sections 2.2.2 and 2.2.3, we show that an additional, slight modification to the model of Section 2.1 makes the modified conceptual representation also valid in the higher than cold ignition T_0 regime.

2.2.1. Iso-octane in the cold ignition regime

In Figs. 1 and 2, $N_c/(\phi \times N^*)$, molar densities of O_2 and H_2O (N_{o2} and N_{h2o}) are illustrated from the LLNL full mechanism [12] in conjunction with CHEMKIN II for the same conditions as in the respective Figs. 2 and 3 of Harstad and Bellan [11] obtained for *n*-heptane. Clearly, $N_c/(\phi \times N^*)$ remains self-similar with θ, and N_{o2} and N_{h2o} remain quasi-linear with θ (for N_{h2o} up to its maximum value; for $\phi = 2$ and 4 after the N_{h2o} maximum value, the curve is multivalued with respect to θ). Visual examination of curves in Figs. 1 and 2 compared to Figs. 2 and 3 of [11] indicates that the curves from the respective figures are superimposable, confirming the similarity concept. Considering iso-octane and *n*-heptane, when moving on the $N_c/(\phi \times N^*)$ curves to increasing θ values, the implication is that heavy species pyrolysis, decomposition and corresponding light species production occur in similar manner for the two fuels.

Further examination of the LLNL full mechanism [12] in conjunction with CHEMKIN II revealed that the molar density production rate of O_2, H_2O, H and H_2 from the heavy species, as shown by Eq. (7), is now governed by KG_i alone, unlike the finding for *n*-heptane. Since O_2 and H_2O are conceptually computable using the quasi-linear form shown in Fig. 2 and since in absence of diffusive mixing the molar density of H is quasi-steady, the *n*-heptane form of the reduced model is simplified for iso-octane by using $K_{net,i} \equiv (KG_i - X_i KL_i)$ which are functions of (T_0, ϕ, N^*, T). All other unsteady light species also have $KL_i \simeq 0$, as for *n*-heptane.

2.2.2. Iso-octane in the high-temperature regime

To reveal the applicability of the conceptual model to higher than cold ignition T_0 values, results are displayed in Fig. 3a showing $N_c/(\phi \times N^*)$ versus θ for T_0 up to 1200 K, as extracted from the LLNL full mechanism [12] using CHEMKIN II. Clearly, for $T_0 = 1000$ K and 1200 K, the values depart from the narrow band in the $T_0 \in [600, 800]$ K regime. In particular, we observe an increase in the initial slope of $N_c/(\phi \times N^*)$ versus θ with increasing T_0, consistent with the increasing pyrolysis rate, as found by Yu et al. [14]. However, similarity still exists at fixed T_0 as shown in Fig. 3b, where it is shown that for $T_0 = 1200$ K the $N_c/(\phi \times N^*)$ values plotted versus θ at various p_0 and ϕ nearly collapse on each other. Thus, the similarity concept still holds at higher T_0 but instead of obtaining a single $N_c/(\phi \times N^*)$ curve versus θ, there is now a family of curves parametrized by T_0. Extension of the *n*-heptane model [11] to incorporate this new aspect is discussed in Section 3.

2.2.3. Primary reference fuels

A sample of results similar to those shown in Section 2.2.1 is presented here to highlight the fact that the similarity concept remains valid for PRFs. Two mixtures are chosen to illustrate the applicability of the concept: (90% iso-octane)/(10% *n*-heptane) and (50% iso-octane)/(50% *n*-heptane). Information extracted from the LLNL full mechanism [12] using CHEMKIN II is exhibited for $N_c/(\phi \times N^*)$ versus θ in Fig. 4; the quasi-linear behavior of N_{o2} and N_{h2o} versus θ still holds but is not illustrated for the purpose of brevity. The results show that whether for (90% iso-octane)/(10% *n*-heptane) or

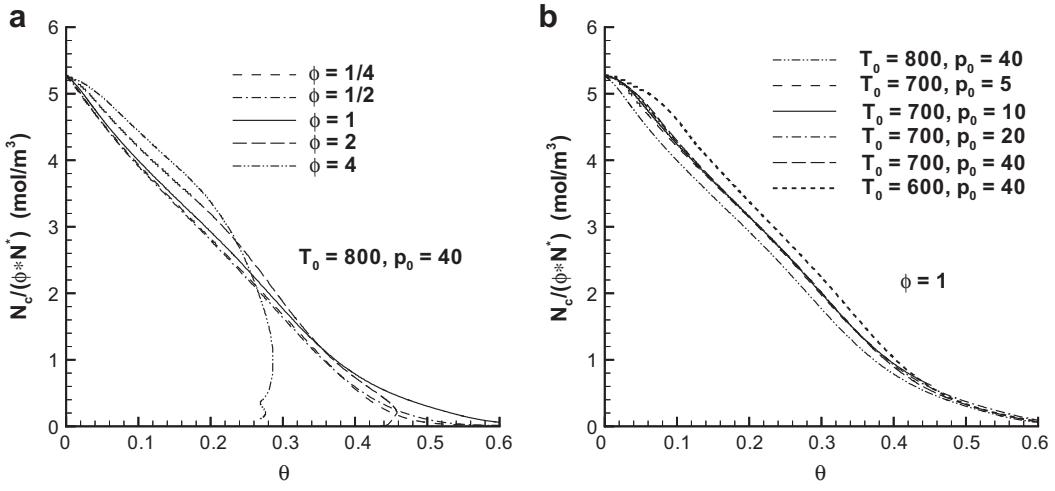

Fig. 1. Similarity plots of parameter $N_c/(\phi \times N^*)$ versus θ for iso-octane oxidation in the cold ignition regime at (a) $T_0 = 800$ K, $p_0 = 40$ bar and (b) $\phi = 1$ (T_0 is in K and p_0 is in bar) using the LLNL full mechanism in conjunction with CHEMKIN II.

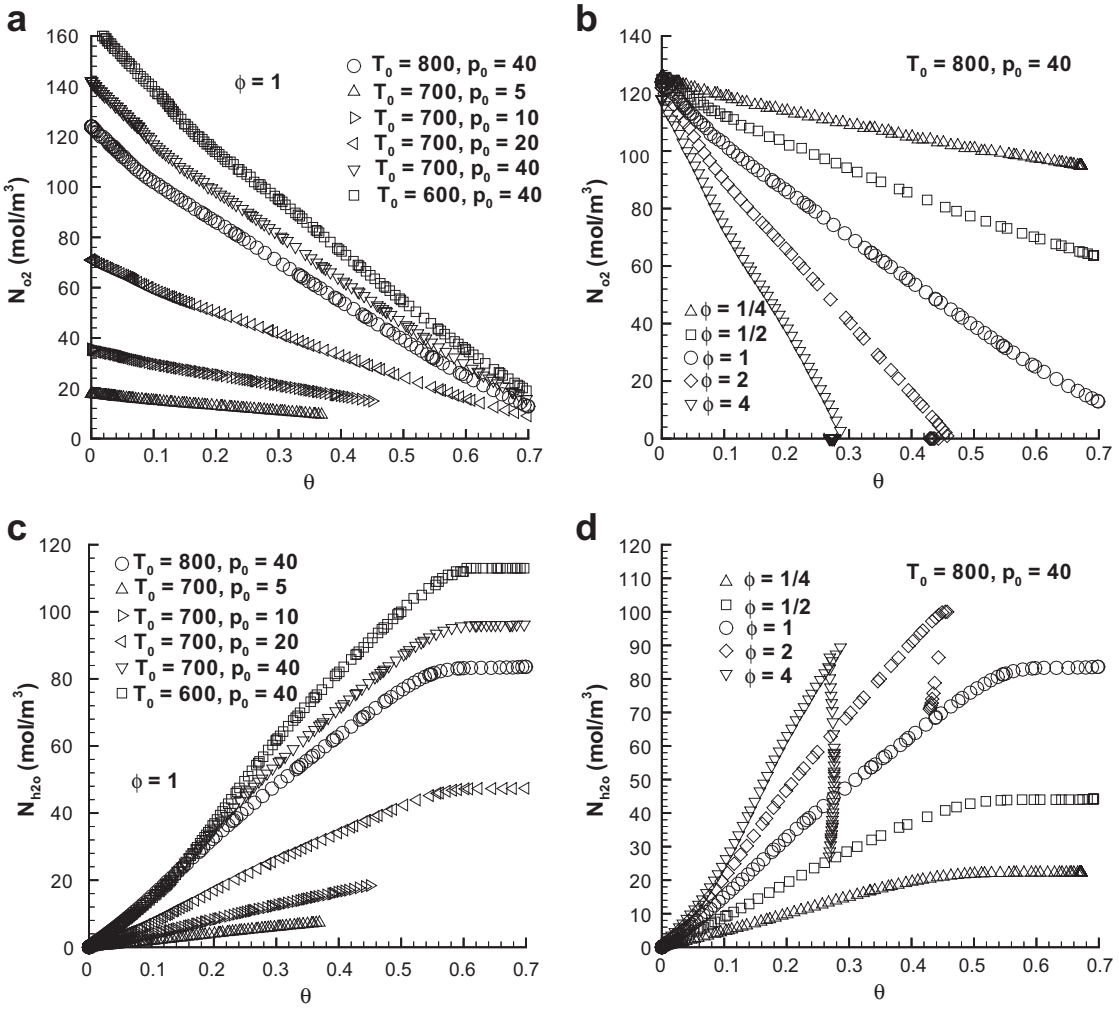

Fig. 2. Oxygen and water molar densities versus θ for iso-octane oxidation in the cold ignition regime as extracted from the LLNL full mechanism in conjunction with CHEMKIN II. T_0 is in K and p_0 is in bar.

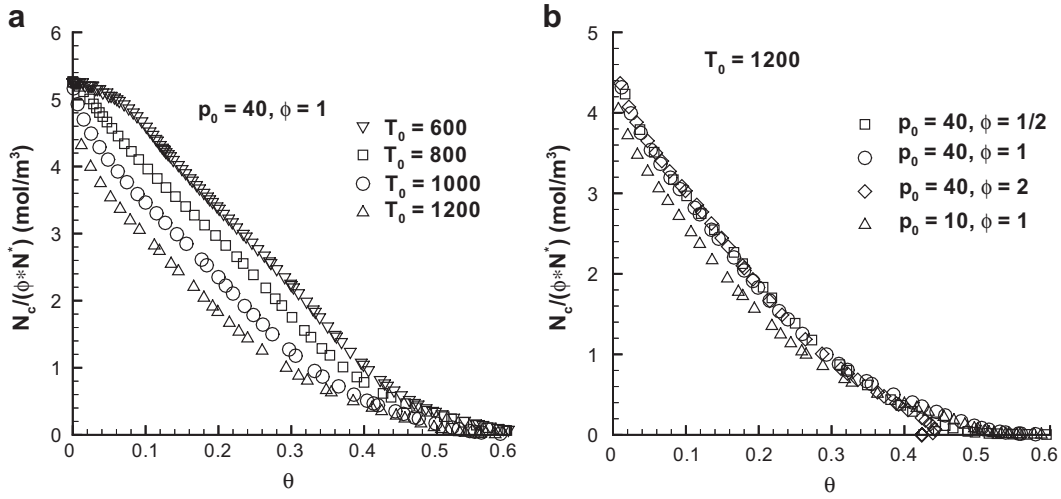

Fig. 3. Similarity plots of parameter $N_c/(\phi \times N^*)$ versus θ for iso-octane oxidation at higher than cold ignition T_0: (a) p_0 = 40 bar, ϕ = 1 and (b) T_0 = 1200 K using the LLNL full mechanism in conjunction with CHEMKIN II. T_0 is in K and p_0 is in bar.

(50% iso-octane)/(50% *n*-heptane), the self-similarity holds very well over the entire range of θ, except for very rich mixtures for which as θ increases there is a departure from the typical behavior since the reaction is incomplete; this departure occurs at smaller θ with increased ϕ. Moreover, in Fig. 5 is an example of self-similarity at higher T_0 for the (90% iso-octane)/(10% *n*-heptane) mixture, showing that the behavior identified for iso-octane holds well for PRFs.

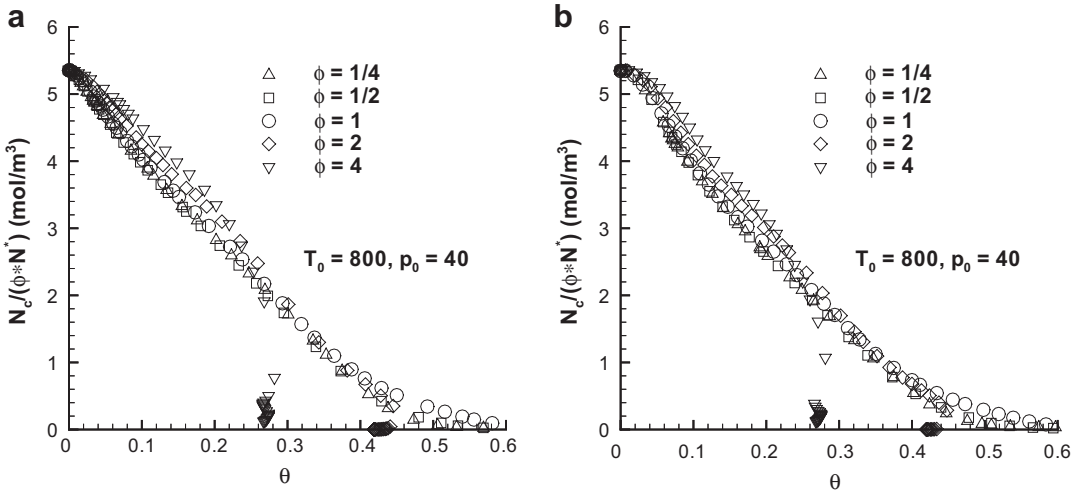

Fig. 4. Similarity plots of parameter $N_c/(\phi \times N^*)$ versus θ at $T_0 = 800$ K and $p_0 = 40$ bar for a range of ϕ values: (a) for (90% iso-octane)/(10% *n*-heptane) oxidation and (b) for (50% iso-octane)/(50% *n*-heptane) oxidation. Results extracted from the LLNL full mechanism in conjunction with CHEMKIN II.

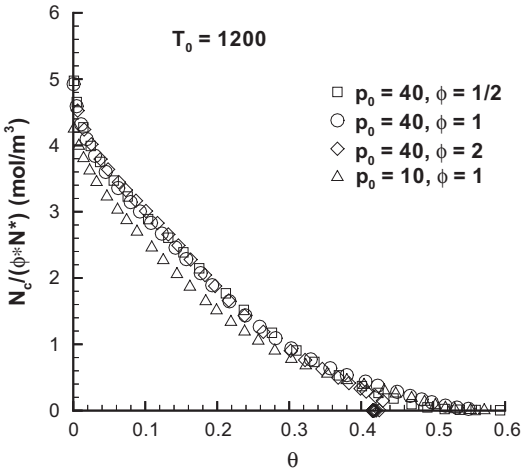

Fig. 5. Example of similarity plot for $N_c/(\phi \times N^*)$ versus θ for (90% iso-octane)/(10% *n*-heptane) at $T_0 = 1200$ K for various p_0 (in bar) and ϕ values. The results are obtained using the LLNL full mechanism in conjunction with CHEMKIN II.

2.2.4. Mixtures of iso-octane and n-pentane or iso-hexane

Mixtures of iso-octane and *n*-pentane or iso-hexane display the same behavior as iso-octane and PRFs. In the interest of brevity, the corresponding plots are not shown, but the predictive capability of the model for such mixtures is addressed in Section 3.3.

3. Results

The extension of the conceptual model to higher T_0 values than for cold ignition, showing now a families of similarity curves according to T_0, leads to making the choice between either correspondingly extending the functional fits of [11] to encompass this new T_0 regime or using the ideal model provided by the LLNL full mechanism in the form of tabular input for the conceptual model. We chose the second option both as a shortcut to investing additional time in functional fitting and as a necessarily more accurate alternative to the fits. The ideal model is read only once in the code, at the beginning of the computation, and is in tabular form; during the computation, instead of accessing a function as was done in [11], one accesses a table. The functions needed for the reduced model are calculated by cubic interpolation in T from the tables, each obtained at fixed (T_0, ϕ, N^*).

The listed tabular information consists of numbers for T, N_c, quasi-steady light mole fractions X_i, $C_{p,h}$ as defined by Eq. (9), $K_{net,i}$ and K_h, all computed from the LLNL full mechanism [12] in conjunction with CHEMKIN II. The tables are obtained for fixed values of (T_0, ϕ, N^*, T) with specified increments in T. Particular attention was devoted to T value increments in the $T \leqslant T_0 + 5$ K regime since T may decrease a few K (especially for rich mixtures) during the initial time when heavy species pyrolysis occurs, and since the reaction spends a relatively long time in this T regime. The first entry for any table is a t-averaged value over an interval up to the t value corresponding to $\theta \simeq 2 \times 10^{-6}$. Further table entries in this $T \leqslant T_0 + 5$ K regime involve two nested criteria to determine the T frequency of the entries. In a first step, table values were generated for T with the goal of computing a table entry when $(T - T_0)$ is close to 0.1, 0.2, 0.3, 0.5, 1.0, and 2.5 K. For each output T, as one marches in t during the full model calculations, the corresponding θ value was calculated and the second criterion was based on the difference between the θ value corresponding to this T and the value of θ corresponding to the previous table value of T. At each occurrence when this difference had a value equal or larger than 10^{-4}, an additional table entry was generated for $(T - T_0) \leqslant 5$ K. However, once $(T - T_0) \simeq 2.5$ K was reached, only the criterion based on the difference between θ values was used until $(T - T_0) \simeq 5$ K was reached. After $(T - T_0) \simeq 5$ K, tables were produced at 5 K increments. The most frequent table entries in the $T \leqslant T_0 + 5$ K regime were required for either larger T_0 values or lean mixtures.

The reduced model computations use the LLNL specified thermodynamic properties for the light species. The species progress variables are the eleven unsteady light species H_2O, CO_2, O_2, H, CO, H_2, CH_4, H_2O_2, C_2H_2, C_2H_4, CH_2O.

Comparisons are presented below between the reduced model predictions and those of the LLNL full mechanism [12] in conjunction with CHEMKIN II. The full model was exercised on a single processor of a supercomputer which had a speed 100 times faster than that of a personal computer on which the reduced model was run. Despite the speed advantage, the full model still required run times which were one to two orders of magnitude larger than the reduced model.

Results are presented here from three perspectives: the recovery by the reduced model of the molar density of important

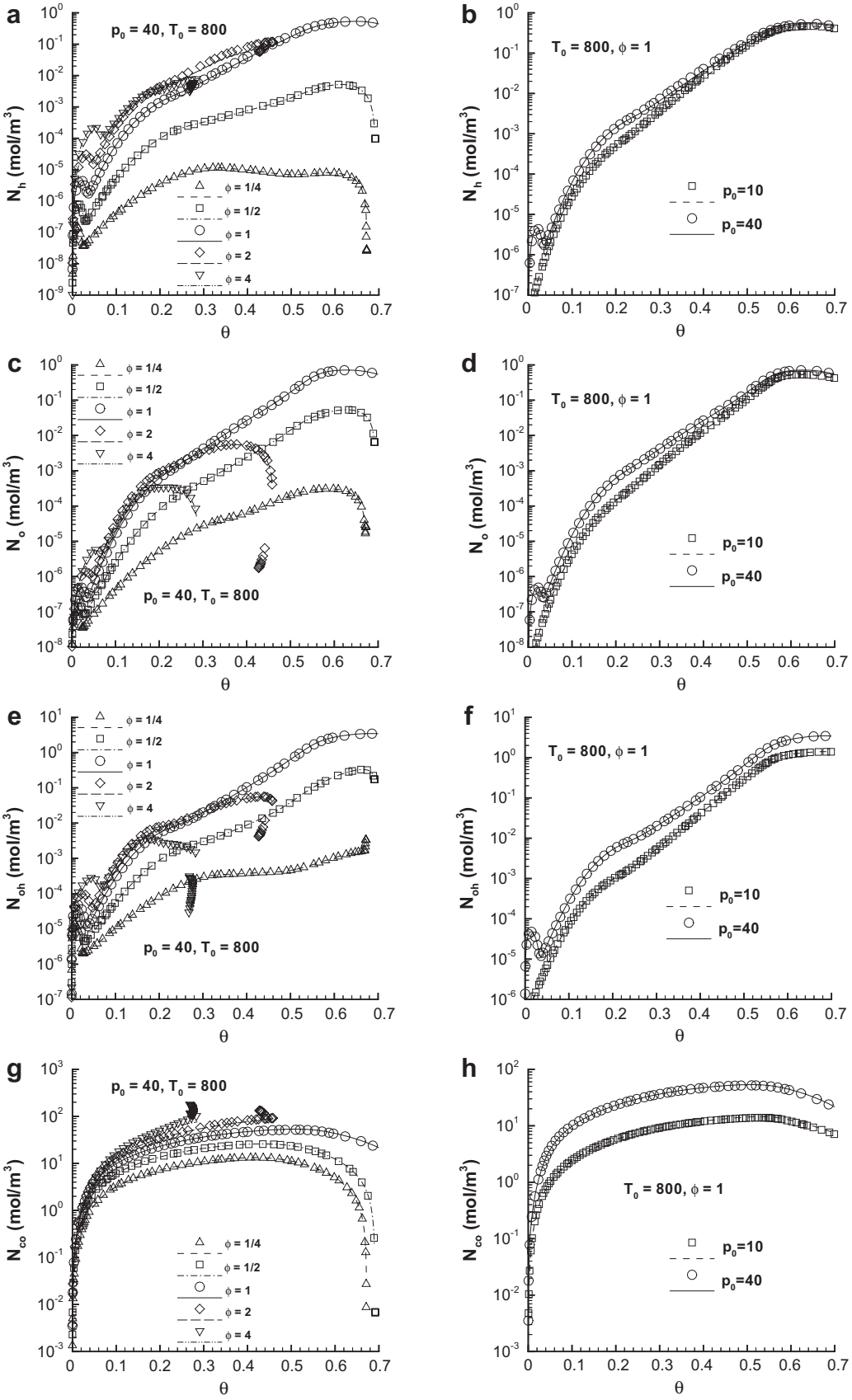

Fig. 6. Molar density of (a and b) H, (c and d) O, (e and f) OH and (g and h) CO versus θ for iso-octane oxidation. (a,c,e,g) T_0 = 800 K, p_0 = 40 bar at various ϕ values and (b,d,f,h) T_0 = 800 K, ϕ = 1 at two p_0 values. Symbols represent selected data from the LLNL runs; lines represent the corresponding reduced model predictions. T_0 is in K and p_0 is in bar.

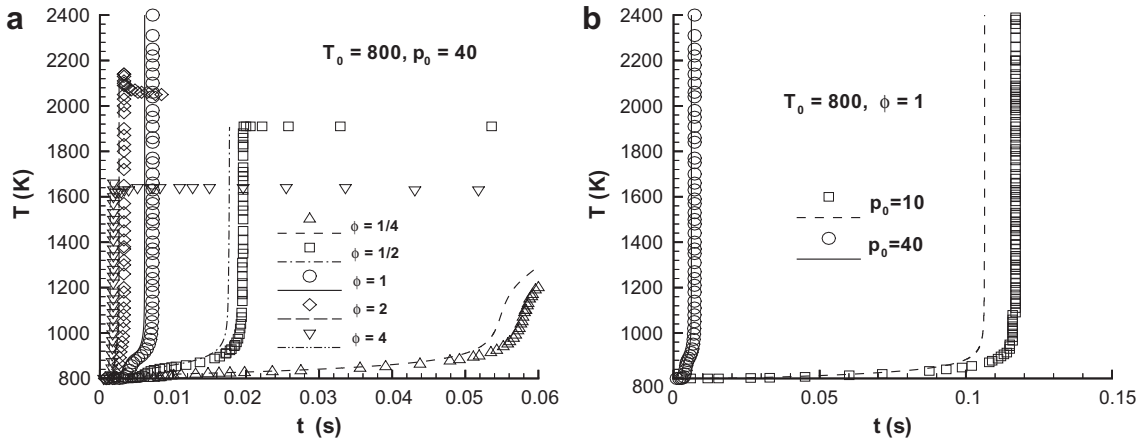

Fig. 7. $T(t)$ for iso-octane oxidation as predicted by the reduced model (lines) compared to the LLNL full mechanism using CHEMKIN II (symbols) for a variety of conditions. T_0 is in K and p_0 is in bar.

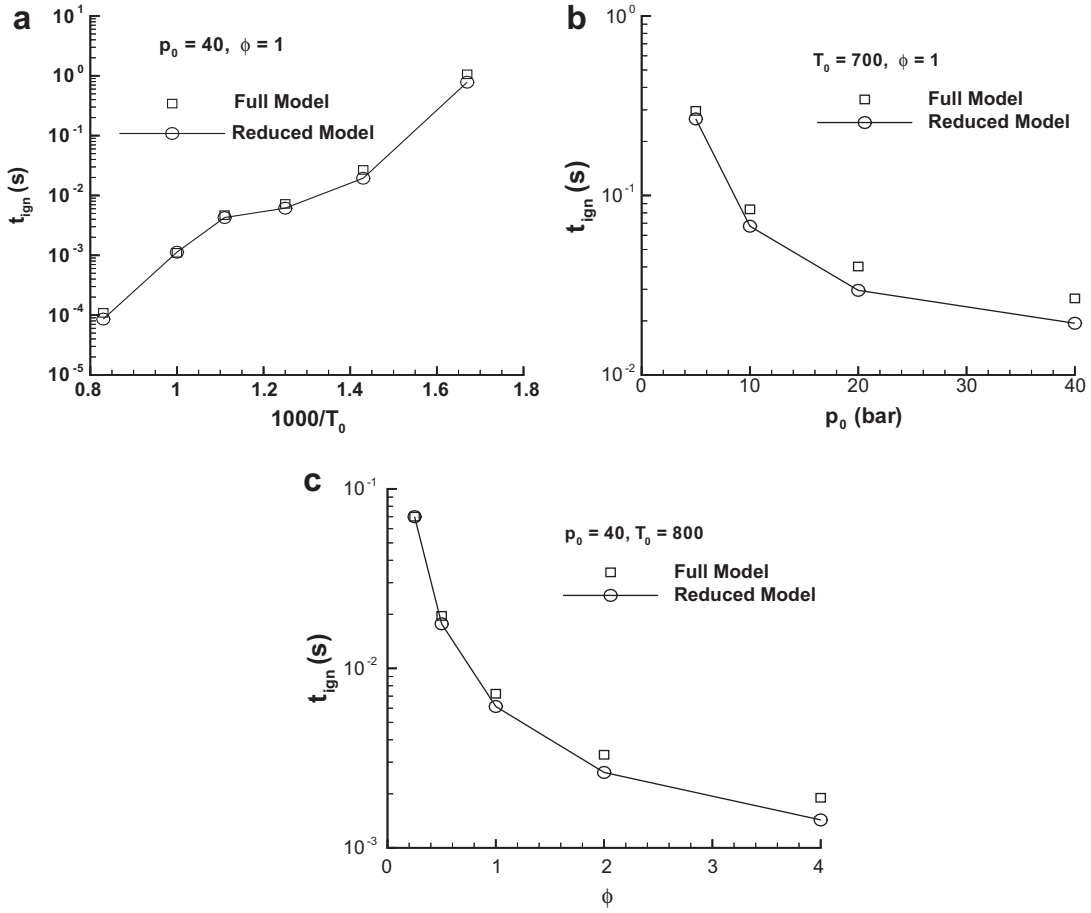

Fig. 8. t_{ign} for iso-octane oxidation as function of T_0, p_0 and ϕ. Where not indicated on the plots, T_0 is in K and p_0 is in bar.

species, the reproduction of $T(t)$, and the prediction of the ignition time, t_{ign}.

3.1. Iso-octane

In Fig. 6 are displayed the molar densities of H, O, OH and CO as a representative sample of the results. H and O are highly reactive radicals, OH is generally used to indicate the location of the flame, and CO is a major product of incomplete combustion. The results are generally excellent over the wide range of $\phi = [1/4, 4]$ (Fig. 6a, c, e and g) and the model even captures the turnover of the curves at large θ when the reaction is nearly completed. In the rich range, the model also captures the turnover of the curves for the incomplete reaction, but any multivalued aspect, if it occurs, is not reproduced. Such lack of complete fidelity is unavoidable in reduced models, as information is discarded in the reduction process. The reduced model is also very successful over the range of p_0 investigated, as can be seen in Fig. 6b, d, f and h.

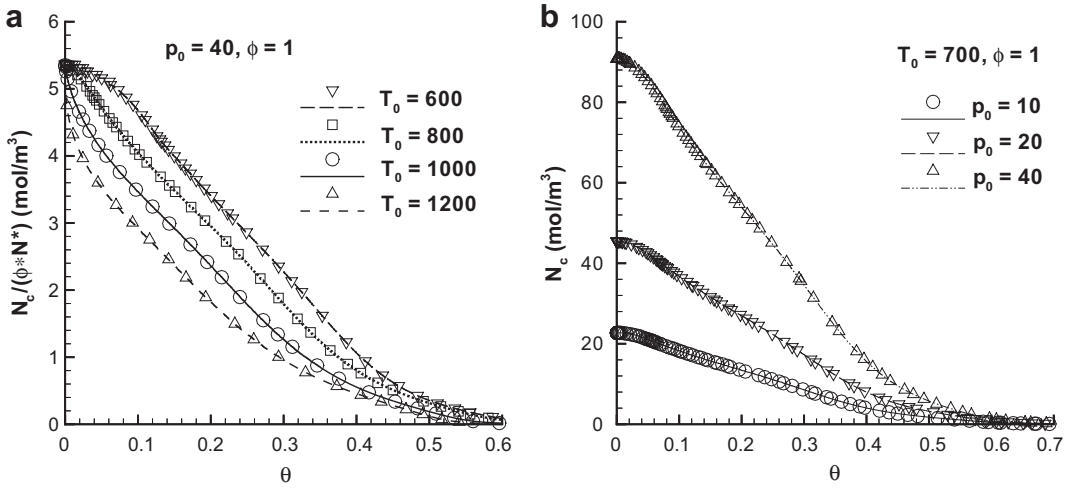

Fig. 9. Recovery by the reduced mechanism (lines) for (90% iso-octane/10% *n*-heptane) of: (a) $N_c/(\phi \times N^*)$ versus θ for $p_0 = 40$ bar, $\phi = 1$ and (b) N_c versus θ for $T_0 = 700$ K, $\phi = 1$. Comparisons are made with the LLNL full mechanism in conjunction with CHEMKIN II (symbols). T_0 is in K and p_0 is in bar.

The prediction of $T(t)$ is illustrated in Fig. 7 for the same conditions as those in Fig. 6. The temperature evolution and the maximum achieved are very well predicted by the reduced model over the entire range of ϕ values (Fig. 7a). A slight exception is the T drop in the rich regime after the maximum T achieved, which is directly connected to the uncaptured multivalued aspect with respect to θ discussed in conjunction with Fig. 6. The decrease of T at the end of rich combustion is due to thermal energy loss resulting from continued heavy species reactions which are not captured by the reduction concept; since this occurs at the end of combustion, it is expected that prediction of t_{ign} values will not be affected by the disparity. For the leanest case studied, the final T is slightly overpredicted and t_{ign} is slightly underpredicted.

Finally, the t_{ign} prediction is shown in Fig. 8 for a wide range of T_0, p_0 and ϕ. In all cases, the quantitative aspect of the prediction ranges from very good to excellent, indicating that the slight underpredictions observed in Fig. 7 are indeed minor. In particular, the Negative Temperature Coefficient (NTC) region is excellently captured, and the ratio of the predicted value by the reduced model to that from the full model is within percentages rather than multiplying factors.

3.2. Iso-octane/n-heptane mixtures

To highlight the flexibility of the model in computing kinetics for PRFs, we present here detailed results for two PRF mixtures of very different compositions.

3.2.1. Ninety percent iso-octane/ten percent n-heptane

Figure 9 displays comparisons between the reduced and full models over a wide range of T_0 and p_0 values. For all runs the predictions of the reduced and full models coincide. Of note is the $N_c/(\phi \times N^*)$ versus θ behavior according to families of T_0 (Fig. 9a) and the lack of self-similarity of N_c alone versus θ (Fig. 9b); indeed, only the normalization $N_c/(\phi \times N^*)$ leads to self-similarity versus θ. To highlight the capabilities of the reduced model, illustrated in Fig. 10 are the molar densities of O_2 and H_2O over a wide parametric range. In all cases with the exception of the very rich cases, N_{o2} and N_{h2o} are excellently predicted. Even for the very rich cases, the prediction is still very good and the model captures the turnover in the curves, however, the multivalued aspect is missed, just as for iso-octane, a fact which is again traced (see below) to the incapability of the kinetic reduction to reproduce the decreased T at the end of combustion. The N_{co} results shown in Fig. 11 emulate those for N_{o2} and N_{h2o} in that the results are excellent with the exception of the very rich cases for which they are still very good. Finally, a sample of the N_o and N_{oh} predictions is exhibited in Fig. 12 showing again the high fidelity of the predictions.

In Fig. 13a and c the temporal variation of T is shown from our reduced model for the (90% iso-octane)/(10% *n*-heptane) mixture oxidation and compared to the full model results. Similarly to the iso-octane results, the ultimate value of T is excellently predicted, but there is an underprediction of t_{ign} that increases with decreasing p_0; that is to say that the best predictions are at high pressure which is the regime of choice for the operation of diesel, gas turbine and HCCI engines. As stated above, for the very rich cases, the temperature decrease at the end of combustion is not captured, which explains the lack of complete accuracy in predicting the molar densities in that regime. Finally, t_{ign} is illustrated for this PRF mixture in Fig. 14a, c and e over a range of $T_0 \in [600,1200]$ K (the plots are versus $1000/T_0$ to emulate similar plots for other reduced kinetics in the literature), $p_0 \in [10,50]$ bar and $\phi = [1/4,4]$. The general observations are that the predictions as a function of T_0 are excellent and capture with high fidelity the NTC region, and those versus p_0 and ϕ are excellent for high p_0 and stoichiometric and lean mixtures. A slight deterioration is observed for small p_0 and large ϕ, but even in those cases the ratio of the prediction by the reduced model to that by the full model is only within percentages. Moreover, the results versus p_0 are plotted using a regular rather than logarithmic axis, and thus indeed the deviation from the full model predictions is very small.

3.2.2. Fifty percent iso-octane/fifty percent n-heptane

The results for the (50% iso-octane)/(50% *n*-heptane) mixture are similar to those for the (90% iso-octane)/(10% *n*-heptane) mixture, and thus we only show some examples to document the reduced model capabilities. Presented in Fig. 15 are N_{o2} and N_{h2o}; displayed in Fig. 16 are the molar densities of the two radicals O and H and the light species H_2; exhibited in Fig. 17 are the molar densities for the flame indicator radical OH and the product of incomplete combustion CO. All evaluations for the (90% iso-octane)/(10% *n*-heptane) mixture remain valid for the (50% iso-octane)/(50% *n*-heptane) mixture.

For comparison with the (90% iso-octane)/(10% *n*-heptane) mixture, $T(t)$ is plotted in Fig. 13b and d and t_{ign} in Fig. 14b, d and f. Compared to the predictions for (90% iso-octane)/(10% *n*-heptane),

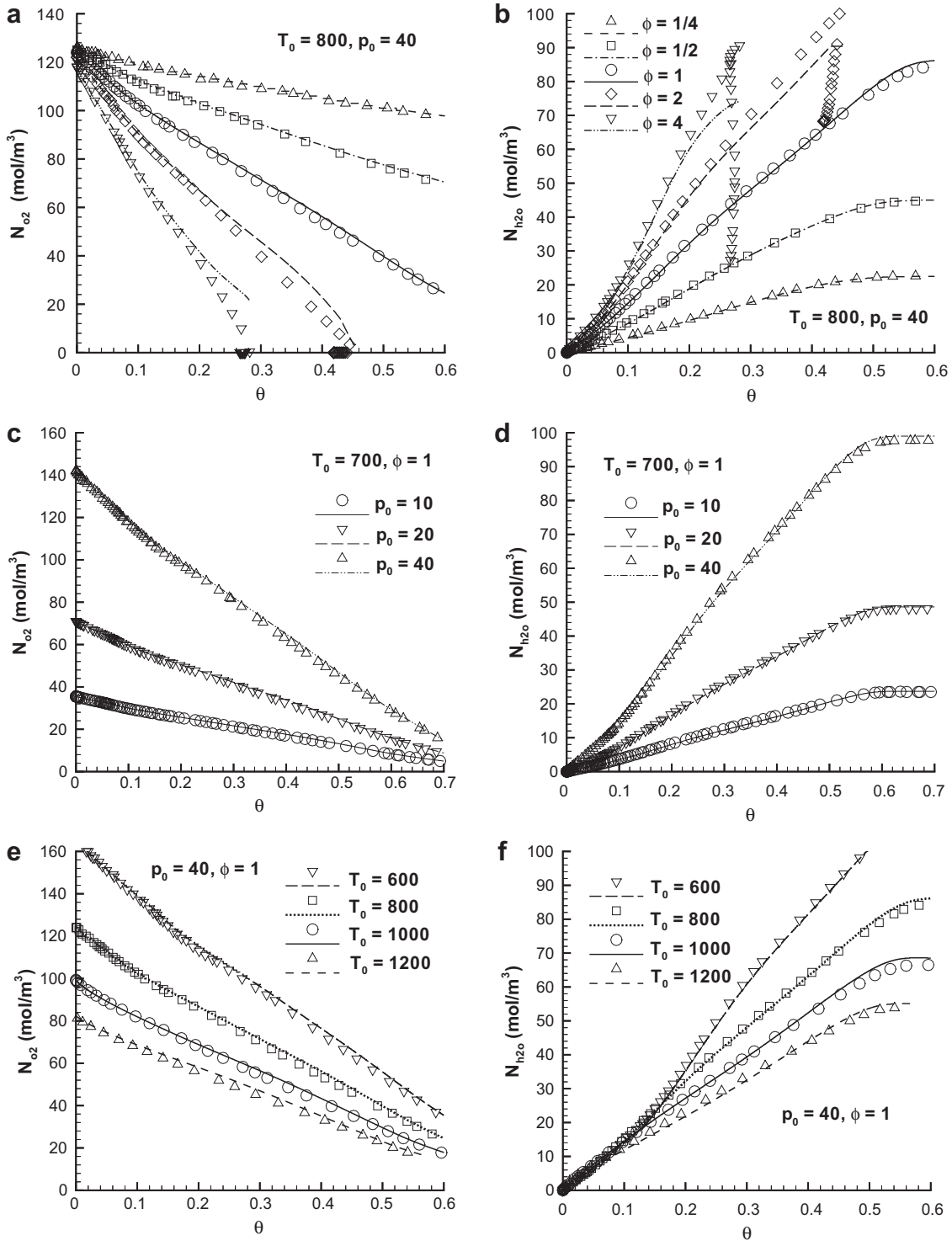

Fig. 10. Comparisons between reduced mechanism predictions (lines) for (90% iso-octane/10% *n*-heptane) and corresponding LLNL full mechanism using CHEMKIN II (symbols) for the molar densities of (a,c,e) O_2 and (b, d, f) H_2O for a variety of conditions. Figure (a) has the same legend as figure (b). T_0 is in K and p_0 is in bar.

those for (50% iso-octane)/(50% *n*-heptane) are somewhat less favorable in the cold ignition regime and also versus the entire range of p_0, although they are still very good; the same quality as for the (90% iso-octane)/(10% *n*-heptane) mixture is maintained versus ϕ.

As a last test, t_{ign} is plotted in Fig. 14g versus the mole fraction of iso-octane in the fuel, X_{oct}, on a regular (rather than logarithmic) axis and the predictions become better with decreasing X_{oct}, although even for $X_{oct} = 1$ they are still very good.

3.3. Iso-octane/n-pentane and iso-octane/iso-hexane mixtures

Since species and temperature predictions are less sensitive to modeling errors than ignition times, for brevity, we only focus here on t_{ign} since any inaccuracies in the model are magnified when predicting this quantity. In Table 1 are listed, as an example, ignition times for iso-octane/*n*-pentane and iso-octane/iso-hexane mixtures obtained with the reduced model and with the LLNL full mechanism with CHEMKIN II; for comparison, the corresponding

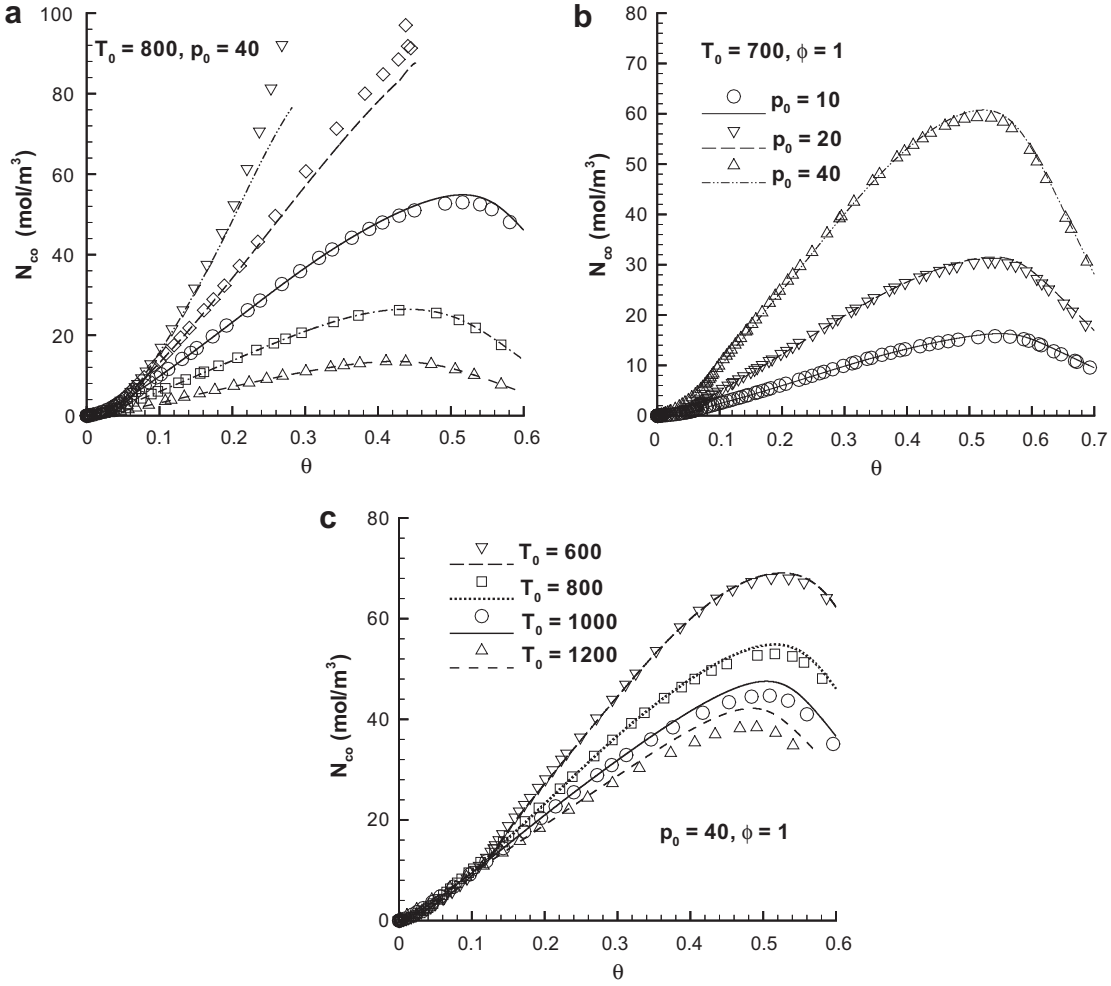

Fig. 11. Predictions of the reduced mechanism (lines) compared to the LLNL full mechanism using CHEMKIN II (symbols) for the (90% iso-octane/10% *n*-heptane) mixture showing the molar density of N_{co} versus θ at various conditions. The legend for figure a is: ▽ and — · · — $\phi = 4$; ◇ and — — $\phi = 2$; ○ and —— $\phi = 1$; □ and — · — $\phi = 1/2$; △ and – – – $\phi = 1/4$. T_0 is in K and p_0 is in bar.

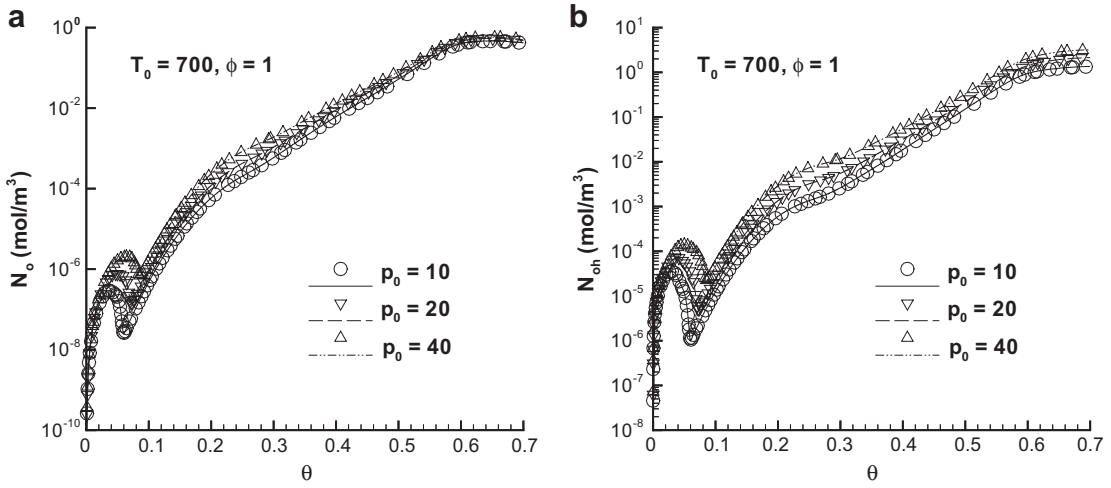

Fig. 12. Predictions of the molar density for radicals O and OH by the reduced mechanism (lines) for (90% iso-octane/10% *n*-heptane) compared to the corresponding LLNL full mechanism in conjunction with CHEMKIN II (symbols). Selected conditions. T_0 is in K, p_0 is in bar.

iso-octane case is listed as well. Clearly, the predictions of the reduced model are within approximately 20% or better with respect to those of the full model. This performance is typical of the suite of results.

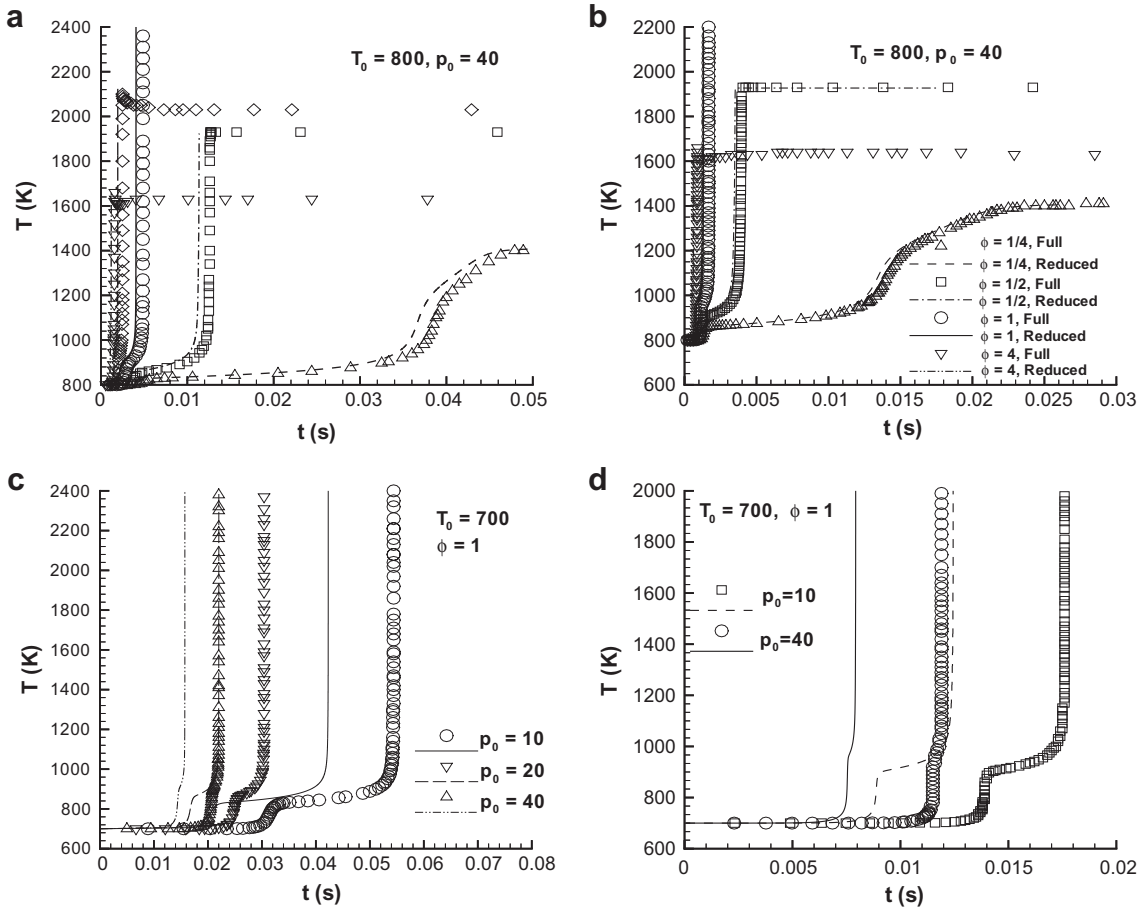

Fig. 13. $T(t)$ for PRF fuels: (a and c) (90% iso-octane)/(10% *n*-heptane) and (b and d) (50% iso-octane)/(50% *n*-heptane) at various conditions. Predictions of the reduced model compared those of the LLNL mechanism used with CHEMKIN II. Figure (a) has the same legend as figure (b). T_0 is in K and p_0 is in bar.

4. Summary and conclusions

A model previously developed for reducing *n*-heptane oxidation kinetics has been here slightly modified to address the oxidation of iso-octane, Primary Reference Fuels (PRFs) and iso-octane mixtures with *n*-pentane and iso-hexane. The conceptual model was based on the identification of constituents as the building blocks of the heavy species and on reducing the species progress variables to following the total constituent molar density and the molar densities of the unsteady light species. A normalized surrogate temperature variable had been defined for which a scaled total constituent molar density exhibited a self-similar behavior for initial temperatures in the cold ignition regime and for a wide range of initial pressures and equivalence ratios; also the molar densities of O_2 and H_2O exhibited a quasi-linear behavior versus the normalized variable. For *n*-heptane, mathematical fits versus the normalized surrogate temperature variable were required in a four-dimensional space to solve the equations and obtain the species and temperature evolution. On going from the previous study of *n*-heptane to the present study of iso-octane and its mixtures, examination of the LLNL full mechanisms using CHEMKIN II showed that the constituent list was augmented by one additional entity, but the molar density of this total constituent remained self-similar versus the previously defined normalized surrogate temperature variable for initial temperature values in the cold ignition regime, and for the wide range of initial pressures and equivalence ratios previously examined. When the higher than cold ignition temperature regime was explored, a family of self-similar curves versus the normalized surrogate temperature variable was obtained according to the initial temperature. The molar densities of O_2 and H_2O remained quasi-linear versus the normalized surrogate temperature variable.

Based on these observations, it was concluded that the effort of extending the mathematical fits developed for *n*-heptane was not warranted, and instead an ideal model in tabular form was used, as extracted from the LLNL full mechanisms using CHEMKIN II and our concept. This tabular information is read into the code only once, at the beginning of the computation, and is accessed similarly to the mathematical fits for *n*-heptane. There are eleven species progress variables, as the molar densities of O_2 and H_2O which were obtained for *n*-heptane using fits for their slopes, are now computed in an unsteady way utilizing the ideal model.

Results were presented from computations using the reduced model for the oxidation of iso-octane, of two different PRF fuels, and of mixtures of iso-octane and *n*-pentane or iso-hexane. These results were compared to the corresponding information extracted from the LLNL full mechanisms using CHEMKIN II. The comparisons were performed for initial temperatures in the [600,1200] K range, initial pressures in the [5,50] bar regime and equivalence ratios encompassing mixtures with air as rich as $\phi = 4$ and as lean as $\phi = 1/4$. The capability of the model was assessed from the viewpoints of predicting species, the temperature evolution and the ignition time. The species prediction was excellent in all cases, with the exception of the multivalued regions occurring for very rich situations. The temperature values were correspondingly excellently to very well predicted, except for the temperature decrease from the maximum observed for rich mixtures. Finally,

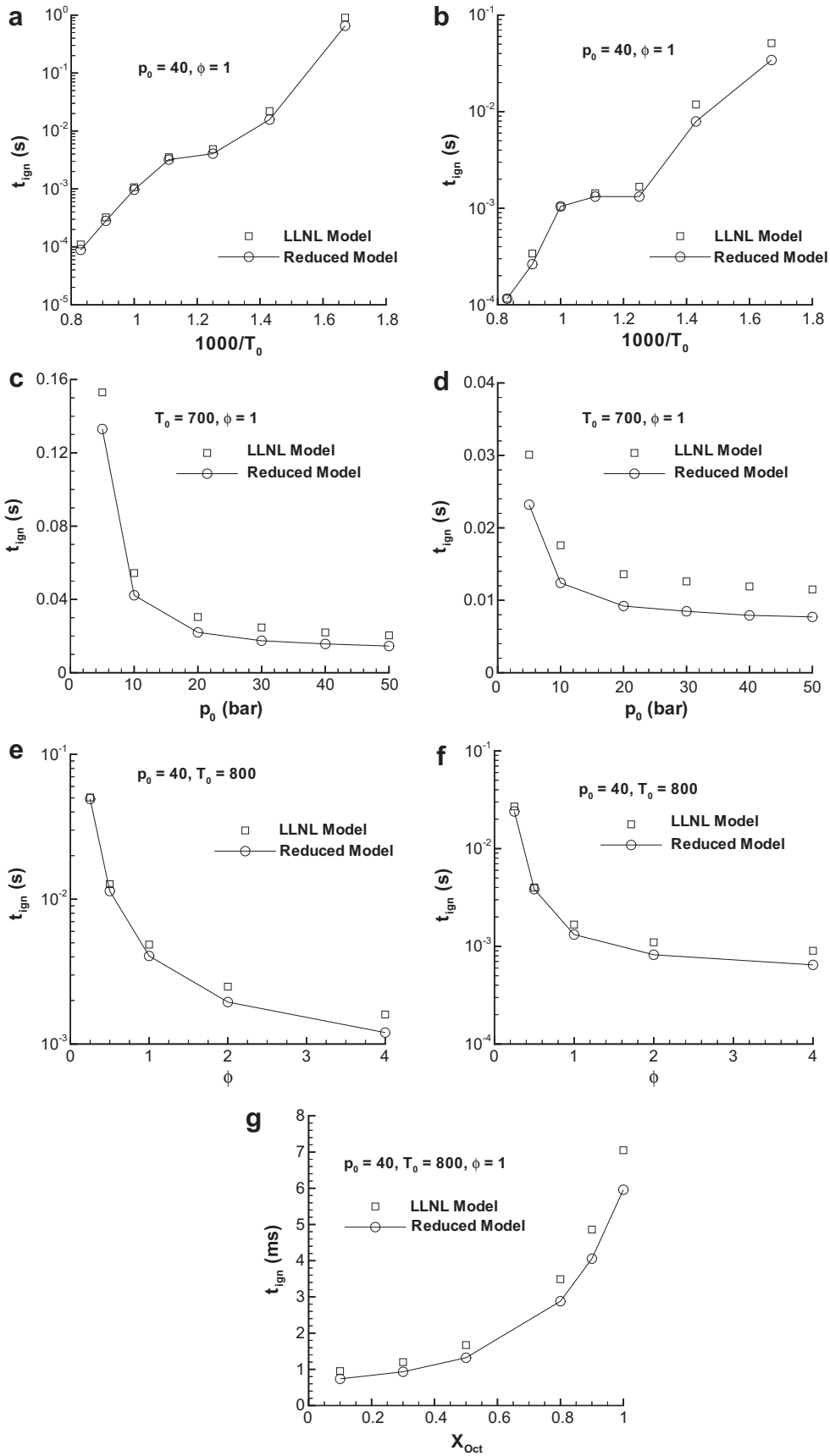

Fig. 14. t_{ign} for PRF fuels: (a,c,e) (90% iso-octane)/(10% *n*-heptane) and (b,d,f) (50% iso-octane)/(50% *n*-heptane) versus $1000/T_0$, p_0 and ϕ; (g) versus the mole fraction of iso-octane in the fuel, X_{oct}. Where not indicated on the plots, T_0 is in K and p_0 is in bar. Comparisons are made between predictions of the reduced model and those of the LLNL mechanism used with CHEMKIN II.

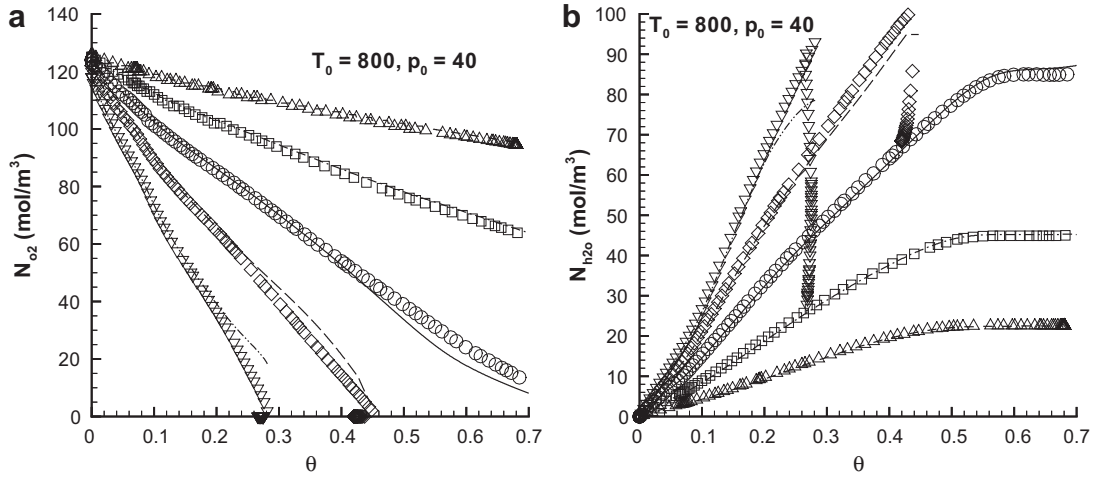

Fig. 15. Molar density of (a) O_2 and (b) H_2O for (50% iso-octane)/(50% *n*-heptane) obtained from the reduced model (lines) and the LLNL mechanism using CHEMKIN II (symbols): ▽ and — · · — $\phi = 4$; ◇ and — — $\phi = 2$; ○ and —— $\phi = 1$; □ and — · — $\phi = 1/2$; △ and – – – $\phi = 1/4$. T_0 is in K and p_0 is in bar.

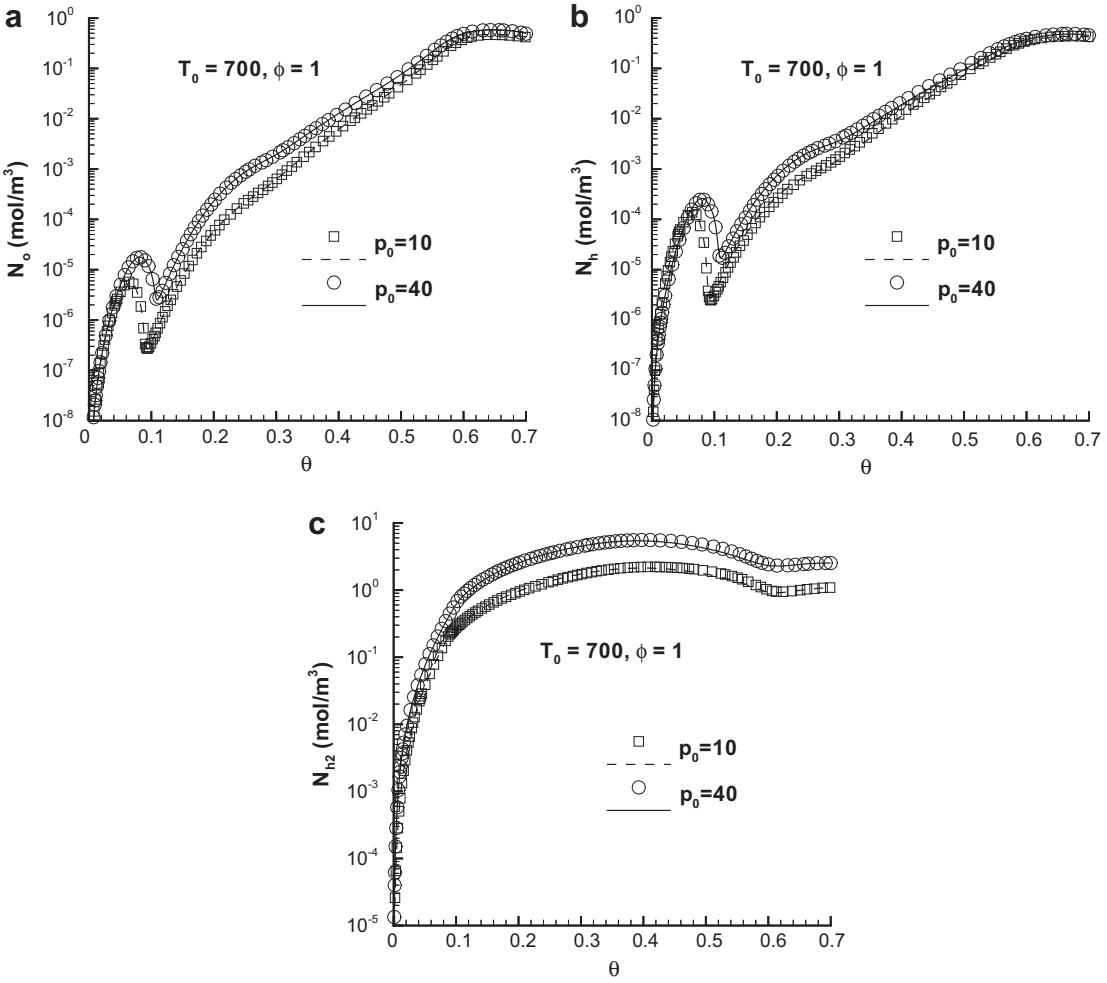

Fig. 16. Predictions of the molar density of (a) O, (b) H and (c) H_2 for (50% iso-octane)/(50% *n*-heptane) from the reduced model (lines) and the LLNL mechanism used with CHEMKIN II (symbols) for selected conditions. T_0 is in K and p_0 is in bar.

the ignition times were reproduced within percentages of those computed with the full mechanism.

The favorable predictive aspect of our model should be contrasted with its relative simplicity, as it has a specified form which is not dynamically changed during the computation and only requires solutions of eleven species progress variables, all of which are light species; the model has much increased range of ϕ validity with respect to other reduced models with a small number of

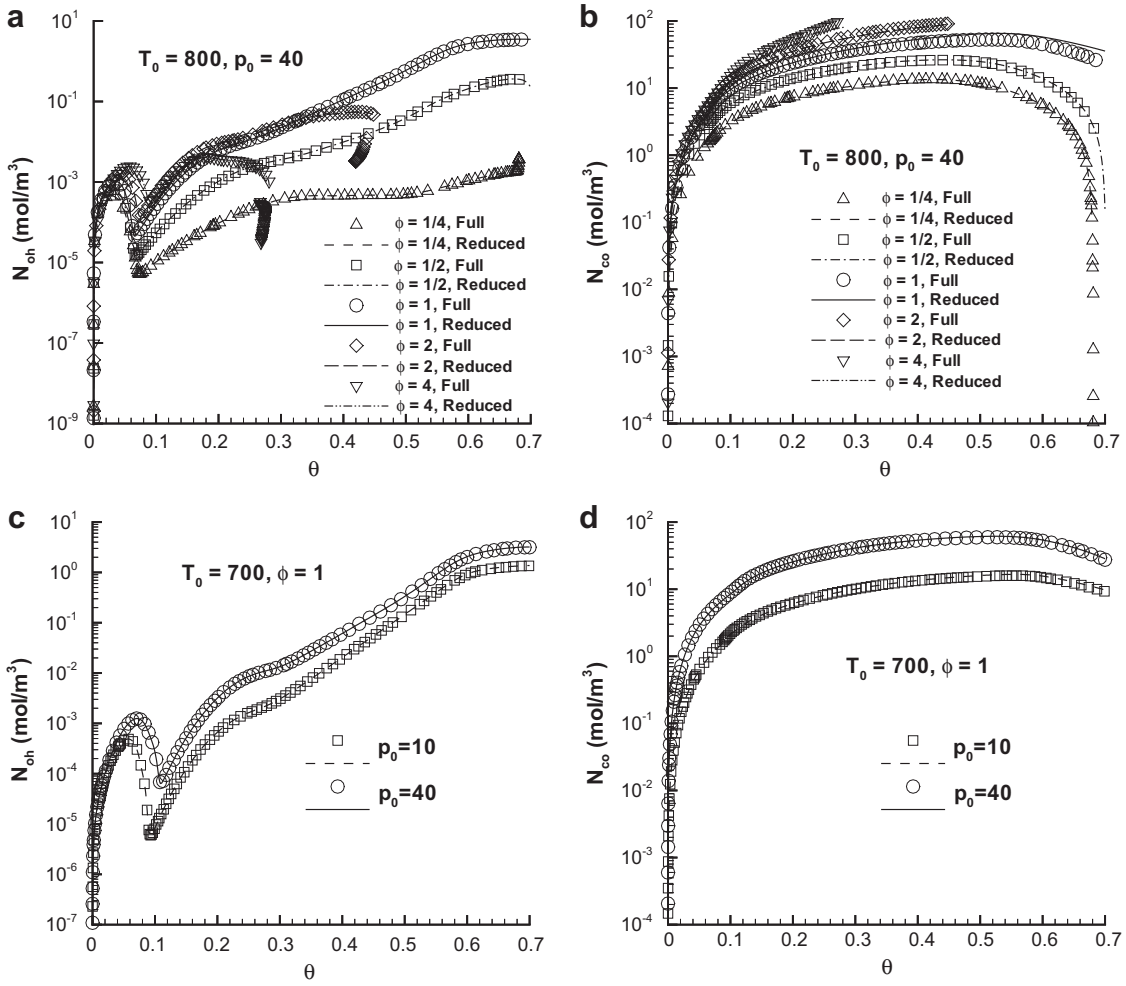

Fig. 17. Predictions of the molar density of (a and c) OH and (b and d) CO for (50% iso-octane/50% *n*-heptane) by the reduced model (lines) and the corresponding LLNL full mechanism used with CHEMKIN II (symbols) at various conditions. T_0 is in K and p_0 is in bar.

Table 1
Ignition times for oxidation of iso-octane and iso-octane/*n*-pentane or iso-octane/iso-hexane mixtures. Comparisons between the LLNL full mechanism used with CHEMKIN II and our reduced model. T_0 = 800 K, p_0 = 40 bar and ϕ = 1.

Fuel composition	LLNL t_{ign} (s)	Reduced model t_{ign} (s)	t_{ign} ratio $(\frac{\text{reduced}}{\text{LLNL}})$
Iso-octane	7.22×10^{-3}	6.13×10^{-3}	0.85
95% iso-octane/5% *n*-pentane	6.60×10^{-3}	5.56×10^{-3}	0.84
90% iso-octane/10% *n*-pentane	6.00×10^{-3}	5.04×10^{-3}	0.84
50% iso-octane/50% *n*-pentane	2.73×10^{-3}	2.19×10^{-3}	0.80
20% iso-octane/80% *n*-pentane	1.80×10^{-3}	1.40×10^{-3}	0.78
90% iso-octane/10% iso-hexane	5.80×10^{-3}	4.88×10^{-3}	0.84
50% iso-octane/50% iso-hexane	3.19×10^{-3}	2.69×10^{-3}	0.84

species [15,16]. The advantage of such a simple model becomes increasingly significant with increasing carbon atoms of the fuel because of the proliferation of relatively heavy species with increasing carbon number; for example, the skeletal mechanism for *n*-heptane was based on 160 species and 1540 reactions, whereas the full iso-octane mechanism has 857 species and 3606 reactions. If the model can be extended to even heavier species, such as *n*-nonane (*n*-C_9H_{20}), *n*-decane (*n*-$C_{10}H_{22}$), *n*-dodecane (*n*-$C_{12}H_{26}$), *n*-tetradecane (*n*-$C_{14}H_{30}$) and *n*-hexadecane (*n*-$C_{16}H_{34}$), it would be very advantageous for performing computations for heavy fuels.

Acknowledgments

This study was conducted at the California Institute of Technology, Jet Propulsion Laboratory (JPL), and was sponsored by the Army Research Office, with Dr. Ralph Anthenien as Program Manager. Computation with the full kinetic mechanisms were performed using the JPL Supercomputing facility.

References

[1] U.C. Müeller, N. Peters, A. Liñan, Proc. Combust. Inst. 24 (1992) 777–784.
[2] M. Bollig, H. Pitsch, J.C. Hewson, K. Sheshadri, Proc. Combust. Inst. 26 (1997) 729–737.
[3] C.J. Sung, C.K. Law, J.-Y. Chen, Proc. Combust. Inst. 27 (1998) 295–304.
[4] S.C. Li, B. Varatharajan, F.A. Williams, AIAA J. 39 (12) (2001) 2351–2356.
[5] J.B. Bell, N.J. Brown, M.S. Day, M. Frenklach, J.F. Grcar, R.M. Propp, S.R. Tonse, Proc. Combust. Inst. 28 (2000) 107–113.
[6] S.B. Pope, Combust. Theory Model. 1 (1997) 41–63.
[7] U. Maas, S.B. Pope, Combust. Flame 88 (3–4) (1992) 239–264.
[8] A. Mitsos, G.M. Oxberry, P.I. Barton, W.H. Green, Combust. Flame 155 (2008) 118–132.
[9] O.O. Oluwole, B. Bhattacharjee, J.E. Tolsma, P.I. Barton, W.H. Green, Combust. Flame 146 (2006) 348–365.
[10] R. Hanson, Private Communication, September 16, 2009.
[11] K.G. Harstad, J. Bellan, Combust. Flame 157 (2010) 1594–1609.
[12] Lawrence Livermore National Laboratory, <http://www-pls.llnl.gov/?url=science_and_technology-chemistry-combustion>.
[13] S.W. Benson, Thermochemical Kinetics, John Wiley & Sons, Inc, 1968.
[14] X. Yu, F.N. Egolfopoulos, H. Wang, Proc. Combust. Inst. 32 (2009) 403–410.
[15] H. Pitsch, N. Peters, SAE paper 98-2464.
[16] C.J. Montgomery, M.A. Cremer, J.-Y. Chen, C.K. Westbrook, L.Q. Maurice, J. Propuls. Power 18 (1) (2002) 192–198.

APPENDIX 3

Alkane Kinetics Reduction Consistent with Turbulence Modeling using Large Eddy Simulation

Kenneth G. Harstad[♦,*] and Josette Bellan[♦,**,†]
Jet Propulsion Laboratory[♦], *California Institute of Technology, Pasadena CA 91109-8099*
California Institute of Technology[**], *Mechanical Engineering, Pasadena, CA 91125*

A methodology for deriving a reduced kinetic mechanism for alkane oxidation is described, inspired by n-heptane oxidation. The model is based on partitioning the species of the skeletal kinetic mechanism into lights, defined as those having a carbon number smaller than 3, and heavies, which are the complement of the species ensemble. For modeling purposes, the heavy species are mathematically decomposed into constituents, which are similar but not identical to groups in the group additivity theory. From analysis of the n-heptane LLNL skeletal mechanism in conjunction with CHEMKIN II, it is shown that a similarity variable can be formed such that the appropriately non-dimensionalized global constituent molar density exhibits a self-similar behavior over a very wide range of equivalence ratios, initial pressures and initial temperatures that is of interest for predicting n-heptane oxidation. Furthermore, the oxygen and water molar densities are shown to display a quasi-linear behavior with respect to the similarity variable. The light species ensemble is partitioned into quasi-steady and unsteady species. The reduced model is based on concepts consistent with those of Large Eddy Simulation in which functional forms are used to replace the small scales eliminated through filtering of the governing equations; these small scales are unimportant as far as dynamic energy is concerned. Here, we remove the scales deemed unimportant for recovering the thermodynamic energy. The concept is tested by using tabular information from the n-heptane LLNL skeletal mechanism in conjunction with CHEMKIN II utilized as surrogate ideal functions replacing the necessary functional forms. The test reveals that the similarity concept is indeed justified and that the combustion temperature is well predicted, but that the ignition time is overpredicted, which is traced to neglecting a detailed description of the processes leading to the heavies chemical decomposition. To palliate this deficiency, functional modeling is incorporated into our conceptual reduction. This functional modeling includes the global constituent molar density, the enthalpy evolution of the heavies, the contribution to the reaction rate of the unsteady lights from other light species and from the heavies, the molar density evolution of oxygen and water, and the mole fractions of the quasi-steady light species. The model is compact in that there are only nine species-related progress variables. Results are presented showing the performance of the model for predicting the temperature and species evolution for n-heptane. The model reproduces the ignition time over a wide range of equivalence ratios, initial pressure and initial temperature. Preliminary results for iso-octane using the full mechanism are also presented, showing encouragingly that the concept may be generalized to other alkanes. The utility of the model and possible improvements are discussed.

I. Introduction

The reduction of elementary or skeletal oxidation kinetics to a subgroup of tractable reactions for inclusion in turbulent combustion codes has been the subject of numerous studies. The skeletal mechanism is obtained from the elementary mechanism by removing from it reactions which are considered negligible for

*Senior Engineer.
†Senior Research Scientist, AIAA Fellow (corresponding author, josette.bellan@jpl.nasa.gov).

the intent of the specific study considered. As of now, there are many chemical reduction methodologies, a few exaples being: reduction to a few significant reactions (Müeller et al.,[1] Bollig et al.,[2] Sung et al.[3] and Li et al[4]); piecewise implementation of solution mapping (PRISM);[5] *in-situ* adaptive tabulation (ISAT);[6] intrinsic low-dimensional manifold (ILDM);[7] the Computational Singular Perturbation (CSP) method of Lam and Goussis;[9] lumping[10,11] and directed relation graph (DRG) reduction.[12–16] These few reduction methodologies only represent a subset of all procedures devised for the goal of obtaining a kinetic mechanism compact enough to be utilizable for turbulent reactive flow calculations and accurate enough to be reliable over a wide range of equivalence ratios, ϕ, initial pressures, p_0 (subscript 0 denotes the initial value), and initial temperatures, T_0. As none of the existing methodologies for mechanism reduction is considered the ultimate answer in the quest for compactness and reliability, the search for novel ideas in kinetic mechanism reduction continues. The study presented here is the result of such a search.

In this study, one of the main concerns was to devise a kinetic reduction procedure which is consistent with the Large Eddy Simulation (LES) concept, as LES has shown considerable promise in simulating turbulent flows and represents the state-of-the-art capability in such simulations. The primary idea in LES is that due to the computational infeasibility of routinely solving the governing equations for fully turbulent flows (i.e. high Reynolds number), one should spatially filter the equations thus removing the dynamic-energy-unimportant small scales, leaving only the large scales to be resolved. The influence of the small scales is re-introduced in the equations through functional modeling, allowing the solution of the large scales, and thus of most of the dynamic energy. The dynamic scales of fluid mechanics have a parallel in chemical kinetics since each species has its own characteristic time and can be thought to be a scale of the problem. The dynamic energy of the flow has a parallel in the thermodynamic energy of the reaction; at this early stage of our reduction model, we are only interested in recovering the energetics of the reaction, the major species, and some of the species through which a reaction is monitored (e.g. OH). Therefore, the idea here is to remove scales unimportant to the energetics, and functionally model them.

As in LES, there are two important components to this study, namely the *a priori* analysis and the *a posteriori* evaluation. In the *a priori* study for turbulence modeling, one examines the behavior of the samll scales and proposes models to duplicate it. For chemical kinetics, the information that could be neglected is contained in the skeletal kinetic mechanism. Therefore, the idea is here that examination of the skeletal mechanism should reveal the functional forms of the kinetic scales which could be neglected. In the *a posteriori* study, one includes the small-scales models in LES and assesses their behavior when interacting with the large scales to replicate the flow which is known by other means, either through Direct Numerical Simulations or from experiments. The same *a posteriori* methodology is used here. The present model is for a constant-volume situation, so as to be consistent with the requirement of a LES grid.

This paper is organized as follows: We first describe the basis leading to our conceptual model. Then, we present the model which results from examination of the n-heptane kinetic mechanism,[17] as n-heptane is the simplest hydrocarbon exhibiting a negative temperature coefficient (NTC) behavior and is a reference fuel. Further, we assess the model by comparing it with the skeletal mechanism and identify modeling needs. The functional model is next presented, and results from it are critically examined. Preliminary results for iso-octane based on the full mechanism are also presented, indicating that the conceptual model is extendable to higher alkanes. Finally, we discuss future work.

II. Conceptual model for n-heptane

The conceptual model seeks to represent the species, thought to be akin to vectors in a mathematical space, by a reduced base set. The species are partitioned into heavies (carbon number, $n \geqslant 3$) and lights (the remaining of the set). The heavies can be either radicals or stable species. The lights are oxygen, nitrogen, the final combustion products and light radicals/molecules (e.g. CH_3, CH_4, H_2O_2). The heavies are decomposed into constituents, as described below, while the lights remain part of the base.

A. Heavy species: the total constituent model as progress variable

The definition of constituents stems from the observations that (i) plots of the heats of combustion for alkanes and for alkenes having a C double bond at the molecular chain end have a linear variation with the C number, n and (ii) at fixed temperature T, the species specific heats at constant pressure, C_p, vary linearly with n. The implications are that (1) heats of combustion and C_p may be considered obtainable by summing those

of constituent radicals CH_2, CH_3 and C_2H_3 that form these hydrocarbons and (2) for $n \geqslant 3$, species may be mathematically decomposed into constituent radicals. This is consistent with group additivity theory,[18,19] however, there are marked differences from it. In group additivity one accounts for interactions with adjacent groups, interactions with non-adjacent groups and for steric effects. In our 'constituents' concept we only account for interactions with adjacent groups and first order (compositional) effects. Also, our process is different from lumping because we are decomposing all heavy species and a constituent may span the entire species set of heavy species. The heavy species constituent radicals are defined as a set of entities (here, 13 of them: CH_2, CH_3, CH, C_2H_3, C_2H_2, C_2, HC_2, CO (keto), HCO, HO, HO_2, OO, O) from which any heavy species or radical may be constructed. The total constituent molar density is

$$N_c \equiv \sum_{k=1}^{13} N_k \tag{1}$$

where the molar density of individual constituent k is N_k.

We define a reference molar density for nitrogen, N_2, from the dry air value at pressure $p_{ref} = 1$ bar and T_{ref}= 298.15 K, giving N_{ref}= 31.5 mol/m^3. Using N_{ref}, a dimensionless N_2 molar density is defined as

$$N^* \equiv \frac{N_{N2}}{N_{ref}} \tag{2}$$

which acts as a convenient surrogate variable for the pressure p since the N^* value is essentially rate invariant. That is, the partial pressure of N_2 is the overwhelming contribution to p; basically, the ratio of N^* to p_0 is nearly constant. A normalized temperature variable θ is defined by

$$\theta \equiv \frac{T - T_0}{T_r(\phi, N^*)} \tag{3}$$

$$T_r \equiv 2065(N^*)^{0.06} w(\phi) \tag{4}$$

$$w(\phi) = \phi \frac{1.5 + 1.31\phi}{1 + 0.71\phi + 1.1\phi^2}. \tag{5}$$

The θ definition is such that N_c decreases by three orders of magnitude (delving into higher order of magnitude decrease runs the risk of encountering round-off and truncation errors) from its initial value during stoichiometric combustion upon reaching $\theta \gtrsim 0.6$. The 0.6 value was chosen to ensure that all θ values remain below unity for all test case calculations. The relationships Eq. 3-5 have been empirically derived upon examining the n-heptane LLNL skeletal mechanism, as described in section A.

B. Light species: a modeled subset and a progress variable subset

According to the above procedure, light species are not subject to meaningful decomposition. Examination of runs made using the LLNL database in CHEMKIN II indicates that the light species should be categorized in two subsets: one which is modeled, and one which is computed subject to the heavy species model, as follows:

1. Quasi-steady light species

The species in the first subset are the radicals O, CH, CH_2, CH_3, HO, HCO, HO_2, HC_2, C_2H_3 which have a quasi-steady behavior and require mathematical fits of their mole fraction, X_i, as a function of the state variables (ϕ, N^*, T) and modeling parameters (here, only T_0). There are nine of these quasi-steady light species.

2. Progress variable light species

The species in the second subset are unsteady and require rate equations. This set consists of H_2O, CO_2, O_2, H, CO, H_2, CH_4, H_2O_2, C_2H_2, C_2H_4, CH_2O. The reaction rate of light species is

$$\mathcal{R}_i \equiv \left(\frac{dN_i}{dt}\right)_{reac} = \left.\frac{dN_i}{dt}\right|_{heavies} + \left.\frac{dN_i}{dt}\right|_{lights}, \tag{6}$$

where the contribution of the heavy group to the rate of change of a light species molar density N_i is expressed in terms of quasi-steady gain and loss rates KG_i and KL_i as

$$\left.\frac{dN_i}{dt}\right|_{heavies} = N_c(KG_i - X_i KL_i). \tag{7}$$

Since KG_i and KL_i are functions of (T_0, ϕ, N^*, T), they must be modeled consistently with the heavy species model. There are eleven of these unsteady light species.

C. Model summary for species and computation of energetics

At this junction, the base set is composed of the global constituent radical mole fraction N_c and of the 11 light molecules or free radicals of the second light species subset. Thus, there are at this stage only 12 species-related progress variables. To use this model, one must first find a strategy for computing N_c; such a strategy will be shown next. To compute the 20 light species, one must model X_i of the first light species subset and compute the conventional light species reaction rates of the second light species subset. For the unsteady light species reaction rates, models of KG_i and KL_i are needed in functional form.

The energy equation is

$$\left(N_c C_{p,h} + \sum_{i \in lights} C_{p,i} N_i\right) \frac{dT}{dt} = -\sum_{i \in lights} h_i \mathcal{R}_i + N_c (R_u T_{ref}) K_h \tag{8}$$

where h_i is the molar enthalpy, $C_{p,i}$ is the molar constant-pressure heat capacity, R_u is the universal gas constant,

$$C_{p,h} \equiv \frac{(\sum_{l \in heavies} C_{p,l} N_l)}{N_c}, \tag{9}$$

and the rate of enthalpy change due to heavy species l chemical kinetic changes is defined as

$$K_h \equiv -\left(\sum_{l \in heavies} h_l \mathcal{R}_l\right) \frac{1}{R_u T_{ref} N_c}. \tag{10}$$

Clearly, since K_h is associated with the heavy species, it must be modeled as a function of (T_0, ϕ, N^*, T).

For each light species C_p is modeled as

$$\frac{C_p}{R_u} = a^h + b^h \ln\left(\frac{T}{T_{ref}}\right). \tag{11}$$

Values of a^h and b^h for the light molecules are given in Table 1,[20–23] where values for the the heat of formation, h_i^0, and the heat of combustion for species i, h_i^c, are also given. Both h_i^0 and h_i^c are needed to compute the enthalpy.

III. Results for n-heptane

A. Examination of the n-heptane skeletal mechanism using our concept

Figure 1 shows $N_c/(\phi \times N^*)$ as a function of θ; the plots were obtained using the LLNL skeletal kinetics in CHEMKIN II. The similarity achieved with the two normalized variables is remarkable despite small departures from the nominal curves. Even for as rich a mixture as $\phi = 2$, similarity holds, making this similarity valid in realms beyond those in advanced reduced schemes where the upper limit of the scheme validity is $\phi = 1.5$ (Lu and Law[13]), at most $\phi = 2.0$ (Peters et al.[24]) or exceptionally $\phi = 3$ (Babushok and Tsang[25]). At $\phi = 4$, the mixture is too rich for the reaction to proceed to its ultimate conclusion, and as a result, the reaction termination induces the disparity from self-similarity at $\theta \simeq 0.24$. This self-similar behavior can be understood as a reduction in dimensionality of the problem but should not be confused with the intrinsic low-dimensional manifold[7] because that concept was developed for actual chemical species, whereas our findings are for N_c. And, as stated above, neither is our model equivalent with lumping[10,11] because we are decomposing all heavy species and because a constituent may span the entire species set of

heavy species. The fact that N_c can embody the evolution of all heavy species is consistent with, and can be traced to, the fact that as T increases, the heavy species chemically decompose and no longer play a role; instead, the products of this decomposition determine the reaction evolution. Once values of $\theta \simeq 0.6$ are achieved, the constituents have been nearly exhausted and the reaction may be considered to have reached fruition. Thus, the normalization achieved through θ may be very useful because over the wide range of ϕ, p_0 and T_0, the reaction is completed at approximately the same θ value.

Plots of the molar densities of oxygen, N_{o2}, and of water, N_{h2o}, versus θ are illustrated in Fig. 2 over the same wide range of ϕ, p_0 and T_0 as in Fig. 1. Remarkably, both types of plots display a quasi-linearity. For H_2O, eventually, an asymptotic behavior is seen at $\theta \simeq 0.6$ indicative of the reaction having reached completion, consistent with the information from Fig. 1.

The above findings suggest that instead of computing N_c from a rate equation (i.e. as a process variable), one may simply fit the $N_c/(\phi \times N^*)$ curves shown in Fig.1; this fitting must be performed in the four parameter space (T_0, ϕ, N^*, T). Similarly, instead of considering O_2 and H_2O as progress variables, it seems reasonable to functionally fit the slope of the curves in Fig. 2 and use this fit in routine calculations to predict these two major species. Thus, this examination of our conceptual model for n-heptane using the LLNL skeletal kinetics in CHEMKIN II leads to further reducing the number of species-related process variables from 12 to 9. These 9 process variables are the molar densities of the lights: CO_2, CO, H, H_2, CH_4, H_2O_2, C_2H_2, C_2H_4, CH_2O.

B. Assessment of the concept's predictive capabilities using an ideal model

Before launching into the task of performing functional fits for rates and X_i, we deemed it instructive to assess the predictive capability of the concept by utilizing ideal functional fits extracted from the LLNL skeletal mechanism using CHEMKIN II. These ideal functions were obtained in tabular form, every 5^oK, and served as input to our conceptual model. Examples of the results are portrayed in Fig. 3 for both N_c and T profiles; indeed, predicting the energetics and more particularly the ignition time, t_{ign}, is an important goal of the model.

Unsurprizingly according to Fig. 1, Fig. 3a shows that N_c is excellently predicted by our conceptual model. However, whereas the value of the combustion T is also excellently predicted, the predicted ignition time is longer than that of the skeletal mechanism. This epitomizes the missing information resulting from the reduction of the LLNL skeletal mechanism from 160 to 9 progress variables. Physically, the missing information is that of how the heavy species evolve over the relatively long initial time of nearly constant T. During this time, although T is almost constant, heavy species decomposition provides the radicals responsible for eventual ignition. Experimentally, it is observed[26] that t_{ign} is an extremely sensitive quantity function of T_0 and even a degree K change in T_0 makes approximately 10% change in t_{ign}. Thus, the accurate prediction of t_{ign} is a very stringent test for a model. From the modeling viewpoint, this means that the neglected scales of the initial pre-ignition process must be reintroduced through very careful modeling. This modeling is described next.

C. Functional fits to emulate the LLNL skeletal mechanism

The functional fits necessary to complete the model fall into two categories: fits for the rates K_h, KG_i, $RL_i \equiv KL_i/KG_i$, for N_c, and for the X_i of the quasi-steady light species; and fits for the slopes of the unsteady quantities N_{o2}, and N_{h2o}.

1. Fits for the rate quantities and quasi-steady light species molar fractions

According to Eq. 8, to recover the value of T in the reduction scheme, the heavy species model should focus on an appropriate representation of $C_{p,h}$ and K_h. Plots (not shown) of $C_{p,h}$ at various p_0 values, calculated using the LLNL model over a wide range of ϕ, show that these curves exhibit a very modest variation over the range of strong N_c decay; moderate (i.e. up to 50%) variation occurs only after N_c values are very small to negligible. This indicates that the T recovery is primarily governed by K_h as far as heavy species modeling is concerned.

The model for K_h, KG_i, RL_i and X_i is constructed considering these quantities as functions of T or θ, with N^*, ϕ and T_0 being parameters. Quantities K_h, KG_i and X_i are split into a very low T region, i.e. $\theta \leqslant 10^{-2}$, termed the incubation region in which there are very slow changes; a low-rate portion corresponding

to $10^{-2} \leqslant \theta \leqslant 0.2$ that exhibits a maximum, K_{mx}, and a minimum, K_{mn}; and a high T, $\theta \geqslant 0.2$, high-rate portion termed the fast-rate region in which a continuous increase is commonly observed. Conversely, RL_i first exhibits a minimum, and then a maximum. Thus, the functional fits are performed in three separate regions, with connection constraints between consecutive regions (the ultimate fits are piecewise continuous). Details of the fitting procedure are given in Harstad and Bellan.[27]

The need to introduce a model to capture t_{ign}, as explained in section B, as well as an extreme sensitivity of K_h on T_0 (e.g. $K_h \sim T_0^{21}$ for $\theta \simeq 10^{-3}$) meant that special care should be devoted to reproduce this dependency. Thus, we developed functional fits to the slopes dK_h/dT at T_0 and made corresponding adjustments to the rates at $\theta \lesssim 10^{-1}$. These turned out to be insufficient to reproduce t_{ign}, and an adjustment was introduced to the initial slope for K_h (for $\theta < 10^{-2}$) by using a multiplying factor determined by trial-and-error calculations, so as to best match the reduced model predictions compared to those of the skeletal mechanism.

This model was used for K_h, for the quasi-steady gain rates KG_i (where i stands for CO_2, H, CO, H_2, CH_4, H_2O_2, C_2H_2, C_2H_4, CH_2O), for the quasi-steady loss rate RL_i (where i stands for H and H_2, this rate being negligible for the other light species) and for the quasi-steady light species molar fractions X_i (O, CH, CH_2, CH_3, HO, HCO, HO_2, HC_2, C_2H_3).

Selected plots of K_h are presented in Fig. 4; KG_{h2} and KG_h are displayed in Fig. 5 and the ratio RL_i is correspondingly illustrated in Fig. 6 for $i = $ H and $i = H_2$. The rates K_h exhibit a variation by as much as seven orders of magnitude, and the task of developing curve fits over this extended regime in the four parameter space (T_0, ϕ, N^*, θ) is far from trivial. Despite the difficulty of developing accurate curve fits, the agreement between the fits and the LLNL skeletal mechanism in excellent to good over $p_0 \in [10, 40]$ bar, $T_0 \in [600, 800]$ K and $\phi \in [0.5, 4]$ and even extends to values as small as $\phi = 1/4$ (not shown). The same comments hold for KG and RL. Discrepancies between fits and the LLNL skeletal mechanism past $\theta \simeq 0.6$ are unimportant for the reduction concept since $N_c/N_{c,0} \ll O(1)$ past that station.

For the quasi-steady species, we chose to display N_o because of the high reactivity of the O radical and N_{oh} because the OH species is generally considered as indicative of the flame location. The quantities N_i were computed as $N_i = X_i N_L$ where $N_L = \sum_{i \in lights} N_i$. Results are presented in Fig. 7 and show that the agreement between fits and the skeletal mechanism is very good, including some extreme ϕ values in the lean regime.

2. Fits for N_{o2} and N_{h2o}

Two quantities were defined that constrain the evolution of N_{o2} and N_{h2o} : the initial value, N_{o2}^i, and the asymptotic value N_{h2o}^a. Fits for N_{o2} and N_{h2o} were constructed as follows:

$$N_{o2}/N_{o2}^i \doteq \max(1.0 - A_{o2} \times \theta,\ 0.0), \tag{12}$$

$$N_{h2o}/N_{h2o}^a \doteq \min(1.0,\ A_{h2o} \times \theta). \tag{13}$$

Fits to the slopes A_{o2} and A_{h2o} were constructed as

$$A_{o2} = C_{o2}(\phi, T_0) \times \phi \times (N^*)^{0.05} \tag{14}$$

$$A_{h2o} = C_{h2o}(\phi, T_0) \times (N^*)^{\varepsilon} \tag{15}$$

where $\varepsilon(\phi) = 0.2 \times \phi \times \exp(-1.4\phi) \leqslant 0.0525$. For computing functions $C_{o2}(\phi, T_0)$ and $C_{h2o}(\phi, T_0)$ a set of ϕ values is first chosen. For a specified value in the set, $C_{o2}(\phi, T_0)$ and $C_{h2o}(\phi, T_0)$ are fitted as a polynomial function (up to quadratic) of T_0/T_{ref}. For arbitrary ϕ, an interpolation is performed over ϕ using C_{o2} and C_{h2o} values at the specified ϕ values in the chosen set.

Figure 8 shows an example of the obtained fits versus the LLNL skeletal mechanism. The agreement ranges from excellent to good and is typical of that obtained over a wide range of (T_0, ϕ, N^*).

D. Model predictions

The model predictions consist of the timewise temperature evolution $T(t)$, t_{ign} as extracted from the $T(t)$ profile, and the timewise evolution of the unsteady light species with the exception of O_2 and H_2O which are modeled as shown in section 2.

1. Temperature profiles

Displayed in Fig. 9 are the reduced model predictions compared to those of the skeletal mechanism, spanning a wide range of ϕ values and two values of each T_0 and p_0. Although t_{ign} is well predicted for all cases, the ultimate combustion temperature is not well predicted at very lean conditions ($\phi = 1/4$) or relatively low pressure (i.e. $p_0 = 10$ bar). It seems likely that with additional modeling effort these limitations could be overcome, but we consider that at this 'proof of principle' stage, the additional effort is not warranted. On the favorable side, at the high temperature conditions representative of diesel, gas turbine and HCCI engines, the model performs very well; the same holds for the very rich conditions (e.g. $\phi = 4$) at which soot forms.

2. Ignition times

The very successful use of the adjusted initial K_h slopes instrumental in predicting t_{ign} is shown in Fig. 10. Noteworthy, the ordinate axis is the typical logarithmic one[28] for Figs. 10a and 10b, but it is here linear for Fig. 10c, so deviations between reduced model and skeletal mechanism observed in Fig. 10c are indeed logarithmically very small. The predictions in Fig. 10 are excellent over a wide range of T_0 including as low a temperature as 600 K, over a range of ϕ including mixtures as rich as $\phi = 4$, and as lean as $\phi = 1/3$ and p_0 from 10 to 40 bar.

3. Predicted unsteady species

The prediction of several unsteady light species is illustrated in Figs. 11 and 12. These are results obtained from solving Eq. 6 with the modeled $\mathcal{R}_i$. The $N_i(\theta)$ is computed from using $N_i(t)$ and $T(t)$, which allows computing $\theta(t)$.

We chose to display N_h and N_{h2} because they both depend on the KG and RL fits and thus they provide a stringent test of the model given the possibility of additive error. N_{co} is chosen since CO is one important product of incomplete combustion. N_{ch4} is selected as a representative intermediary in the oxidation process. As discussed above, only prediction up to $\theta \simeq 0.6$ should be considered, as past that station the reaction is practically finished.

Generally, the agreement between the reduced model and the skeletal mechanism is very good, including at $p_0 = 10$ bar for which the combustion temperature was not well predicted. With the exception of N_h for which the comparison is just as favorable at $\phi = 4$ as at $\phi = 1/3$, for all other species the lean region is much better reproduced by the model than the rich region. The fact that good agreement is obtained for such extreme ϕ values is desirable since, as already stated such values are generally not considered in advanced reduced schemes. Also, the results seem to be slightly more accurate with increasing T_0.

IV. Preliminary assessment of the n-heptane model for iso-octane

To test the capability of the proposed technique for other alkanes, iso-octane was chosen as the next one in degree of difficulty. Not only is iso-octane the next higher C number species with respect to n-heptane, by also these two species are prominently featured in JP-8 surrogate fuels because they both display the NTC behavior of the heavier real fuels in the ignition regime and the feature of two-stage ignition.[24] The level of modeling difficulty increases substantially for the n-heptane mechanism having 160 species (progress variables) and 1540 reactions to the iso-octane full (rather than skeletal) oxidation mechanism[30] containing 857 species and 3606 reactions. The substantial effort of decomposing in constituents the heavy species of the 857-species ensemble led to the iso-octane ensemble of constituents being essentially the same as for n-heptane, with the sole addition of the carbon atom C. That is, now

$$N_c \equiv \sum_{k=1}^{14} N_k \tag{16}$$

and the ensemble of constituents is (CH_2, CH_3, CH, C_2H_3, C_2H_2, C_2, HC_2, CO (keto), HCO, HO, HO_2, OO, O, C).

There are four questions that are of interest is assessing the n-heptane conceptual model for iso-octane: (1) Is θ defined in Eq. 3 still a valid similarity variable in that $N_c/(\phi \times N^*)$ as a function of θ, such

as shown in Fig. 1 for n-heptane? (2) If the similarity variable holds, are the concentrations of O_2 and H_2O decreasing and increasing, respectively, in a quasi-linear manner with θ? (3) Is the ensemble of light species partitionable into the same two sub-ensembles of quasi-steady and unsteady species, and do these sub-ensembles contain the same species as for n-heptane? (4) If the three above items hold, are the functional fits derived for n-heptane also valid for iso-octane? The preliminary results derived for iso-octane allow to cautiously affirmative answer the first two questions, with the understanding that a much more extensive study is necessary for incontrovertible affirmation.

Figure 13a illustrates $N_c/(\phi \times N^*)$ as a function of θ at three ϕ values and two T_0 values. We first note that the temperature normalization holds in that $N_c/(\phi \times N^*) \ll 1$ by $\theta \simeq 0.6$. Second, all plots of $N_c/(\phi \times N^*)$ approximately coincide, showing for this limited set of cases that the similarity concept holds. Displayed in Fig. 13b are the temperature profiles corresponding to the Fig. 13a cases, showing that the choice of the runs spans more than one order of magnitude range in t_{ign}.

The O_2 and H_2O concentrations versus θ are plotted in Figs. 14a and 14b. The quasi-linear aspect of the curves is very similar to that observed for n-heptane in Fig. 2, indicating that the same behavior prevails.

Although considerably more tests are necessary to ascertain that the concept and model developed for n-heptane also holds for iso-octane, the preliminary results seem promising.

V. Conclusions and discussion

A kinetic reduction model has been developed based on the concept of constituents representing the evolution of all heavy species, and on light species representing the complementary chemistry to that of heavy species. The light species fall into two categories: quasi-steady, for which no differential equation must be solved, and unsteady light species some of which are progress variables and others which have fitted rates of their evolution as function of the similarity variable. A thorough examination of the LLNL skeletal mechanism for n-heptane revealed that it is possible to empirically define a similarity variable which is function of the initial temperature, initial pressure and equivalence ratio, and for which a non-dimensionalized global-constituents' molar density exhibits a self-similar behavior across initial temperatures, initial pressures and equivalence ratios. The significance of this finding is that there is a reduction in the dimensionality of the problem. We found a lower-dimensional manifold which is not to be confused with ILDM because the latter is for species, whereas the present model is for N_c. The fact that the constituents rather than the heavy species are important can be directly traced to the fact that the heavy species decompose and it is the reaction of these products of decomposition that matters for the energetics. Thus, rather than solving a differential equation to obtain the evolution of the global constituents, their behavior may be functionally fitted, thereby reducing the number of progress variables. Further examination of the skeletal mechanism revealed that the molar density of oxygen and that of water displayed a quasi-linear variation with the similarity variable over the entire range of parameters surveyed. The suggestion was that the molar densities of these two unsteady light species could be functionally modeled rather than computed from differential equations.

The concept was tested by using the n-heptane LLNL skeletal mechanism in conjunction with CHEMKIN II. That is, instead of a model consisting of functional fits, we used an ideal model represented by tables extracted from the LLNL skeletal mechanism in the form needed in our conceptual model. Our conceptual model was found to be sound, but the ignition time it predicted was too long compared to the template. The meaning of this discrepancy is that the neglect of the chemical processes during the initial time of very small temperature changes results in the overprediction of the ignition time. The situation is equivalent to turbulent modeling using the Large Eddy Simulation (LES) concept in which the spatial filtering of scales results in the need to re-introduce the effect of these small scales through models. Following the LES modeling philosophy, a small-scale model was developed and implemented at temperatures very close (1-2 degrees K) to the initial temperature, to be used with the conceptual model.

Moreover, also paralleling the LES concept, fits in functional form were developed for the sensible enthalpy production due the constituents' reaction, for the quasi-steady light species mole fractions and for the reaction rate of the unsteady light species. The reaction rate of each unsteady light species was decomposed into contributions from the lights which were directly taken from the LLNL skeletal mechanism and contributions from the heavy species which were modeled. The heavy species rate contribution was further categorized into a gain rate and possibly a loss rate, which were individually modeled. The modeling effort was by no means trivial as the rates and molar fractions varied by as much as seven orders of magnitude and this

variation needed to be captured in the four parameter space of the initial pressure, the initial temperature, the equivalence ratio and the temperature.

The consequence of providing functional fits over a wide range of equivalence ratios encompassing mixtures as rich as $\phi = 4$ and as lean as $\phi = 1/4$ was that generally the fits were very good to excellent, but sparse regions of good to fair results could also be identified. The ignition times were excellently to very well reproduced by the model, and so were some major species (e.g. O_2 and H_2O). Other major species (e.g. CO) and OH, which is an indicator of the flame location, were also well reproduced, but the value of the final combustion temperature was not always well predicted. To improve the combustion temperature prediction, one could either refine the K_h functional fit or use the ideal model provided by the tables extracted from the LLNL mechanism using CHEMKIN II as done in section B, but now in conjunction with our model in the vicinity of T_0 so as to capture the ignition time. To improve light species predictions, one could either refine their functional fit if the species is quasi-steady, or refine the functional fits for KG and RL if the species is unsteady; alternately, one could use the the ideal model provided by the tables extracted from the LLNL mechanism using CHEMKIN II.

Instead of improving the n-heptane model, we turned attention to investigating whether the proposed concept also holds for higher C alkanes, such as iso-octane. Preliminary results indicate that the conceptual model of the similarity variable and the quasi-linear dependence of the O_2 and H_2O concentrations of the similarity variable, indeed holds; although it remains to be seen if the present curve fits are valid for higher C alkanes or must be modified.

Finally, the usefulness of our model, which contains only nine species-related progress variables, is that it is less computational intensive than other reduced models having $O(50)$ species-related progress variables (e.g. Lu and Law[29]) while giving much improved predictions compared to the expedient one-step reaction models. As usual, information loss increases with increasing chemical kinetics simplification; the balance between the desired information to be obtained from exercising the model and computational cost is the paramount consideration. Since results for most reduction schemes are presented in a much more restricted ϕ region than the $\phi \in [1/4, 4]$ considered here, it is difficult to directly evaluate our model with respect to other models. It is understood that for any given model, predictions will improve if a less ambitious validity regime is considered.

Acknowledgements

This study was conducted at the Jet Propulsion Laboratory (JPL), California Institute of Technology (Caltech) and sponsored at Caltech by the Army Research Office under the direction of Drs. David Mann, Kevin McNesby and Ralph Anthenien.

References

[1]U. C. Müeller, N. Peters, A. Liñan, Proc. Comb. Inst. 24 (1992) 777-784.

[2]M. Bollig, H. Pitsch, J. C. Hewson, K. Sheshadri, Proc. Comb. Inst. 26 (1997) 729-737.

[3]C. J. Sung, C. K. Law, J.-Y. Chen, Proc. Comb. Inst. 27 (1998) 295-304.

[4]S. C. Li, B. Varatharajan, F. A. Williams, AIAA J. 39(12) (2001) 2351-2356.

[5]J. B. Bell, N. J. Brown, M. S. Day, M. Frenklach, J. F. Grcar, R. M. Propp, S. R. Tonse, Proc. Comb. Inst. 28 (2000) 107-113.

[6]S. B. Pope, Combust. Theory Model. 1 (1997) 41-63.

[7]U. Maas, S. B. Pope, Combust. Flame 88(3-4) (1992) 239-264.

[8]C. Correa, H. Niemann, B Schramm, J Warnatz, Proc. Comb. Inst. 28 (2000) 1607-1614.

[9]S. H. Lam, D. A. Goussis, Int. J. Chem. Kinetics 26 (1994) 461-486.

[10]E. Ranzi, T. Faravelli, P. Gaffuri, A. Sogaro, Comb. Flame 102 (1995) 179-192.

[11]E. Ranzi, M. Dente, A. Goldaniga, G. Bozzano, T. Faravelli, Prog. Energy Comb. Sci. 27 (2001) 99-139.

[12]T. F. Lu, C. K. Law, Proc. Combust. Inst. 30 (2005) 1333-1341.

[13]T. F. Lu, C. K. Law, Combust. Flame 144 (2006) 24-36.

[14]T. F. Lu, C. K. Law, Combust. Flame 146 (2006) 472-483.

[15]X. L. Zheng, T. F. Lu, C. K. Law, Proc. Combust. Inst. 31 (2007) 367-375.

[16]P. Pépiot-Desjardins, H. Pitsch, Combust. Flame 154 (2008) 67-81.

[17]Lawrence Livermore National Laboratory, http://www-cms.llnl.gov/combustion/combustion2.html.

[18]S. W. Benson, Thermochemical Kinetics., John Wiley & Sons, Inc., 1968.

[19]R. C. Reid, J. M. Prausnitz, B. E. Poling, The Properties of Gases and Liquids, McGraw-Hill Book Co., 4th edition, 1987, Chapt. 6.

[20]National Institute of Standards and Technology, Chemistry WebBook; http://webbook.nist.gov/chemistry/.

[21]CRC Handbook of Chemistry and Physics, 86th Ed., D. R. Lide (Ed.-in-Chief), CRC Press, Boca Raton, Fl., 2005 (internet edition).

[22]Gas Research Institute, http://www.me.berkeley.edu/gri-mech/.

[23]NASA Glenn Research Center, http://cea.grc.nasa.gov/.

[24]N. Peters, G. Paczko, R. Seiser, K. Sheshadri, Combust. Flame 128 (2002) 38-59.

[25]V. I. Babushok, W. Tsang, J. Propul. Power 20(3) (2004) 403-414.

[26]R. Hanson, private communication, September 16, 2009.

[27]K. G. Harstad, J. Bellan, A model of reduced kinetics for alkane oxidation using constituents and species: proof of concept for n-heptane, submitted 2009.

[28]H. J. Curran, P. Gaffuri, W. J. Pitz, C. K. Westbrook, Combust. Flame 114 (1998) 149-177.

[29]T. F. Lu, C. K. Law, Strategies for Mechanism Reduction for Large Hydrocarbons: n-Heptane, paper #C21, presented at the 5th US Combustion Meeting, March 25-28, 2007, San Diego, CA.

[30]Lawrence Livermore National Laboratory, http://www-pls.llnl.gov/?url=science_and_technology-chemistry-combustion-ic8h18

Mo/Ra	h^0	h^c	a^h	b^h
H_2	0.0	241.5	3.282	0.400
O_2	0.0	0.0	3.476	0.5663
N_2	0.0	0.0	3.388	0.469
C	717	1111	2.50	0.0
H_2O	-241.5	0.0	3.688	1.217
CO_2	-393.5	0.0	4.690	1.390
N	473	473	2.50	0.0
H	218.0	339	2.50	0.0
HO	38	159	3.385	0.3637
HOO	10.5	131	4.150	1.307
O	249.2	249.2	2.536	0.0
CO	-110.5	283	3.426	0.4749
HCO	43.1	558	4.154	1.2875
CH_4	-74.6	802	3.797	4.305
CH_3	146	902	4.440	2.249
CH_2	390	1025	3.973	1.3015
CH	596	1110	3.220	0.7136
C_2H_3	300	1449	5.1	3.5
HC_2	566	1474	4.434	1.404
C_2	838*	1625	4.58	0.0
NO	90.3	90.3	3.533	0.4508
NO_2	33.2	33.2	4.691	1.151
H_2O_2	-136	106	5.269	1.880
HCOH	-109	526.5	4.27	2.546
C_2H_2	228	1257	5.368	2.294
C_2H_4	52.5	1323	5.383	4.676

*Alternate value of 832 from the CRC tables.

Table 1. Thermodynamic properties of molecules and free radicals. h^0 and h^c (heats of formation and combustion, respectively), in kJ/mol; constants a^h and b^h for molar heat capacity in the form $C_p/R_u = a^h + b^h ln(T/T_{ref})$; T_{ref} = 298.15 K. "Mo" denotes "molecule". "Ra" denotes "radical".

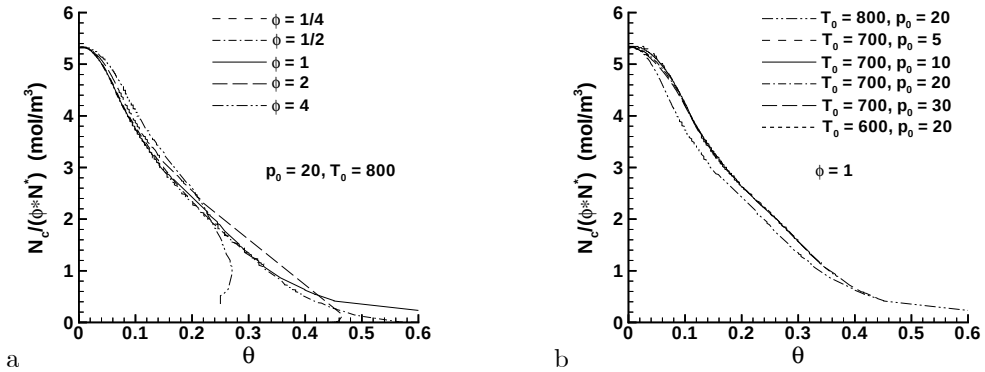

Figure 1. Similarity plots of parameter $N_c/(\phi \times N^*)$ versus θ at (a) $p_0 = 20$ bar and (b) $\phi = 1$ using the LLNL skeletal mechanism in conjunction with CHEMKIN II. T_0 **is in K.**

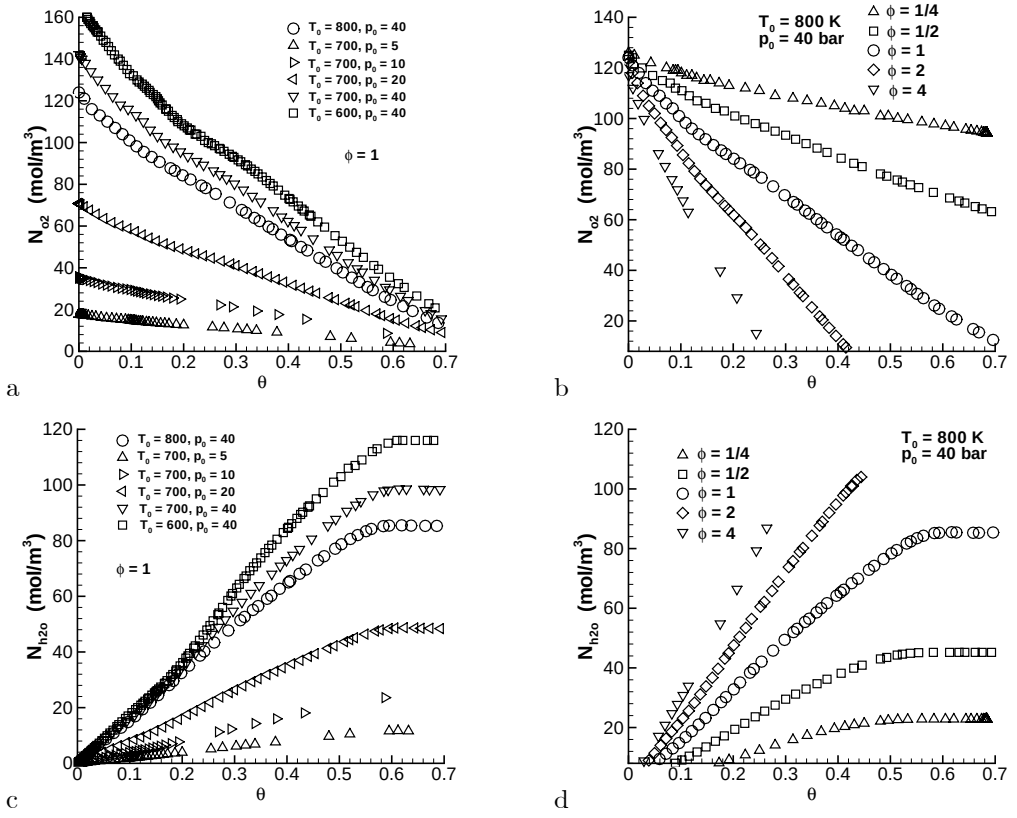

Figure 2. Oxygen and water molar densities versus θ as extracted from the LLNL skeletal mechanism in conjunction with CHEMKIN II.

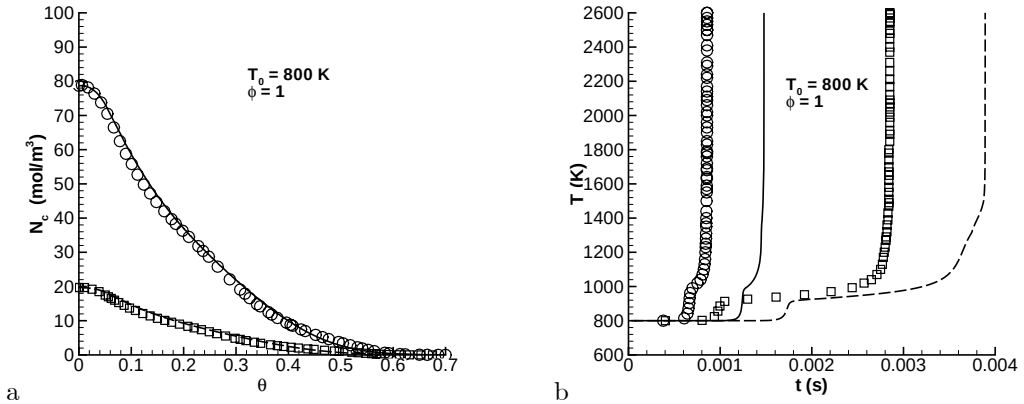

Figure 3. Molar density of constituents (a) and temperature (b) obtained with our conceptual model and tabular information from the LLNL skeletal mechanism using CHEMKIN II. The symbols are from the LLNL skeletal mechanism in conjunction with CHEMKIN II (□ □ □ p_0 =10 atm; ◯ ◯ ◯ p_0= 40 atm), and the lines are obtained using tabular information from the LLNL skeletal mechanism with CHEMKIN II in our conceptual model (- - - - p_0 =10 atm; ——— p_0= 40 atm).

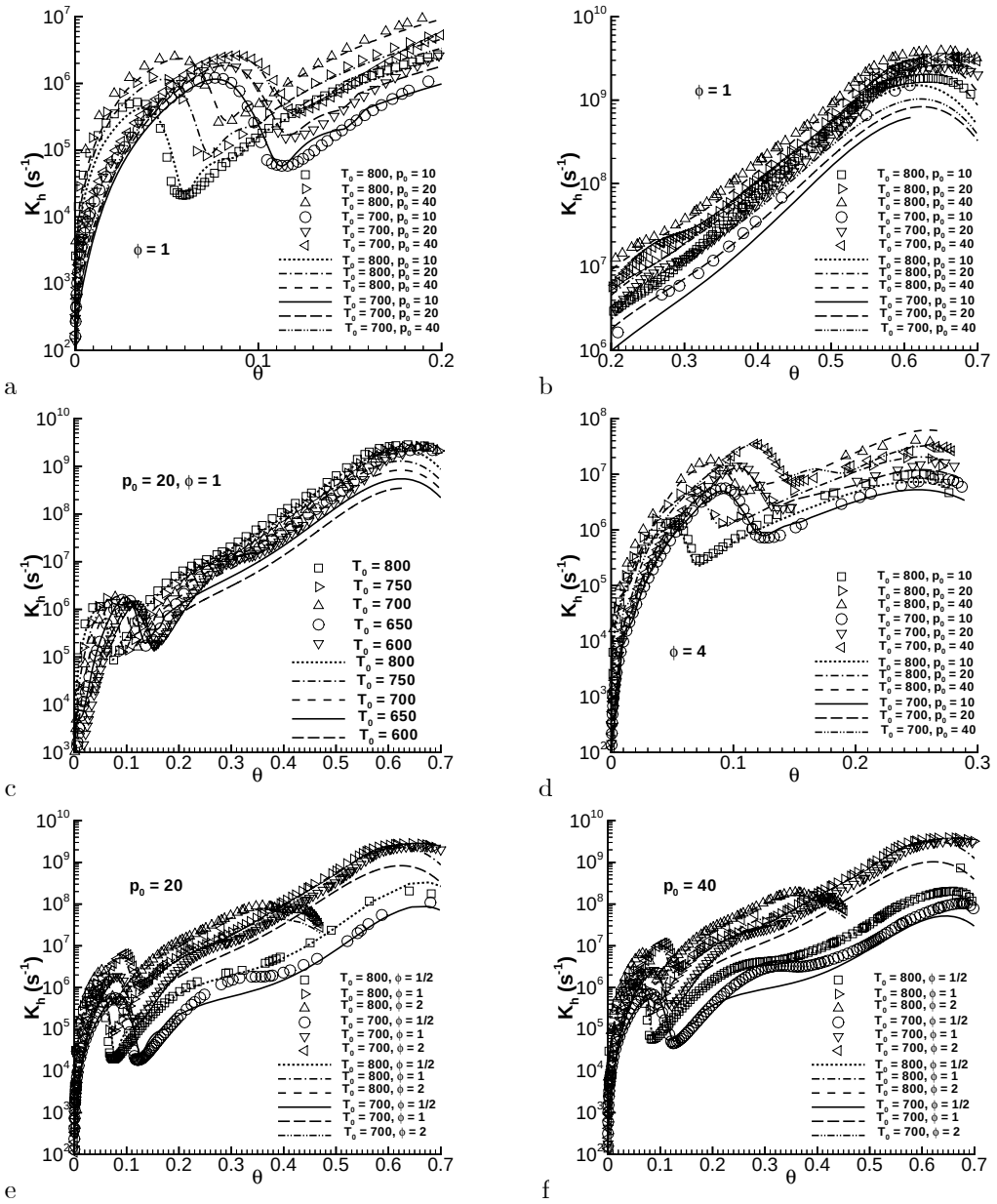

Figure 4. K_h **versus** θ **for different conditions. Symbols represent selected data from the LLNL runs; lines represent the corresponding fits.** T_0 **is in degrees K and** p_0 **is in bar.**

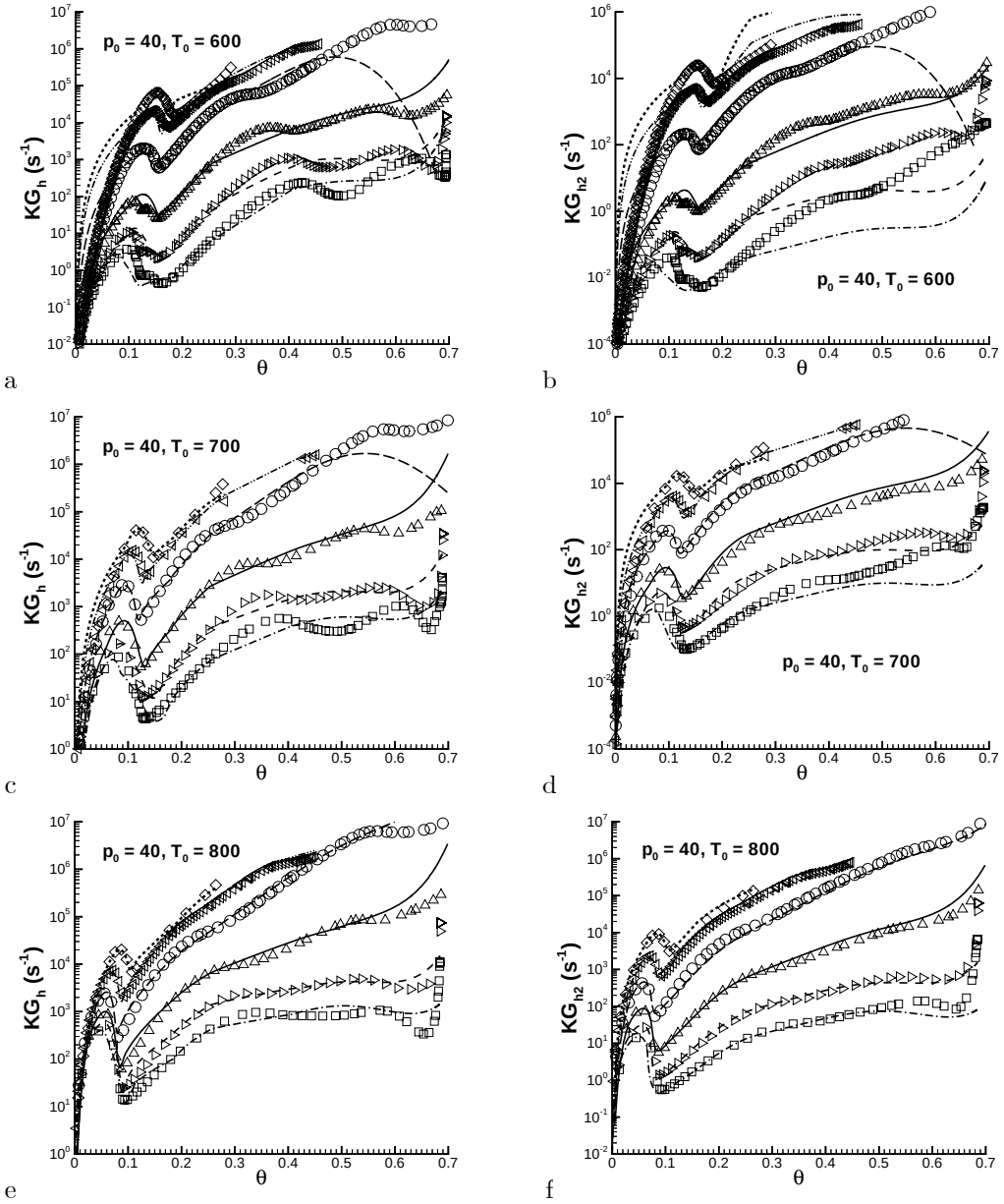

Figure 5. KG_h **and** KG_{h2} **versus** θ **for** $p_0 = 40$ **bar at different** T_0 **and** ϕ**. Symbols represent selected data from the LLNL skeletal mechanism; lines represent the corresponding fits.**

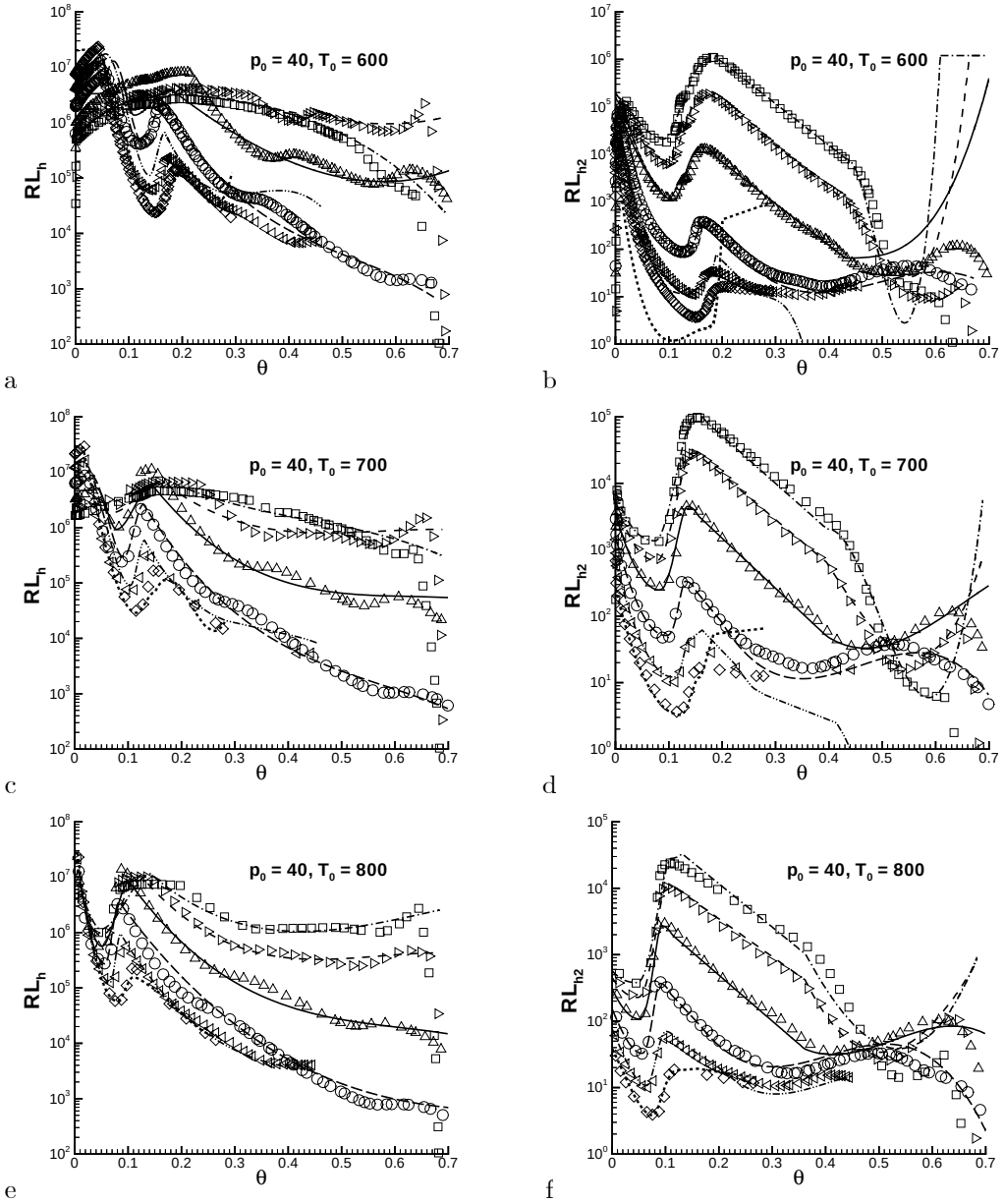

Figure 6. RL_h **and** RL_{h2} **versus** θ **for** $p_0 = 40$ **bar at different** T_0 **and** ϕ**. Symbols represent selected data from the LLNL skeletal mechanism; lines represent the corresponding fits.**

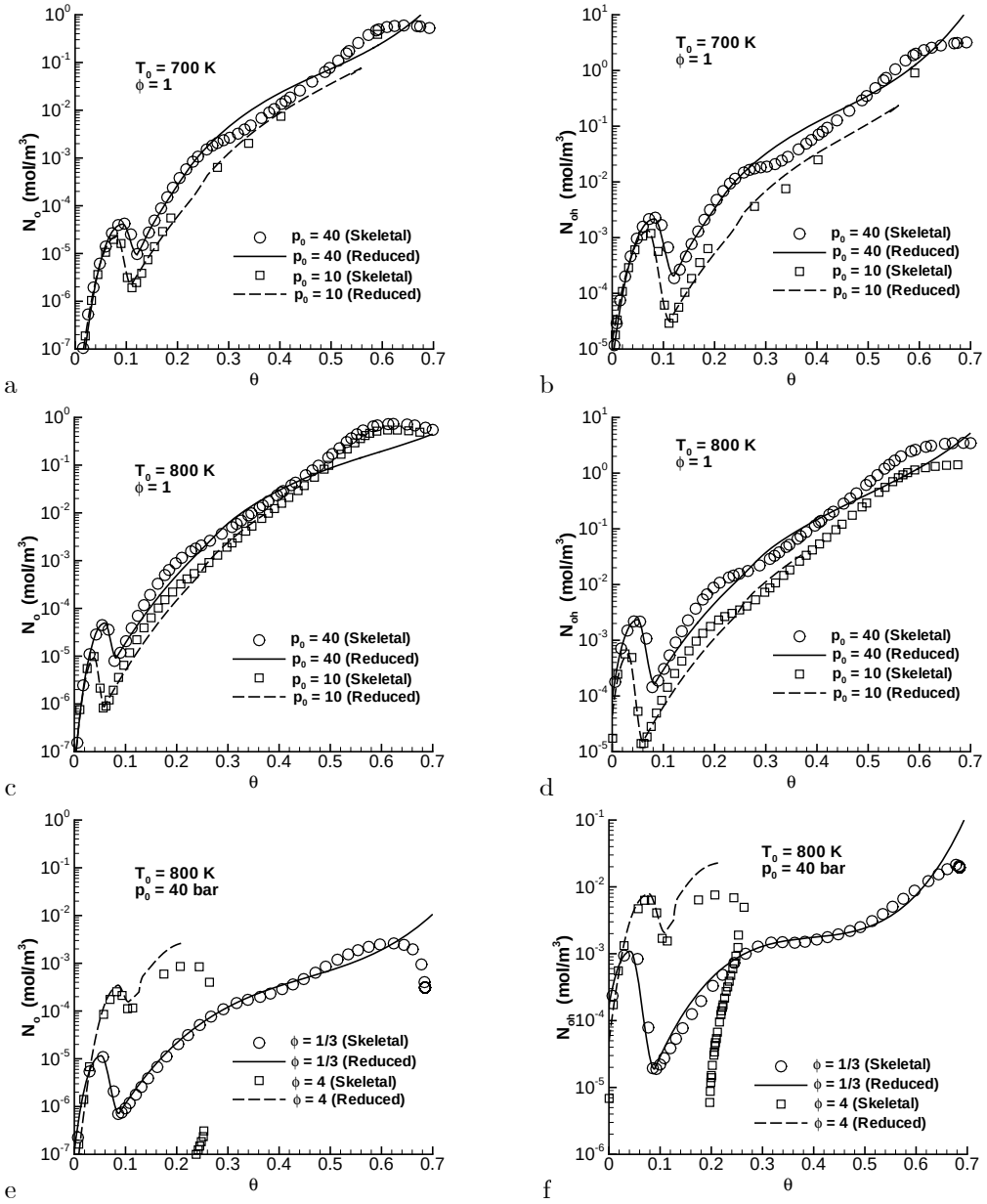

Figure 7. Modeling results for the quasi-steady molar densities N_o and N_{oh} and comparison with those of the skeletal mechanism at various T_0, p_0 and ϕ conditions.

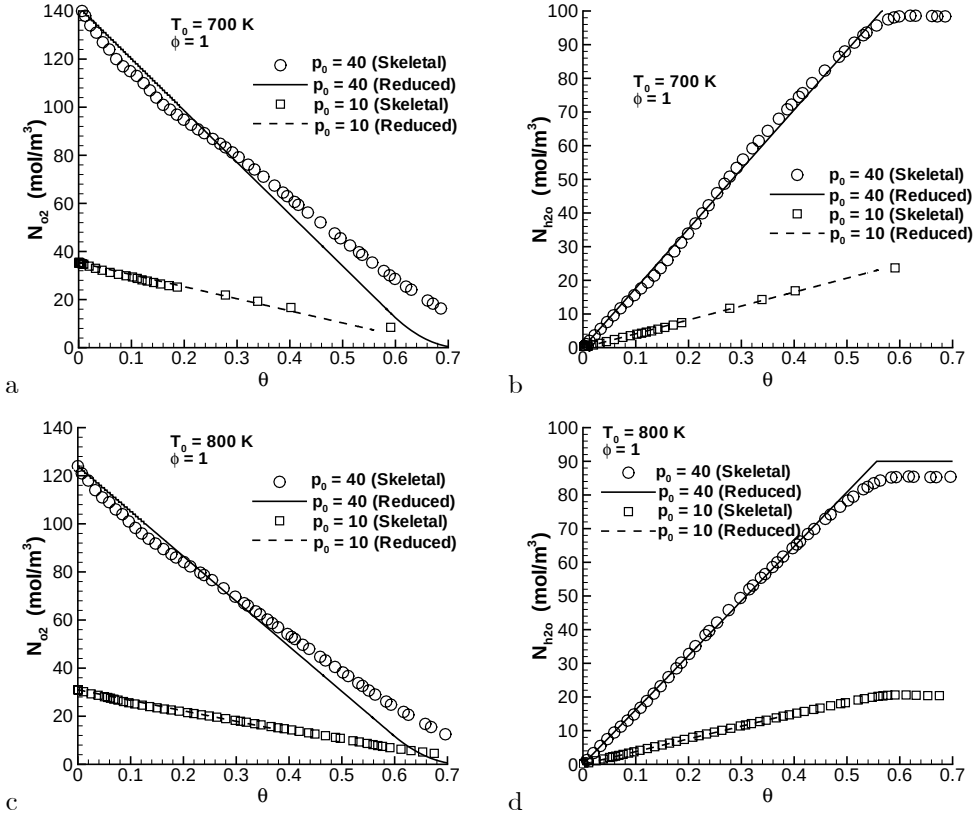

Figure 8. N_{o2} **and** N_{h2o} **versus** θ **at fixed** $p_0 = 10$ **and** 40 **bar for** $\phi = 1$ **and** $T_0 = 700$ **and** 800 **K.**

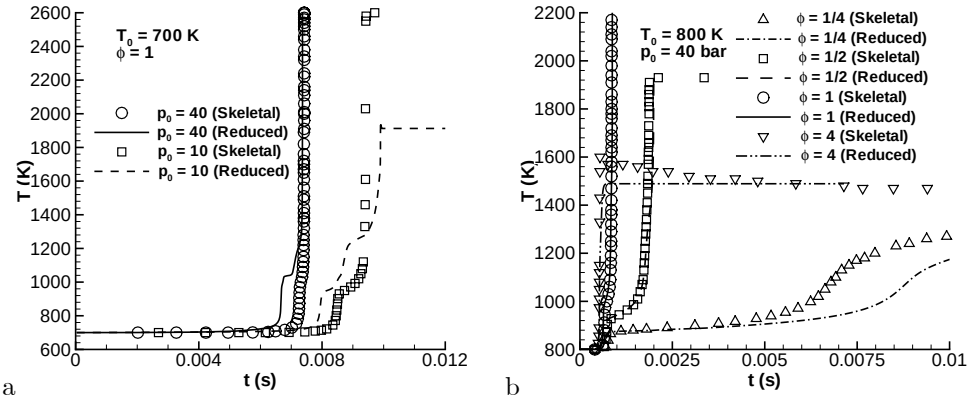

Figure 9. $T(t)$ **as predicted by the reduced model compared to the LLNL skeletal mechanism predictions for a variety of conditions.**

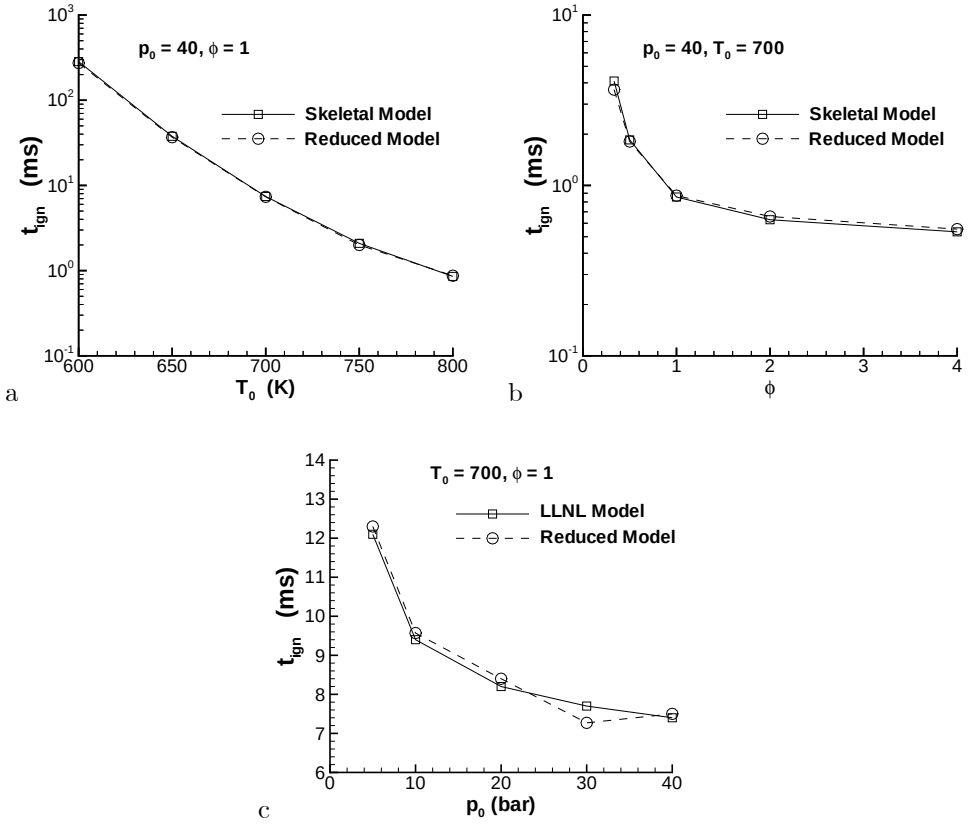

Figure 10. t_{ign} **as function of** T_0, ϕ **and** p_0**. Where not indicated on the plots,** T_0 **is in degrees K and** p_0 **is in bar.**

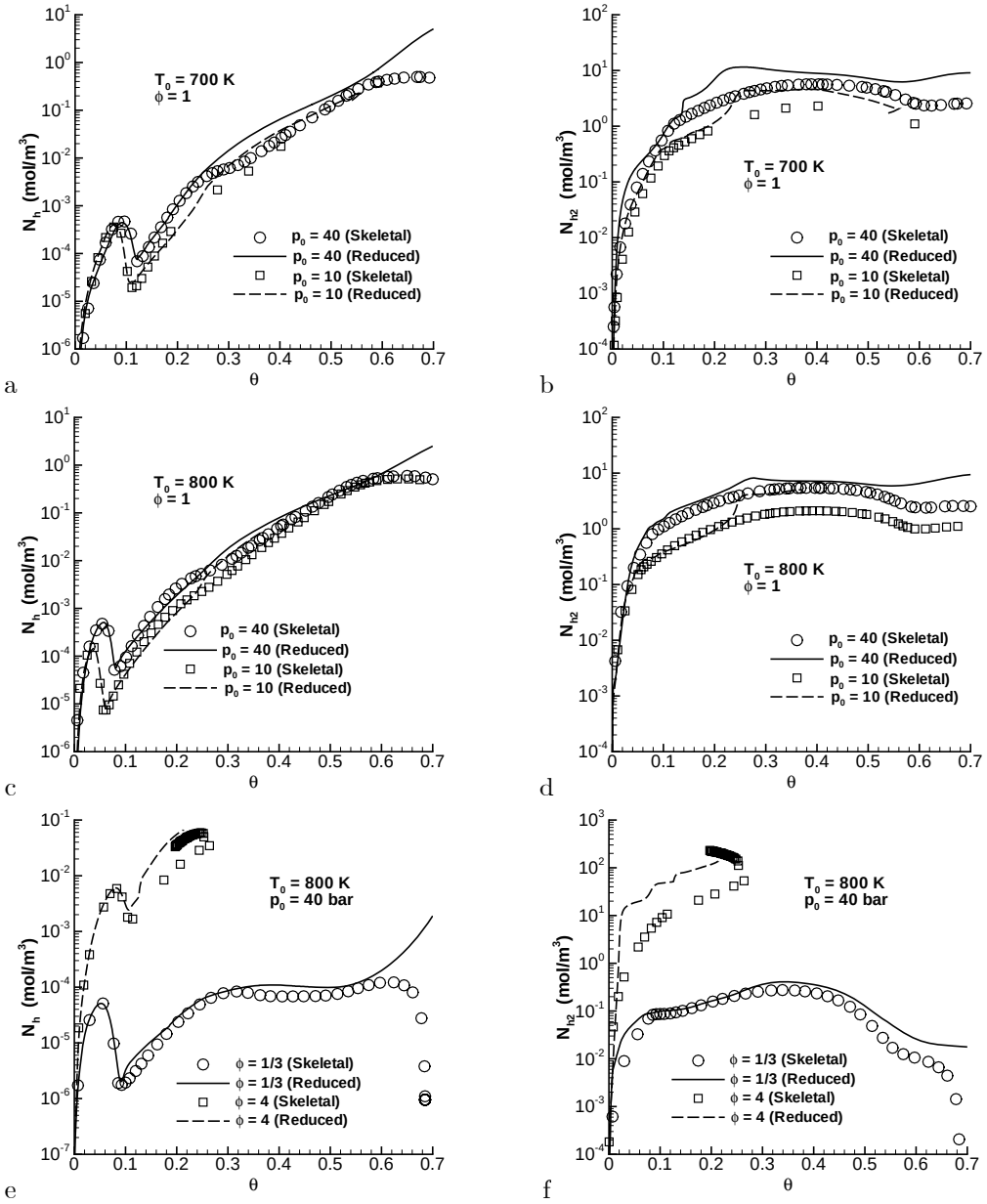

Figure 11. Predictions of the reduced model for N_h and N_{h2} compared to those of the skeletal mechanism at various T_0, p_0 and ϕ conditions.

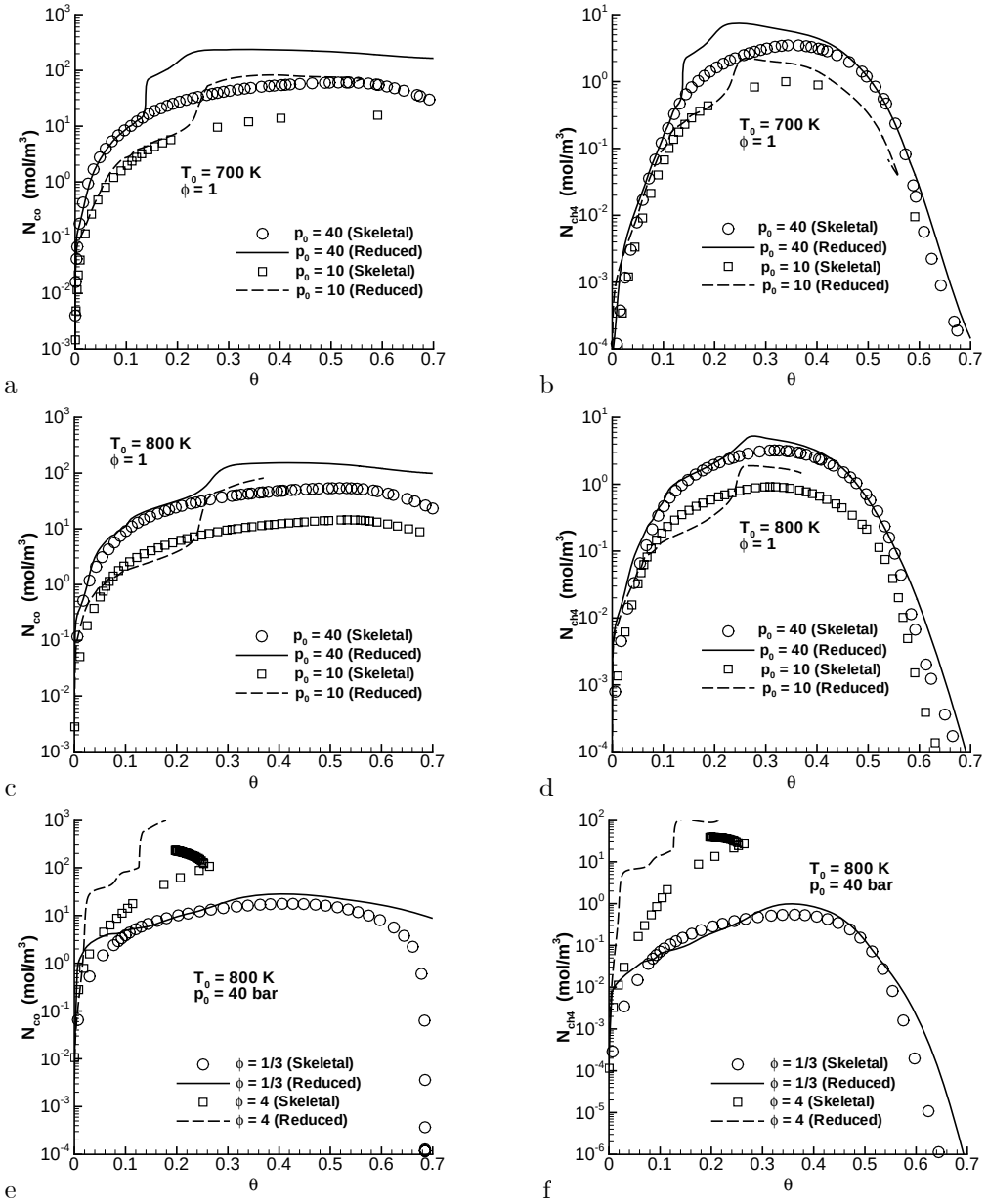

Figure 12. Predictions of the reduced model for N_{co} and N_{ch4} compared to those of the skeletal mechanism at various T_0, p_0 and ϕ conditions.

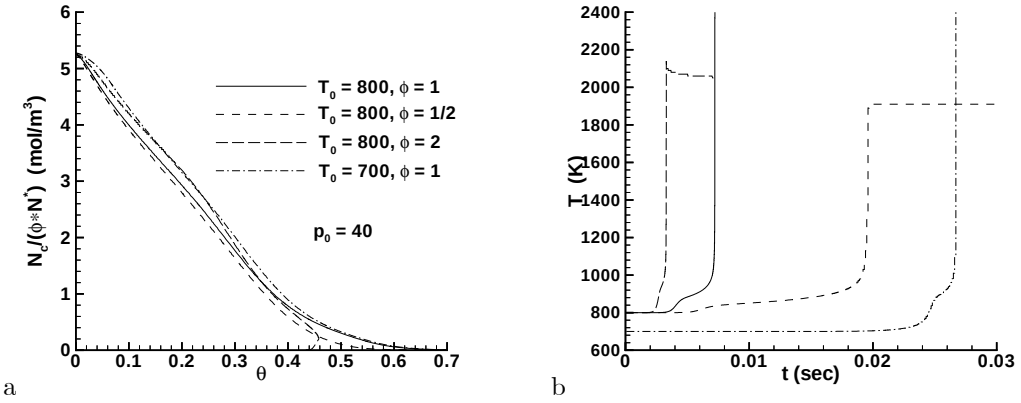

a b

Figure 13. Iso-octane results obtained using the LLNL full mechanism in conjunction with CHEMKIN II: (a) similarity plot of parameter $N_c/(\phi \times N^*)$ versus θ at $p_0 = 40$ bar and (b) T time-wise evolution. T_0 is in K.

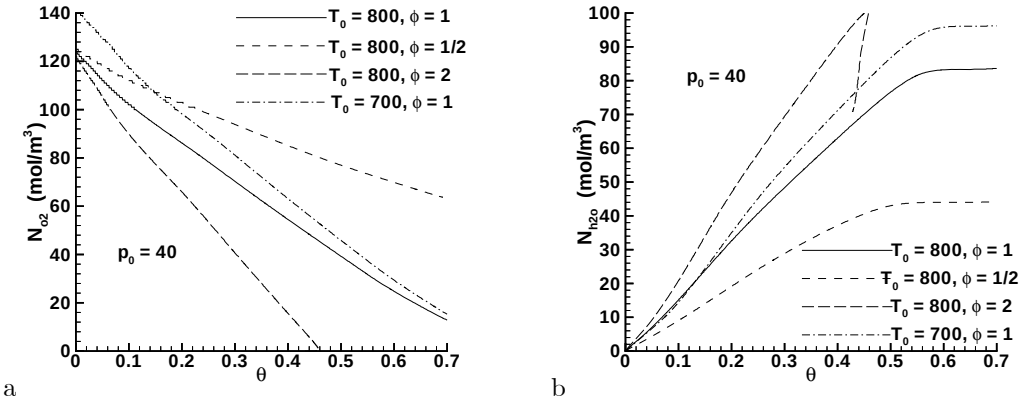

a b

Figure 14. Oxygen and water molar densities versus θ as extracted from the iso-octane LLNL full mechanism in conjunction with CHEMKIN II. p_0 is in bar, T_0 is in K.

APPENDIX 4

Computation of Laminar Premixed Flames Using Reduced Kinetics Based on Constituents and Species

Kenneth G. Harstad[♦,*] and Josette Bellan[♦,**,†]
Jet Propulsion Laboratory[♦], *California Institute of Technology,*
Pasadena CA 91109-8099
California Institute of Technology[**], *Mechanical Engineering, Pasadena, CA 91125*

A model is proposed for quasi-one-dimensional steady flame development in the configuration of an inviscid, premixed fuel jet injected into air. The governing equations are written within the framework of a reduced kinetic model based on constituents and species. The reduced kinetic model, previously exercised in a constant-volume perfectly-stirred reactor mode, has been successful at predicting ignition and combustion product and temperature evolution for n-heptane, iso-octane, PRF fuel combinations, and mixtures of iso-octane with either n-pentane or iso-hexane. The differential governing equations have the option of an axially variable area and they are coupled with a real gas equation of state. The flame development model accounts for a full diffusion matrix, and thermal conductivity computed for the species mixture. Preliminary results are presented.

I. Introduction

To predict the initiation and evolution of turbulent reacting flows in practical devices one must couple chemical kinetics and turbulence models. Because codes resulting from these models are very computationally intensive, the chemical kinetic mechanisms cannot be utilized in their entire complexity and instead they are reduced to mechanisms that are sought to be compact as well as reliable. Recently a reduced kinetic model relying on constituents and species[1,2] has been developed, which was successful in reproducing ignition time, and combustion product and temperature evolution for n-heptane, iso-octane, PRF fuel combinations, and mixtures of iso-octane with either n-pentane or iso-hexane.

In this conceptual model,[1,2] the ensemble of species in a full (or skeletal) mechanism is partitioned into heavies (carbon number, $n \geqslant 3$) and lights (the remaining of the set). The heavies can be either radicals or stable species. The lights are oxygen, nitrogen, the final combustion products and light radicals/molecules (e.g. CH_3, CH_4, H_2O_2). The heavies are not treated as a species set, but as a set of base constituent radicals which correspond to radicals as used in group additivity theory.[3] Sometimes light species are radicals which may have the same chemical formula as constituents, however, the difference between constituents and these light species is that the later are unbound to other chemical entities whereas the former are bound to other chemical entities, i.e. other constituents. For each constituent k, its molar density, N_k, is the sum, over all heavy species, of the count of the constituent in each heavy species multiplied by the molar density of that species. The constituents are not just based on atom counts and their element composition is not linearly independent, however, the constituents are linearly independent. Thus, the constituents are independent structural elements which have individual valence bond topologies.

For each heavy species, and thus for the entire set of heavy species, there is a unique and complete set of constituents. The subset of constituents that have a very small contribution to the total constituent count having molar density N_c, is replaced by the complementary subset of constituents already accounted for in N_c. The rule for replacement is that each constituent having a small contribution to N_c is replaced by one having, first, close valence structure and second, close composition to the constituent neglected. After this

*Senior Engineer.
†Senior Research Scientist, AIAA Fellow (corresponding author, josette.bellan@jpl.nasa.gov).

replacement, one obtains an optimal N_k set. It is this optimal set of constituents that is used in the kinetic reduction.

To test the capability of the reduced kinetic model in the a simple flow model, the first step is to evaluate it in a steady, quasi-one-dimensional configuration before undertaking the more arduous task of the counter-flow configuration for which the overwhelming experimental data has been obtained. This first step is the purpose of this study. In this paper, we first present the governing equations, as they are more general than the typical ones for steady one-dimensional flow which use approximate transport properties and the perfect gas equation of state. Further, we discuss some preliminary results obtained with the model. Finally, we elaborate on the future work necessary before such a model is ready for incorporation in turbulent flow models and codes.

II. Governing equations

The configuration of interest is that of a steady, round jet in a system of coordinates (x, r, θ) where it is assumed that there is uniformity in the θ direction and thus the coordinates of interest are (x, r). The entrance of the jet $(x = 0)$ is labeled by the subscript 0 and the far field boundary is at $x = L$. Within the quasi-one-dimensional framework, all quantities are averaged in the r direction, and thus the jet boundary is located at $r = R(x)$. Therefore, the jet area is $A(x) = \pi R^2(x)$. A quantity $\xi(x) \equiv R_0/R(x)$ is defined to track the jet spacewise variation.

A. Continuity and momentum

We define the mass density ρ, and the axial and radial velocities, u and v. Radial averages are designated by $\overline{()}$, as for example

$$\overline{\rho}(x) = \frac{2}{R^2} \int_0^R \rho(x, r)\ r\ dr. \tag{1}$$

In the entire derivation below, all quantities will be considered as radial averages, but the $\overline{()}$ symbol will be omitted for notation simplicity.

1. *Continuity equation*

Defining the mass flow rate $\dot{M}$, the steady flow assumption implies $\rho u A = \dot{M} = \text{constant}$, which means that

$$\rho u = \dot{M}/A \equiv \dot{M}/\pi R^2(x). \tag{2}$$

Replacing eq. 2 in the steady continuity equation

$$\frac{1}{r}\frac{\partial(r\rho v)}{\partial r} + \frac{\partial(\rho u)}{\partial x} = 0 \tag{3}$$

leads to

$$\rho v = r\frac{\dot{M}}{\pi R^3}\frac{dR}{dx}. \tag{4}$$

2. *Momentum equation*

Under the assumption of an inviscid fluid, the steady momentum equation components are

$$\rho\left(u\frac{\partial}{\partial x} + v\frac{\partial}{\partial r}\right)u + \frac{\partial p}{\partial x} = 0 \tag{5}$$

$$\rho\left(u\frac{\partial}{\partial x} + v\frac{\partial}{\partial r}\right)v + \frac{\partial p}{\partial r} = 0. \tag{6}$$

To make progress in obtaining an equation for the jet area, we expand p and ρ^{-1} in even powers of r (due to symmetry conditions), as a means of taking advantage of the configuration symmetry. Thus, we postulate

that

$$p = p_0 + \frac{1}{2}\rho_0 u_0^2 \sum_{n=0}^{n_{\max}} \sigma_n(x) \frac{r^{2n}}{R^{2n}}, \tag{7}$$

$$\frac{\rho_0}{\rho} = \sum_{n=0}^{n_{\max}} f_n(x) \frac{r^{2n}}{R^{2n}}, \tag{8}$$

where σ_n and f_n are arbitrary functions. Replacing these expressions in eqs. 5 and 6 yields

$$-\frac{1}{2}\frac{d\sigma_n}{dx} = \xi^2 \frac{d(\xi^2 f_n)}{dx} + R_0^2 \frac{d\xi}{dx}\frac{d}{dx}\left(f_{n-1}\frac{d\xi}{dx}\right) \tag{9}$$

$$n\sigma_n = R_0^2 \xi \frac{d}{dx}\left(f_{n-1}\frac{d\xi}{dx}\right) \quad \text{for } n > 0. \tag{10}$$

Combining eqs. 9 and 10 for $n = 1$, leads to

$$2\xi^4 \frac{d(\xi^2 f_1)}{dx} + R_0^2 \frac{d}{dx}\left[\xi^3 \frac{d}{dx}\left(f_0 \frac{d\xi}{dx}\right)\right] = 0. \tag{11}$$

An analysis of eq. 11 provides insights from which further simplifications are obtained. For example, near a stagnation point, which is obtained for $\xi \to 0$, the second term on the left hand side of eq. 11 dominates the first term which can then be neglected. Also, near the $x = 0$ boundary, the jet is nearly radially uniform, which means that $f_1 \doteq 0$. These simple considerations indicate that f_1 can be neglected over the entire length of the jet. More generally, if $x \neq x_a$, where x_a is one of the elements in the set defined by those x values for which $\left|R_0 \frac{d\ln\overline{\rho}}{dx}\right| \ll 1$, the jet area can be computed from

$$\xi \doteq 1 - (1 - \xi_L)\left[\int_0^x \left(\frac{\overline{\rho}}{\rho_0}\right)_{x\neq x_a} dx\right] / \left[\int_0^L \left(\frac{\overline{\rho}}{\rho_0}\right)_{x\neq x_a} dx\right] \tag{12}$$

where ξ_L is the eigenvalue corresponding to the variable $A(x)$ situation. For A constant, none of these considerations apply and the momentum equation becomes a vehicle to compute ∇p, but under the assumption of very small Mach number the pressure is assumed constant for the calculation of the equation of state (EOS).

B. Species and energy equations

The complete formulation for the species and the energy equations has been presented elsewhere.[4] However, that formulation was for species and it is not applicable here where the model is for both constituents and species. In this reduced kinetic model, the evolution of the global constituents molar density is found from input tables and it is only the light-species equations that are progress variables, together with the energy; however, the constituents make contributions to the light, and these contributions must be now formulated in the species equations in terms of the constituents. To this end, we assign indices i, j and q to an ensemble L denoting the lights, k to the ensemble C of the constituents and l, m to the ensemble H of the heavies. Ensemble L is further partitioned into that of the quasi-steady species, LQS, and that of the unsteady species, $LUNS$. All quantities are assumed averaged over the r direction, so there is only a variation with x.

1. *Species equation*

We partition the species molar flux in the light-species governing equation in two categories as $J_{i,light}$ which represents the contributions on light species i of all lights, and $J_{i,heavy}$ which represents contributions on light species i from all heavies

$$J_i = J_{i,light} + J_{i,heavy} \tag{13}$$

$$J_{i,light} = -n\left(X_i D_{T,i}\frac{d\ln T}{dx} + \sum_j \mathcal{D}_{ij}\frac{dX_j}{dx}\right) \tag{14}$$

$$J_{i,heavy} = -n\sum_l \mathcal{D}_{il}\frac{dX_l}{dx} \equiv J_{H,i} \tag{15}$$

where n is the molar density, X is the mole fraction, T is the temperature and quantities $\mathcal{D}_{ij}$ are pairwise diffusion coefficients for the lights that are computable from the binary diffusion coefficients through mixing rules; ways to compute binary diffusion coefficients have been given by Harstad and Bellan[5] and mixing rules were derived by Harstad and Bellan.[6] The term proportional to ∇T includes the entire Soret effect (in J_i the term proportional to ∇p is considered negligible because it is usually small and we additionally make the small Mach number approximation) and it is included in $J_{i,light}$ because, as for $\mathcal{D}_{ij}$, $D_{T,i}$ can be computed using mixing rules. These mixing rules generally include contributions from the heavies, however, since the individual heavies are not individually tracked, we use a single mean heavy species dynamically computed from the injected alkane fuel as it pyrolyses. The goal is now to express $J_{H,i}$ as a function of a constituent equivalent of a mole fraction.

If one considers a constituent N_k, then

$$N_k \equiv \sum_l C_{kl} N_l, \;\; N_c \equiv \sum_k N_k \tag{16}$$

where C_{kl} is the count of constituent k in species l. To find a way of writing the heavies as a function of the constituents, one must invert the matrix of elements C_{kl}. However, because there are fewer equations (i.e. constituents) than unknowns (i.e. heavies), the inversion can only be approximately performed. To perform this inversion, we select the Householder transformation which when utilized, yields

$$\widehat{N}_m = \sum_k \widehat{C}_{mk} N_k \;\; \text{where} \;\; \delta_{ml} = \sum_k \widehat{C}_{mk} C_{kl} \tag{17}$$

with δ_{ml} being the Kronecker symbol. One may interpret $\widehat{N}_m$ as the minimum norm of heavy molar densities for given N_k. This norm favors heaviest species and it is thus most accurate at early times, when diffusion is important. Since $X_l = N_l/n$,

$$J_{H,i} = -\sum_k \left(\sum_l \mathcal{D}_{il} \widehat{C}_{lk} \right) \frac{dN_k}{dx} + \left(\sum_l \mathcal{D}_{il} N_l \right) \frac{d\ln(n)}{dx}. \tag{18}$$

Since ultimately only $N_c \equiv \sum_k N_k$ is available in the model, an additional transformation is needed in the expression of eq. 18. Under the verified assumption that individual dominant constituents of molar density N_k are quasi-steady, it was postulated[1] that there exists a mole fraction XC_k such that $N_k \simeq N_c XC_k$. Therefore,

$$\sum_{l,k} \mathcal{D}_{il} \widehat{C}_{lk} \; XC_k = \frac{1}{N_c} \sum_l \mathcal{D}_{il} \widehat{N}_l = \frac{1}{N_c} \sum_l \mathcal{D}_{il} \left(\sum_k \widehat{C}_{lk} N_k \right). \tag{19}$$

Finally, it is necessary to compute, from the $\mathcal{D}_{il}$ coefficients, a global diffusion coefficient for the term accounting in the formulation for the global constituent molar density. For this purpose, we define

$$\mathcal{D}_{H,i} \equiv \frac{1}{n} \sum_l \mathcal{D}_{il} N_l = \sum_l \mathcal{D}_{il} X_l = X_H \mathcal{D}_{iH} \tag{20}$$

where X_H is the global mole fraction of the heavies and $\mathcal{D}_{iH}$ is a mean diffusion coefficient from the light species i to the ensemble of the heavies. If one defines a mean total constituent count as

$$C_{ave} \equiv \frac{N_c}{n} = \sum_{k,l} C_{kl} X_l, \tag{21}$$

then one may approximate $J_{H,i}$ by

$$J_{H,i} \doteq -n \mathcal{D}_{H,i} \frac{d\ln C_{ave}}{dx}. \tag{22}$$

This leads to

$$J_i = -n \left[\sum_j \mathcal{D}_{ij} \frac{dX_j}{dx} + X_H \mathcal{D}_{iH} \frac{d\ln C_{ave}}{dx} + X_i D_{T,i} \frac{d\ln T}{dx} \right]. \tag{23}$$

To write J_i as a function of mass fraction gradients and take advantage of the partition of the lights set into unsteady and quasi-steady species, we now assign indices i and j to the unsteady light species and q to the quasi-steady light species. Thus the total unsteady mole fraction is

$$X_u = 1 - X_H - \sum_q X_q \tag{24}$$

and the mixture mean mass becomes

$$m = \frac{X_u}{\sum_i \frac{Y_i}{m_i}}. \tag{25}$$

Introducing these definitions in eq. 23 yields

$$\begin{aligned} J_i &= -n\left[\sum_j \mathcal{D}_{ij}\frac{dX_j}{dx} + \sum_q \mathcal{D}_{iq}\frac{dX_q}{dx} + X_H\mathcal{D}_{iH}\frac{d\ln C_{ave}}{dx} + X_i D_{T,i}\frac{d\ln T}{dx}\right] \\ &= -n\left[\mathcal{D}_i^a\frac{dX_u}{dx} + \sum_j(\mathcal{D}_{ij}-\mathcal{D}_i^a)\frac{m}{m_j}\frac{dY_j}{dx} + \sum_q \mathcal{D}_{iq}\frac{dX_q}{dx} + X_H\mathcal{D}_{iH}\frac{d\ln C_{ave}}{dx} + X_i D_{T,i}\frac{d\ln T}{dx}\right] \end{aligned} \tag{26}$$

having used $dX_j = (m/m_j)dY_j + X_j d\ln(m)$ and having defined a mean unsteady-lights mass diffusion coefficient

$$\mathcal{D}_i^a \equiv \frac{1}{X_u}\sum_j \mathcal{D}_{ij}X_j. \tag{27}$$

Writing eq. 26 consistent with the kinetic reduction model[1,2] in which variables X_q, X_H and C_{ave} are obtained from the reduced model as functions of the temperature, so that, for example $dX_H/dx = (\delta X_H/\delta T)(dT/dx)$, leads to

$$J_i = -n\left[\sum_j(\mathcal{D}_{ij}-\mathcal{D}_i^a)\frac{m}{m_j}\frac{dY_j}{dx} + B_{T,i}^e\frac{dT}{dx}\right] \tag{28}$$

where

$$B_{T,i}^e \equiv X_i\frac{D_{T,i}}{T} + \sum_q(\mathcal{D}_{iq}-\mathcal{D}_i^a)\frac{\delta X_q}{\delta T} + X_H\mathcal{D}_{iH}\frac{\delta\ln C_{ave}}{\delta T} - \mathcal{D}_i^a\frac{\delta X_H}{\delta T} \tag{29}$$

acts as an effective Soret coefficient for the reduced model.

Denoting the total reaction rate of species i by $\mathcal{R}_i$, the governing equation for species of mass fraction Y_i is

$$\frac{dY_i}{dx} = \frac{A}{\dot{M}}m_i\mathcal{R}_i - \frac{d}{dx}\left(\frac{A}{\dot{M}}m_i J_i\right). \tag{30}$$

In accordance with the reduced kinetic model

$$\mathcal{R}_i = \mathcal{R}_i|_{lights} + \mathcal{R}_i|_{heavies} \tag{31}$$

where $\mathcal{R}_i|_{lights}$ is computed using CHEMKIN II in conjunction with the LLNL rate data, and $\mathcal{R}_i|_{heavies} = N_c K_{net,i}$ where $K_{net,i}$ is computed by interpolation from tables where it is listed as a function of T for fixed (T_0, p_0, ϕ) with ϕ being the equivalence ratio and subscript 0 denoting initial conditions.

2. Energy equation

We write the energy equation under the assumption that the Dufour effect has a negligible contribution to the heat flux. Additionally, since in our model the heavy species are combined into a single constituent, we approximate the molar enthalpy of all heavy species averaged over the molar fluxes by the enthalpy $h_H = (1/X_H)\sum_l X_l h_l$ which is the mean heavy-species enthalpy based on an average of heavy species molar enthalpies h_l. The result is

$$q \doteq -\lambda\frac{dT}{dx} - \sum_i\left(\frac{m_i}{m_H}h_H - h_i\right)J_i \tag{32}$$

where λ is the mixture thermal conductivity. The energy equation is thus

$$\frac{C_p}{m}\frac{dT}{dx} = \frac{d}{dx}\left(\frac{A}{\dot{M}}\lambda\frac{dT}{dx}\right) - \frac{A}{\dot{M}}\left\{\frac{dT}{dx}\left[\sum_i\left(\frac{C_{p,i}}{m_i} - \frac{C_{p,H}}{m_H}\right)(m_i J_i)\right] + \sum_i h_i\mathcal{R}_i - R_u T_{ref} N_c K_H\right\} \tag{33}$$

where C_p is the heat capacity at constant pressure and K_H is computed by interpolation from tables[2] where it is listed as a function of T for fixed (T_0, p_0, ϕ).

C. Equation of state

The pressure is calculated from the Peng-Robinson (PR) EOS

$$p = \frac{R_u T}{(v_{PR} - b_{mix})} - \frac{a_{mix}}{(v_{PR}^2 + 2b_{mix}v_{PR} - b_{mix}^2)}, \tag{34}$$

where v_{PR} is the molar volume and a_{mix} and b_{mix} are functions of T and X_i (see Appendix A).

D. Transport properties

To derive transport properties consistent with the kinetic model approach, we define an ensemble of all light species and one mole-averaged heavy species: $L \cup H$. Indices p, n and r refer to any species from this ensemble. The transport properties under consideration are the diffusion coefficients $\mathcal{D}_{pn}$, the thermal diffusion factors $D_{T,p}$, and the thermal conductivity; the viscosity does not enter the calculations, since an inviscid situation is assumed, however, because transport property calculations of thermal conductivity and viscosity are very much related, we borrow from methods to compute viscosity in order to compute the thermal conductivity.

For the diffusion coefficients, the first task is to compute the binary diffusion coefficients which are the building blocks of the pairwise diffusion coefficients. To this end, we adopt the method of Harstad and Bellan[5] which gives (in cgs units)

$$nD_{pn} = 2.81\times10^{-5}\frac{f_D(T)}{r_D v_{C,pn}^{2/3}}\left[\left(\frac{1}{m_p} + \frac{1}{m_n}\right)T\right]^{1/2}, \tag{35}$$

where the subscript C denotes the critical state, $f_D(T) \equiv (T_{red})^s$ with $\ln s = \sum_{\alpha=0}^{5} a_\alpha^s (\ln T_{red})^\alpha$ where the a^s vector has elements {-0.84211, -0.32643, -0.10053, 0.07747, 0.0127, -0.00995}, and r_D is a constant $O(1)$ which provides an empirical adjustment for the specifics of the collisional interactions of a selected pair of species. Values of r_D are listed in Harstad and Bellan[5] for species pairs relevant to combustion. The heavy species molar mass is part of the reduced model tables and decreases as the reaction proceeds.

From the D_{pn} 's, the pairwise diffusion coefficients[6] can now be computed using, as an approximation (a truncated series proposed by Ern and Giovangigli[7]),

$$\mathcal{D}_{pr} \doteq X_p\sum_n \widetilde{D}_{pn}\alpha_{D,nr}, \tag{36}$$

$$\widetilde{D}_{pn} = \frac{(1+Y_p)}{X_p}\mathcal{D}_p^*\delta_{pn} + (1-\delta_{pn})\frac{\mathcal{D}_p^*\mathcal{D}_n^*}{D_{pn}} - (\sigma_p\mathcal{D}_p^* + \sigma_n\mathcal{D}_n^*) + \sum_{r=1}^{N}(Y_r\sigma_r\mathcal{D}_r^*), \tag{37}$$

$$\mathcal{D}_p^* \equiv (1-Y_p)\left(\sum_{n\neq p}\frac{X_n}{D_{pn}}\right)^{-1}, \tag{38}$$

$$\sigma_p = \frac{m_p}{m}(1+Y_p) + \sum_{n\neq p}^{N} Y_n\frac{\mathcal{D}_n^*}{D_{pn}}, \tag{39}$$

where the mass diffusion factors are computed as

$$\alpha_{D,pn} = \frac{\partial X_p}{\partial X_n} + X_p\frac{\partial \ln\gamma_p}{\partial X_n} \tag{40}$$

from the EOS, with $\gamma_p \equiv \varphi_p/\varphi_p^o$, where φ is the fugacity coefficient and the superscript o denotes the pure ($X_p = 1$) limit.

According to Harstad and Bellan[6]

$$D_{T,p} \equiv \sum_{n=1}^{N} \left(\sum_{\substack{r=1 \\ r\neq n}}^{N} X_r \zeta_{r\ n}(T_{red,r\ n}) \frac{(m_r \omega_n^T - m_n \omega_r^T)}{(m_r + m_n) D_{r\ n}} \right) X_n \widetilde{D}_{np}, \tag{41}$$

$$\omega_p^T = \frac{\omega_p^Q \lambda_p}{R_u n}, \tag{42}$$

where λ_p is the species p thermal conductivity computed according to eq. 50 and ω_p^Q is a weighting factor given by eq. 45. Factors $\zeta_{r\ n}(T_{red,r\ n})$ are closely related to the temperature derivative of D_{pn} taken at constant pressure,[9] and they are computed from

$$\zeta_{r\ n}(T_{red,r\ n}) = \frac{1}{5} - \frac{2}{5}\left[s_{r\ n} + T_{red,r\ n} \ln(T_{red,r\ n}) \frac{\partial s_{r\ n}}{\partial T_{red,r\ n}} \right], \tag{43}$$

where $T_{red,r\ n}$ is defined in Appendix A.

To compute λ, we use the Wassiljewa-Mason-Saxona method described in Reid et al.,[8]

$$\lambda = \sum_{n \in L \cup H} X_n \omega_n^Q \lambda_n \tag{44}$$

where the weighting factors ω_n^Q are computed as recommended in Reid et al.,[8]

$$(\omega_n^Q)^{-1} = \sum_j \phi_{pn} X_n, \tag{45}$$

$$\phi_{pn} = \frac{\left[1 + \left(\frac{m_n}{m_p}\right)^{1/4} \left(\frac{\eta_p}{\eta_n}\right)^{1/2}\right]^2}{\sqrt{8\left(1 + \frac{m_p}{m_n}\right)}}, \tag{46}$$

where η_p represents the viscosity of species p. To compute the individual species viscosities, we adopt a method explained in Reid et al.[8] whereby

$$\eta_p = \eta_{ref,p}\ f_{R-T}(T_{red,p}), \tag{47}$$

where the subscript $R-T$ stands for "Roy-Thodos" and

$$f_{R-T}(T_{red,p}) = 2.25(\exp(0.0464 T_{red,p}) - \exp(-0.2412 T_{red,p})), \tag{48}$$

$$\eta_{ref,p} = 1.08 \times 10^{-4} (m_p T_{C,p})^{1/2} \left(\frac{Z_{C,p}}{v_{C,p}}\right)^{2/3}. \tag{49}$$

The other ingredient entering the λ calculation is the expression for λ_p which is here computed (in cgs units) using the Stiel-Thodos method (Reid et al.[8]) as

$$\lambda_p = \lambda_{ref,p} \left(f_\lambda f_{R-T}(T_{red,p}) + \frac{1}{Z_{C,p}^5} f_{E,p}(\rho_{red,p}) \right), \tag{50}$$

$$f_\lambda = 3.75 + \frac{\frac{C_p}{R_u} - \frac{5}{2}}{0.7862 - 0.7109\Omega + 1.3168\Omega^2} \tag{51}$$

where f_λ is a function of the acentric factor Ω given by the Chung at al. formula,[8] $f_{R-T}(T_{red,p})$ of eq. 50 accounts for the small ρ_{red} (i.e. kinetic theory) limit whereas $f_{E,p}$ is an excess function of importance for larger ρ_{red}. According to the Stiel-Thodos method,

$$\lambda_{ref,p} = 8.9775 \times 10^3 \left(\frac{T_{C,p}}{m_p}\right)^{1/2} \left(\frac{Z_{C,p}}{v_{C,p}}\right)^{2/3}, \tag{52}$$

$$f_{E,p}(\rho_{red,p}) = 1.223 \times 10^{-2} [\exp(0.535 \rho_{red,p}) - 1]. \tag{53}$$

Properties used in these calculations are provided in Table 1 for n-heptane, iso-octane and all light species and in Table 2 for the quasi-steady radicals. For these latter, estimates of p_C and v_C are made using the group contribution method of Joback (Reid et al.[8]). Then, T_C is estimated assuming $Z_C = 0.28$; the same assumption is made to estimate the p_C, v_C and Ω values in parentheses in Table 1.

III. Numerical method

The equations are solved under the large Péclet number, Pe, assumption which is consistent with using the inviscid momentum equation. Basically, a large Pe value implies that convection dominates diffusion which is the essence of the problem under consideration. If one defines a dimensionless parameter $\varepsilon_i \equiv -m_i J_i/(\rho u)_0$, then one may construct $\varepsilon_i' \equiv -\varepsilon_i/Y_i = \rho u_{D,i}/(\rho u)_0$ where $u_{D,i}$ is the species diffusion velocity. The large Pe value means that $|\varepsilon_i'| \ll 1$.

Three dimensionless parameters are defined

$$\widetilde{T} \equiv \frac{T}{T_{ref}}, \quad \widetilde{A} = \frac{A}{A_0}, \quad \widetilde{C_p} = \frac{C_p}{R_u} \tag{54}$$

along with characteristic chemical kinetic rate-based gradient quantities

$$GYR_i \equiv \frac{m_i \mathcal{R}_i}{(\rho u)_0} \tag{55}$$

$$GTR \equiv \frac{m}{\widetilde{C_p}(\rho u)_0}\left(N_C K_H - \frac{1}{R_u T_{ref}}\sum_{i\in L} h_i \mathcal{R}_i\right) \tag{56}$$

and a characteristic conduction length

$$l_T \equiv \frac{m\lambda}{R_u(\rho u)_0} \tag{57}$$

which is of same order as ε_i. Then, the governing equations become

$$\frac{dY_i}{dx} = \widetilde{A} \times GYR_i + \frac{d(\widetilde{A}\varepsilon_i)}{dx} \tag{58}$$

$$\frac{\widetilde{C_p}}{m}\left(\frac{d\widetilde{T}}{dx} - \widetilde{A} \times GTR\right) = \frac{d}{dx}\left(\frac{\widetilde{A}\, l_T}{m}\frac{d\widetilde{T}}{dx}\right) + \widetilde{A}\frac{d\widetilde{T}}{dx}\sum_{i\in L}\varepsilon_i\left(\frac{\widetilde{C_{p,i}}}{m_i} - \frac{\widetilde{C_{p,H}}}{m_H}\right). \tag{59}$$

The idea is to expand the terms of these equations in function of ε_i and retain only the lowest order terms. Doing so results in

$$\frac{dY_i}{dx} = \widetilde{A} \times (GYR_i + GYD_i) \tag{60}$$

$$\frac{d\widetilde{T}}{dx} = \widetilde{A} \times (GTR + GTD) \tag{61}$$

where quantities GYD_i and GTD are listed in Appendix B.

The equations are solved using a stiff-equations integrator.[17]

IV. Results

Preliminary results are discussed here, obtained for $\widetilde{A} = 1$, so as to be relatable to other simulations described in the literature using this typically made assumption. These results are meant to probe (1) the impact of diffusion with respect to a case where there is no diffusion, and (2) the validity of the large Pe assumption on which the numerical method was constructed. All computations were performed for a fuel that was a mixture of 90% iso-octane and 10% n-heptane, with $(\rho u)_0 = 0.8$ g/cm^2-s and stoichiometric equivalence ratio, i.e. $\phi = 1$.

Figures 1 and 2 illustrate the results without diffusion and with diffusion and Tables 4 and 5 both pertain to simulations performed including diffusion. Without diffusion (fig. 1), the calculation proceeds through

an incubation region and a sharp increase starting at a location , x_{fs}, defined as the flame location (for accounting purposes, x_{fs} occurs at $T_0 + 900$ K). After that location, T increases within a short distance to almost its final value which is in excess of 2800 K. Defining u_{fs} as the characteristic velocity at x_{fs}, without diffusion, $u_{fs} = 120$ cm/s and the value reached for the asymptotic T value is 250 cm/s. With diffusion (fig. 2) it was verified that the large Pe assumption assumption (i.e. $|\varepsilon_i'| \ll 1$) holds in the incubation region. However, as the flame is approached, there is an indication that this assumption is no longer valid. This finding is not unexpected since the flame is inherently a small-scale structure involving very large gradients. As a results of the $|\varepsilon_i'| \ll 1$ assumption breakdown, the calculation stalls at T values or x positions corresponding to past the flame initiation. Values of x_{fs} at two T_0 and three p_0 conditions are listed in Table 4 and the corresponding u_{fs} is listed in Table 5.

V. Conclusions

A model has been developed for simulating quasi-steady quasi-one-dimensional laminar premixed flames in the configuration of a jet injected in air. The model has been derived in the framework consistent with it being used in conjunction with a reduced chemical kinetic model based on constituents and species. As such, the formulation includes the option of a jet variable-area with position, a complete mass-diffusion matrix, and a mixture thermal conductivity computed taking into account the global constituent and all species. Furthermore, a real-gas equation of state is used.

The equations are solved under the large Péclet number assumption. Results show that this assumption is appropriate in the flame incubation region but, not unexpectedly, it breaks down very near the flame. Further efforts will be devoted to enlarging the numerical technique to accommodate both the incubation region and the flame region. Simulations performed devoid of diffusion show that the numerical method can handle the strong reaction region of the flame very well.

Acknowledgements

This study was conducted at the Jet Propulsion Laboratory (JPL), California Institute of Technology (Caltech) and sponsored at Caltech by the Army Research Office under the direction of Dr. Ralph Anthenien.

Appendix A

Miscellaneous relationships relevant to the EOS are

$$a_{mix} = \sum_p \sum_n X_p X_n a_{pn}(T), \quad b_{mix} = \sum_p X_p b_p, \tag{62}$$

where indices do not follow here the Einstein notation, and

$$a_{pn} = (1 - k')\sqrt{\alpha_{pp}\alpha_{nn}}, \tag{63}$$

$$\alpha_{pp}(T) \equiv 0.457236(R_u T_{C,p})^2 \left[1 + c_p(1 - \sqrt{T_{red,p}})\right]^2 / p_{C,p}, \tag{64}$$

$$c_p = 0.37464 + 1.54226\Omega_p - 0.26992\Omega_p^2, \tag{65}$$

where $T_{red,p} \equiv T/T_{C,p}$, $T_{C,p}$ is the critical temperature and Ω_p is the acentric factor. Also,

$$b_p = 0.077796 \frac{R_u T_{C,p}}{p_{C,p}}, \tag{66}$$

$$T_{C,pn} = (1 - k_{pn})\sqrt{T_{C,p} T_{C,n}} \text{ with } k_{pp} = 0, \tag{67}$$

$$v_{C,pn} = \frac{1}{8}\left(v_{C,p}^{1/3} + v_{C,n}^{1/3}\right)^3, \tag{68}$$

$$Z_{C,pn} = \frac{1}{2}(Z_{C,p} + Z_{C,n}), \tag{69}$$

$$p_{C,pn} = \frac{R_u T_{C,pn} Z_{C,pn}}{v_{C,pn}}, \tag{70}$$

with $T_{red,pn} \equiv T/T_{C,pn}, Z_{C,p}$ being the critical compression factor defined as $Z = p/(\rho T R_u/m)$, $v_{C,p}$ being the critical volume, and $p_{C,p}$ being the critical pressure. k_{pn} is an empirical mixing parameter. The relationship between the parameters k_{pn} and k'_{pn} is

$$(1 - k_{pn}) = (1 - k'_{pn}) \frac{(v_{C,p} v_{C,n})^{1/2}}{v_{C,pn}}. \tag{71}$$

Values of k'_{pn} are listed in Table 3, where the values were obtained from Reid et al.[8] or Knapp et al.[10] Otherwise, for pairs involving O_2, N_2, CO, CO_2 or H_2O, $k'_{pn} \simeq 0$.

Appendix B

The coefficients of eqs. 60 and 61 are

$$GTD \doteq \varepsilon_T \times GTR \times (1 + \varepsilon_T + \varepsilon'_T + \varepsilon_T^2 + 3\varepsilon_T \varepsilon'_T + (\varepsilon'_T)^2) \tag{72}$$

$$GYD_i \doteq \sum_{j \in LUNS} (\delta_{ij} + M_{ij}) F_j \tag{73}$$

where

$$\varepsilon_T \equiv \frac{1}{\widetilde{C_p}} \left[l_T \frac{d\widetilde{A}}{dx} + m(\widetilde{A})^2 \frac{\delta\left(\frac{l_T}{m} \times GTR\right)}{\delta \widetilde{T}} + m\widetilde{A} \sum_{i \in L} \left(\frac{\widetilde{C_{p,i}}}{m_i} - \frac{\widetilde{C_{p,H}}}{m_H} \right) \varepsilon_{R,i} + (\widetilde{A})^2 \sum_{j \in LUNS} l_{c,j} \times GYD_j \right], \tag{74}$$

$$\varepsilon_{R,i} \equiv \frac{m_i n}{(\rho u)_0} \widetilde{A} \left[T_{ref} B^e_{T,i} \times GTR + \sum_{j \in LUNS} (\mathcal{D}_{ij} - \mathcal{D}^a_i) \frac{m}{m_j} \times GYR_j \right], \tag{75}$$

$$l_{c,j} \equiv \frac{\rho}{\widetilde{C_p}(\rho u)_0} \sum_{i=L} \left(\widetilde{C_{p,i}} - \frac{m_i}{m_H} \widetilde{C_{p,H}} \right) (\mathcal{D}_{ij} - \mathcal{D}^a_i) \frac{m}{m_j}, \tag{76}$$

$$\varepsilon'_T \equiv (\widetilde{A})^2 \times GTR \times \frac{\rho T_{ref}}{\widetilde{C_p}(\rho u)_0} \sum_{i=L} \left(\widetilde{C_{p,i}} - \frac{m_i}{m_H} \widetilde{C_{p,H}} \right) B^e_{T,i}, \tag{77}$$

$$F_i \equiv \frac{d \ln \widetilde{A}}{dx} \times \varepsilon_{R,i} + \widetilde{A} \times GTR \frac{\delta \varepsilon_{R,i}}{\delta \widetilde{T}}, \tag{78}$$

$$M_{ij} \equiv \frac{m_i n}{(\rho u)_0} \frac{d\widetilde{A}}{dx} (\mathcal{D}_{ij} - \mathcal{D}^a_i) \frac{m}{m_j} \tag{79}$$

In eqs. 74-79, the following replacements were made

$$\frac{d}{dx}\left(\frac{l_T}{m} \frac{d\widetilde{T}}{dx} \right) \quad \text{by} \quad \widetilde{A} \frac{\delta\left(\frac{l_T}{m} \times GTR\right)}{\delta \widetilde{T}} \frac{d\widetilde{T}}{dx}$$

$$\frac{d\varepsilon_{R,i}}{dx} \quad \text{by} \quad \frac{\delta \varepsilon_{R,i}}{\delta \widetilde{T}} \frac{d\widetilde{T}}{dx}$$

and quantities $\delta()/\delta\widetilde{T}$ are numerically calculated using finite differences.

References

[1]K. G. Harstad, J. Bellan, Combustion and Flame 157 (2010) 1594-1609.
[2]K. G. Harstad, J. Bellan, Combustion and Flame 157 (2010) 2184-2197.
[3]S. W. Benson, Thermochemical Kinetics., John Wiley & Sons, Inc., 1968.
[4]N. A. Okong'o, J. Bellan, J. Fluid Mech. 464 (2002)1-34.
[5]K. Harstad and J. Bellan, Ind. & Eng. Chem. Res., 43(2) (2004) 645-654.
[6]K. G. Harstad and J. Bellan, Journal of Chemical Physics, 120(12) (2004) 5664-5673.
[7]A. Ern, V. Giovangigli, Combust. Theory Modelling 2 (1998) 349-372.
[8]R. C. Reid, J. M. Prausnitz, B. E. Poling, The Properties of Gases and Liquids, 4th edition, McGraw-Hill, NY, 1987.

[9]J. O. Hirshfelder, C. F. Curtis, R. B. Bird, Molecular Theory of Gases and Liquids, John Wiley & Sons, Inc., 1954.

[10]H. Knapp, R. Doring, L. Oellrich, U. Plocker, J. M. Prausnitz, DECHMA Chem. Data Series, 6 (1982) DECHMA, Frankfurt.

[11]Lawrence Livermore National Laboratory, http://www-cms.llnl.gov/combustion/combustion2.html.

[12]National Institute of Standards and Technology, Chemistry WebBook; http://webbook.nist.gov/chemistry/.

[13]CRC Handbook of Chemistry and Physics, 86th Ed., D. R. Lide (Ed.-in-Chief), CRC Press, Boca Raton, Fl., 2005 (internet edition).

[14]Gas Research Institute, http://www.me.berkeley.edu/gri-mech/.

[15]NASA Glenn Research Center, http://cea.grc.nasa.gov/.

[16]Lawrence Livermore National Laboratory, http://www-pls.llnl.gov/?url=science_and_technology-chemistry-combustion-ic8h18

[17]www.netlib.org/ode/

Species	m (g/mol)	T_C (K)	p_C (bar)	v_C (cm^3/mol)	Ω
C_7H_{16}	100.2	540.2	27.4	432	0.349
C_8H_{18}	114.23	568.8	24.9	492	0.396
N_2	28.013	126.26	33.4	89.8	0.39
H_2O	18.015	647.3	221	57.1	0.344
CO_2	44.01	304.1	73.8	93.9	0.225
O_2	32.0	154.6	50.43	73.4	0.025
H	1.008	33.15	(12)	64.2	(0.)
H_2	2.016	32.94	12.84	64.3	-0.216
CO	28.01	132.9	35	93.2	0.066
CH_4	16.04	190.6	45.94	99.2	0.0108
H_2O_2	34.015	728	220	(77)	(0.1)
C_2H_2	26.04	308.3	61.4	112.7	0.19
C_2H_4	28.054	282.4	50.4	130.4	0.089
CH_2O	30.026	408	65.9	(144)	0.253

Table 1. Fuel and unsteady light species properties.

Radicals	m (g/mol)	T_C (K)	p_C (bar)	v_C (cm^3/mol)	Ω
O	16.0	116	76	35	0.
CH	13.02	183	73	58	0.
CH_2	14.027	210	66	73	0.
CH_3	15.034	221	62	82	0.
OH	17.01	167	85	45	0.
HCO	29.02	299	70	99	0.25
OOH	33.01	226	83	63	0.
HC_2	25.03	291	67	100	0.2
C_2H_3	27.044	292	57	119	0.1

Table 2. Quasi-steady radicals properties.

p	n	k'
alkane	alkane	0.0
alkane	N_2, O_2	0.15
alkane	CO_2	0.11
alkane	H_2O	0.093-0.006n_c
alkane	H_2	0.099n_c-0.81
H_2	N_2, O_2	0.12
H_2	CO_2	-0.162
CO_2	H_2O	0.095
CO_2	N_2, O_2	-0.017
H_2O	N_2, O_2	0.17

Table 3. Values of $k^{'}$ for species pairs. n_c is the number of C atoms in the species.

p_0, bar / T, K	20	30	40
700	2.39	1.36	0.9
800	0.9	0.4	0.2

Table 4. Flame position, x_{fs} (cm) for stoichiometric conditions and simulations including diffusion.

p_0, bar / T, K	20	30	40
700	118	88	64.4
800	132	91	73.4

Table 5. Characteristic speed (cm/s) at x_{fs} for stoichiometric conditions and simulations including diffusion.

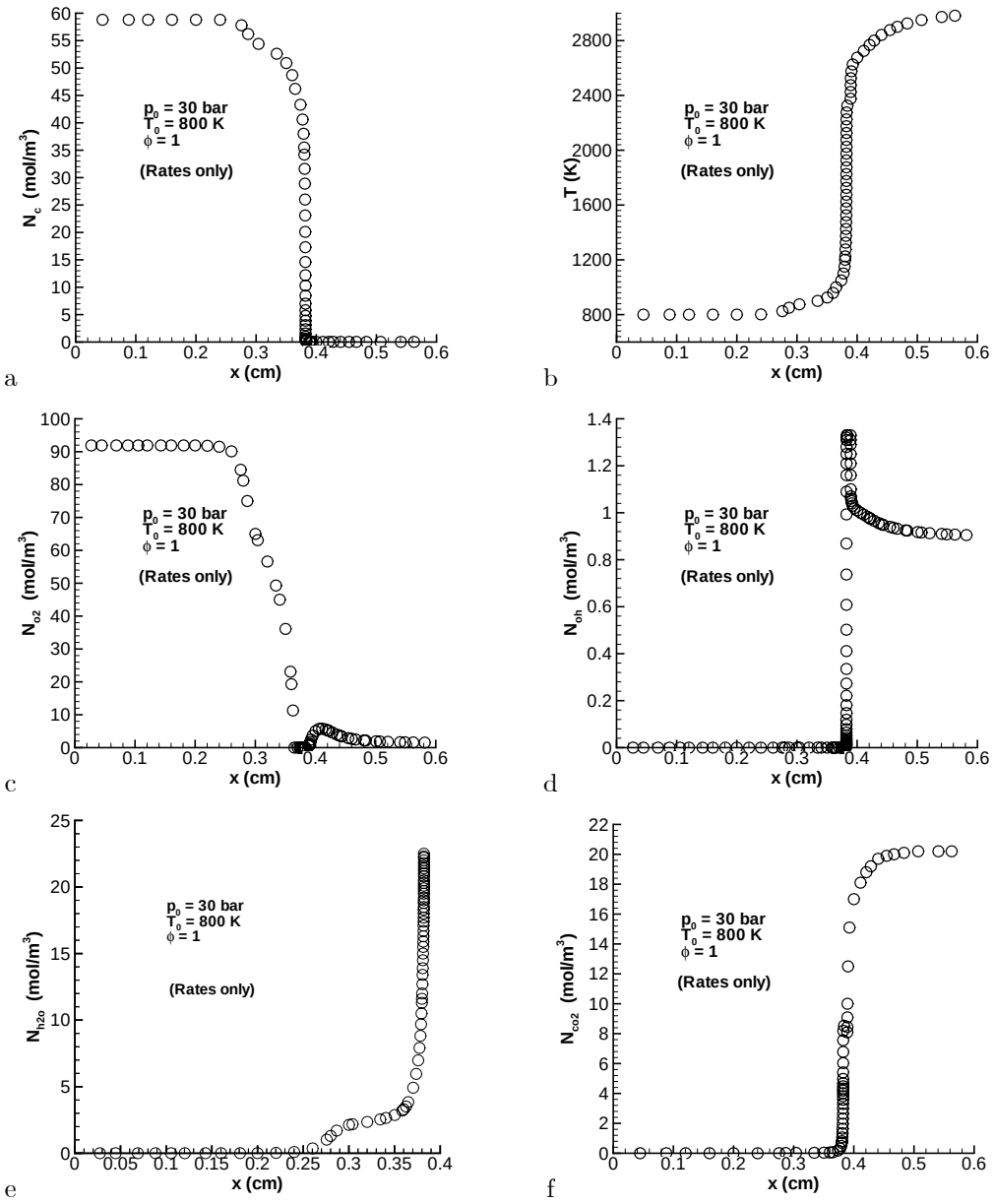

Figure 1. Predictions of the reduced model without diffusion at $p_0 = 30$ bar, $T_0 = 800$ K and $\phi = 1$ conditions.

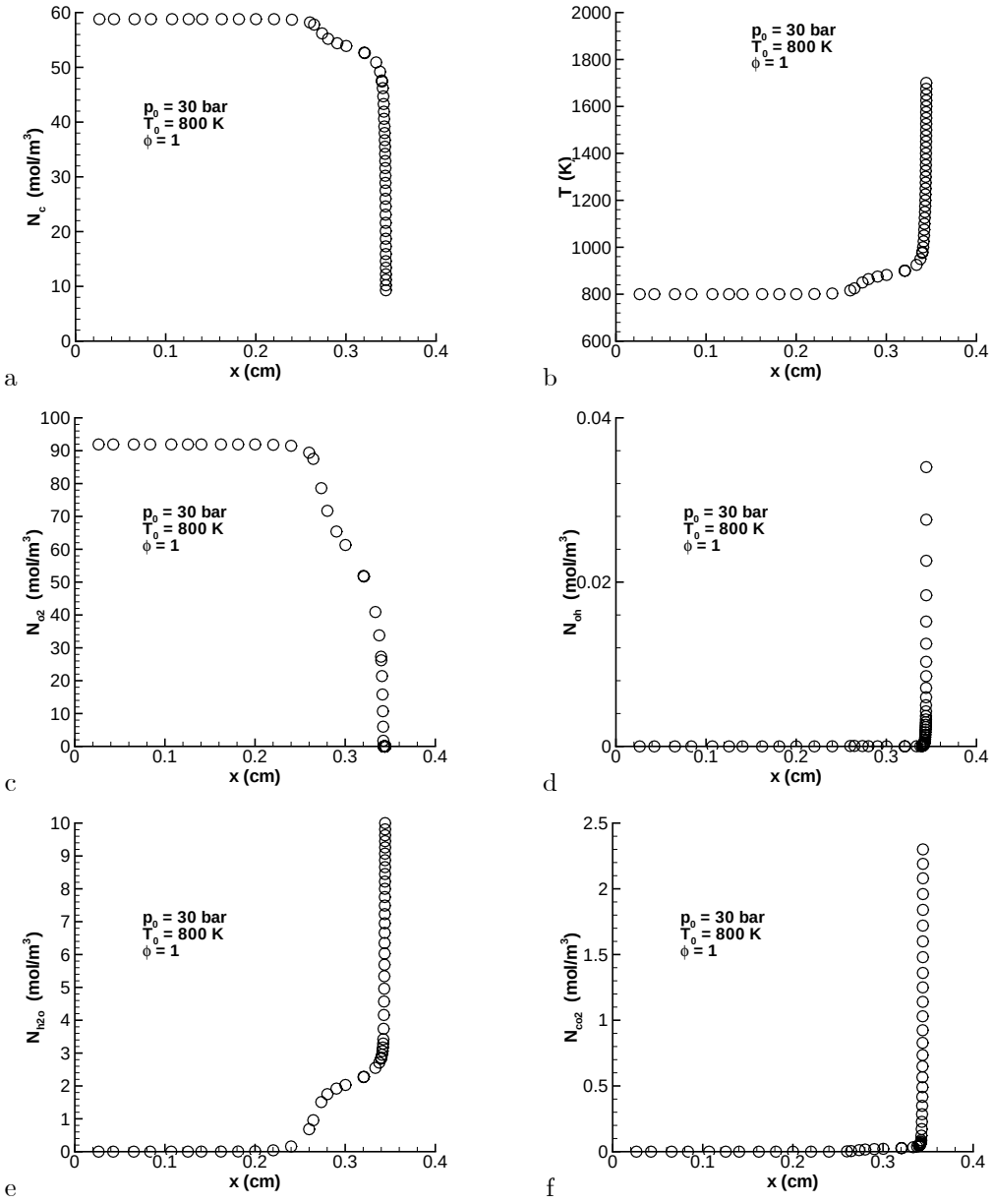

Figure 2. Predictions of the reduced model with diffusion at $p_0 = 30$ bar, $T_0 = 800$ K and $\phi = 1$ conditions.

APPENDIX 5

Modeling of Steady Laminar Flames for One-dimensional Premixed Jets of Heptane/Air and Octane/Air Mixtures

Kenneth G. Harstad[♦,*] and Josette Bellan[♦,**,†]
Jet Propulsion Laboratory[♦], *California Institute of Technology, Pasadena CA 91109-8099*
California Institute of Technology[**], *Mechanical Engineering, Pasadena, CA 91125*

A model is proposed for quasi-one-dimensional steady flame development in the configuration of an inviscid, premixed fuel jet injected into air. The governing equations are written within the framework of a reduced kinetic model based on constituents and species. The reduced kinetic model, previously exercised in a constant-volume perfectly-stirred reactor mode, has been successful at predicting ignition and combustion product and temperature evolution for n-heptane, iso-octane, PRF fuel combinations, and mixtures of iso-octane with either n-pentane or iso-hexane. The differential governing equations have the option of an axially variable area and they are coupled with a real gas equation of state. The flame development model accounts for a full diffusion matrix, and thermal conductivity computed for the species mixture. Results from four simulations at various conditions are presented.

I. Introduction

To predict the initiation and evolution of turbulent reacting flows in practical devices one must couple chemical kinetics and turbulence models. Because codes resulting from these models are very computationally intensive, the chemical kinetic mechanisms cannot be utilized in their entire complexity and instead they are reduced to mechanisms that are sought to be compact as well as reliable. Recently a reduced kinetic model relying on constituents and species[1,2] has been developed, which was successful in reproducing ignition time, and combustion product and temperature evolution for n-heptane, iso-octane, PRF fuel combinations, and mixtures of iso-octane with either n-pentane or iso-hexane.

In this conceptual model,[1,2] the ensemble of species in a full (or skeletal) mechanism is partitioned into heavies (carbon number, $n \geqslant 3$) and lights (the remaining of the set). The heavies can be either radicals or stable species. The lights are oxygen, nitrogen, the final combustion products and light radicals/molecules (e.g. CH_3, CH_4, H_2O_2). The heavies are not treated as a species set, but as a set of base constituent radicals which correspond to radicals as used in group additivity theory.[3] Sometimes light species are radicals which may have the same chemical formula as constituents, however, the difference between constituents and these light species is that the later are unbound to other chemical entities whereas the former are bound to other chemical entities, i.e. other constituents. For each constituent k, its molar density, N_k, is the sum, over all heavy species, of the count of the constituent in each heavy species multiplied by the molar density of that species. The constituents are not just based on atom counts and their element composition is not linearly independent, however, the constituents are linearly independent. Thus, the constituents are independent structural elements which have individual valence bond topologies.

For each heavy species, and thus for the entire set of heavy species, there is a unique and complete set of constituents. The subset of constituents that have a very small contribution to the total constituent count having molar density N_c, is replaced by the complementary subset of constituents already accounted for in

*Senior Engineer.
†Senior Research Scientist, AIAA Fellow (corresponding author, josette.bellan@jpl.nasa.gov).

N_c. The rule for replacement is that each constituent having a small contribution to N_c is replaced by one having, first, close valence structure and second, close composition to the constituent neglected. After this replacement, one obtains an optimal N_k set. It is this optimal set of constituents that is used in the kinetic reduction.

To test the capability of the reduced kinetic model in the a simple flow model, the first step is to evaluate it in a steady, quasi-one-dimensional configuration before undertaking the more arduous task of the counter-flow configuration for which the overwhelming experimental data has been obtained. We first present the governing equations, as they are more general than the typical ones for steady quasi-one-dimensional flow; in particular we use here accurate transport properties and a real-gas equation of state. Further, we discuss some results obtained with the model and then present a concise summary and conclusions.

II. Governing equations

The configuration of interest is that of a steady, round jet in a system of coordinates (x, r, θ) where it is assumed that there is uniformity in the θ direction and thus the coordinates of interest are (x, r). The entrance of the jet $(x = 0)$ is labeled by the subscript 0 and the far field boundary is at $x = L$. Within the quasi-one-dimensional framework, all quantities are averaged in the r direction, and thus the jet boundary is located at $r = R(x)$. Therefore, the jet area is $A(x) = \pi R^2(x)$. A quantity $\xi(x) \equiv R_0/R(x)$ is defined to track the jet spacewise variation.

A. Continuity and momentum

We define the mass density ρ, and the axial and radial velocities, u and v. Radial averages are designated by $\overline{()}$, as for example

$$\overline{\rho}(x) = \frac{2}{R^2} \int_0^R \rho(x, r)\ r\ dr. \tag{1}$$

In the entire derivation below, all quantities will be considered as radial averages, but the $\overline{()}$ symbol will be omitted for notation simplicity.

1. *Continuity equation*

Defining the mass flow rate $\dot{M}$, the steady flow assumption implies $\rho u A = \dot{M} = \text{constant}$, which means that

$$\rho u = \dot{M}/A \equiv \dot{M}/\pi R^2(x). \tag{2}$$

Replacing eq. 2 in the steady continuity equation

$$\frac{1}{r}\frac{\partial(r\rho v)}{\partial r} + \frac{\partial(\rho u)}{\partial x} = 0 \tag{3}$$

leads to

$$\rho v = r\frac{\dot{M}}{\pi R^3}\frac{dR}{dx}. \tag{4}$$

2. *Momentum equation*

Under the assumption of an inviscid fluid, the steady momentum equation components are

$$\rho\left(u\frac{\partial}{\partial x} + v\frac{\partial}{\partial r}\right)u + \frac{\partial p}{\partial x} = 0 \tag{5}$$

$$\rho\left(u\frac{\partial}{\partial x} + v\frac{\partial}{\partial r}\right)v + \frac{\partial p}{\partial r} = 0. \tag{6}$$

To make progress in obtaining an equation for the jet area, we expand p and ρ^{-1} in even powers of r (due to symmetry conditions), as a means of taking advantage of the configuration symmetry. Thus, we postulate

that

$$p = p_0 + \frac{1}{2}\rho_0 u_0^2 \sum_{n=0}^{n_{\max}} \sigma_n(x) \frac{r^{2n}}{R^{2n}}, \tag{7}$$

$$\frac{\rho_0}{\rho} = \sum_{n=0}^{n_{\max}} f_n(x) \frac{r^{2n}}{R^{2n}}, \tag{8}$$

where σ_n and f_n are arbitrary functions. Replacing these expressions in eqs. 5 and 6 yields

$$-\frac{1}{2}\frac{d\sigma_n}{dx} = \xi^2 \frac{d(\xi^2 f_n)}{dx} + R_0^2 \frac{d\xi}{dx}\frac{d}{dx}\left(f_{n-1}\frac{d\xi}{dx}\right) \tag{9}$$

$$n\sigma_n = R_0^2 \xi \frac{d}{dx}\left(f_{n-1}\frac{d\xi}{dx}\right) \quad \text{for } n > 0. \tag{10}$$

Combining eqs. 9 and 10 for $n = 1$, leads to

$$2\xi^4 \frac{d(\xi^2 f_1)}{dx} + R_0^2 \frac{d}{dx}\left[\xi^3 \frac{d}{dx}\left(f_0 \frac{d\xi}{dx}\right)\right] = 0. \tag{11}$$

An analysis of eq. 11 provides insights from which further simplifications are obtained. For example, near a stagnation point, which is obtained for $\xi \to 0$, the second term on the left hand side of eq. 11 dominates the first term which can then be neglected. Also, near the $x = 0$ boundary, the jet is nearly radially uniform, which means that $f_1 \doteq 0$. These simple considerations indicate that f_1 can be neglected over the entire length of the jet. To analyze the last term of eq. 11, we define

$$\xi^2 = 1 - k \int_0^x \zeta(x') \frac{\rho(x')}{\rho_0} x' dx' \tag{12}$$

where k is determined by the downstream boundary condition and is therefore constant. Then, the last term of eq. 11 contains

$$\xi^3 \frac{d}{dx}\left(\frac{\rho_0}{\rho}\frac{d\xi}{dx}\right) = -\frac{k}{2}\xi^2 x \frac{d\zeta}{dx} - \frac{k}{2}\zeta\left[1 + k\left(\frac{1}{2}x^2\zeta\frac{\rho}{\rho_0} - \int_0^x \zeta(x')\frac{\rho(x')}{\rho_0}x'dx'\right)\right]. \tag{13}$$

Outside of the flame, $(\rho/\rho_0) \approx 1$, which together with the fact that the right hand side of eq. 11 must be constant, leads to assuming that ζ is constant. This implies that the right hand side of eq. 13, i.e. $(-k\zeta/2)$ is also nearly constant. To remove the ambiguity of dealing with the product of two constants, we take $\zeta = 1$ which is a good approximation for satisfying eq. 11**.** In the flame region, $\rho/\rho_0 < 1$; for fixed p, its typical (or mean) value is that of $T_0/T \approx 1/4$ found in flames. However, the flame thickness is small, and a value of $\zeta \neq 1$ but varying weakly may be used in this region since the right hand side of eq. 11 will still be nearly constant. For the results presented in section IV, the deviation of ζ from unity was $O(10^{-2})$.

For A constant, none of these considerations apply and the momentum equation becomes a vehicle to compute ∇p, but under the assumption of very small Mach number the pressure is assumed constant for the calculation of the equation of state (EOS).

B. Species and energy equations

The complete formulation for the species and the energy equations has been presented elsewhere.[4] However, that formulation was for species and it is not applicable here where the model is for both constituents and species. In this reduced kinetic model, the evolution of the global constituents molar density is found from input tables and it is only the light-species equations that are progress variables, together with the energy; however, the constituents make contributions to the light, and these contributions must be now formulated in the species equations in terms of the constituents. To this end, we assign indices i, j and q to an ensemble L denoting the lights, k to the ensemble C of the constituents and l, m to the ensemble H of the heavies. Ensemble L is further partitioned into that of the quasi-steady species, LQS, and that of the unsteady species, $LUNS$. All quantities are assumed averaged over the r direction, so there is only a variation with x.

1. Species equation

We partition the species molar flux in the light-species governing equation in two categories as $J_{i,light}$ which represents the contributions on light species i of all lights, and $J_{i,heavy}$ which represents contributions on light species i from all heavies

$$J_i = J_{i,light} + J_{i,heavy} \tag{14}$$

$$J_{i,light} = -n\left(X_i D_{T,i}\frac{d\ln T}{dx} + \sum_j \mathcal{D}_{ij}\frac{dX_j}{dx}\right) \tag{15}$$

$$J_{i,heavy} = -n\sum_l \mathcal{D}_{il}\frac{dX_l}{dx} \equiv J_{H,i} \tag{16}$$

where n is the molar density, X is the mole fraction, T is the temperature and quantities $\mathcal{D}_{ij}$ are pairwise diffusion coefficients for the lights that are computable from the binary diffusion coefficients through mixing rules; ways to compute binary diffusion coefficients have been given by Harstad and Bellan[5] and mixing rules were derived by Harstad and Bellan.[6] The term proportional to ∇T includes the entire Soret effect (in J_i the term proportional to ∇p is considered negligible because it is usually small and we additionally make the small Mach number approximation) and the Soret effect is included in $J_{i,light}$ because, as for $\mathcal{D}_{ij}$, $D_{T,i}$ can be computed using mixing rules. These mixing rules generally include contributions from the heavies, however, since the individual heavies are not individually tracked, we use a single mean heavy species dynamically computed from the injected alkane fuel as it pyrolyses. The goal is now to express $J_{H,i}$ as a function of a constituent equivalent of a mole fraction.

If one considers a constituent N_k, then

$$N_k \equiv \sum_l C_{kl}N_l,\ \ N_c \equiv \sum_k N_k \tag{17}$$

where C_{kl} is the count of constituent k in species l. To find a way of writing the heavies as a function of the constituents, one must invert the matrix of elements C_{kl}. However, because there are fewer equations (i.e. constituents) than unknowns (i.e. heavies), the inversion can only be approximately performed. To perform this inversion, we select the Householder transformation which when utilized, yields

$$\widehat{N}_m = \sum_k \widehat{C}_{mk}N_k \ \text{ where } \ \delta_{ml} = \sum_k \widehat{C}_{mk}C_{kl} \tag{18}$$

with δ_{ml} being the Kronecker symbol. One may interpret $\widehat{N}_m$ as the minimum norm of heavy molar densities for given N_k. This norm favors heaviest species and it is thus most accurate at early times, when heavy species diffusion is important. Since $X_l = N_l/n$,

$$J_{H,i} = -\sum_k \left(\sum_l \mathcal{D}_{il}\widehat{C}_{lk}\right)\frac{dN_k}{dx} + \left(\sum_l \mathcal{D}_{il}N_l\right)\frac{d\ln(n)}{dx}. \tag{19}$$

Since ultimately only $N_c \equiv \sum_k N_k$ is available in the model, an additional transformation is needed in the expression of eq. 19. Under the verified assumption that individual dominant constituents of molar density N_k are mostly quasi-steady, it was postulated[1] that there exists a mole fraction XC_k such that $N_k \simeq N_c XC_k$. Therefore,

$$\sum_{l,k} \mathcal{D}_{il}\widehat{C}_{lk}\ XC_k = \frac{1}{N_c}\sum_l \mathcal{D}_{il}\widehat{N}_l = \frac{1}{N_c}\sum_l \mathcal{D}_{il}\left(\sum_k \widehat{C}_{lk}N_k\right). \tag{20}$$

Finally, it is necessary to compute, from the $\mathcal{D}_{il}$ coefficients, a global diffusion coefficient for the term accounting in the formulation for the global constituent molar density. For this purpose, we define

$$\mathcal{D}_{H,i} \equiv \frac{1}{n}\sum_l \mathcal{D}_{il}N_l = \sum_l \mathcal{D}_{il}X_l = X_H\mathcal{D}_{iH} \tag{21}$$

where X_H is the global mole fraction of the heavies and $\mathcal{D}_{iH}$ is a mean diffusion coefficient from the light species i to the ensemble of the heavies. If one defines a mean total constituent count as

$$C_{ave} \equiv \frac{N_c}{n} = \sum_{k,l} C_{kl} X_l, \tag{22}$$

then one may approximate $J_{H,i}$ by

$$J_{H,i} \doteq -n\mathcal{D}_{H,i} \frac{d\ln C_{ave}}{dx}. \tag{23}$$

This leads to

$$J_i = -n \left[\sum_j \mathcal{D}_{ij} \frac{dX_j}{dx} + X_H \mathcal{D}_{iH} \frac{d\ln C_{ave}}{dx} + X_i D_{T,i} \frac{d\ln T}{dx} \right]. \tag{24}$$

To write J_i as a function of mass fraction gradients and take advantage of the partition of the lights set into unsteady and quasi-steady species, we now assign indices i and j to the unsteady light species and q to the quasi-steady light species. Thus the total unsteady mole fraction is

$$X_u = 1 - X_H - \sum_q X_q \tag{25}$$

and the mixture mean mass becomes

$$m = \frac{X_u}{\sum_i \frac{Y_i}{m_i}}. \tag{26}$$

Introducing these definitions in eq. 24 yields

$$\begin{aligned} J_i &= -n \left[\sum_j \mathcal{D}_{ij} \frac{dX_j}{dx} + \sum_q \mathcal{D}_{iq} \frac{dX_q}{dx} + X_H \mathcal{D}_{iH} \frac{d\ln C_{ave}}{dx} + X_i D_{T,i} \frac{d\ln T}{dx} \right] \\ &= -n \left[\mathcal{D}_i^a \frac{dX_u}{dx} + \sum_j (\mathcal{D}_{ij} - \mathcal{D}_i^a) \frac{m}{m_j} \frac{dY_j}{dx} + \sum_q \mathcal{D}_{iq} \frac{dX_q}{dx} + X_H \mathcal{D}_{iH} \frac{d\ln C_{ave}}{dx} + X_i D_{T,i} \frac{d\ln T}{dx} \right] \end{aligned} \tag{27}$$

having used $dX_j = (m/m_j)dY_j + X_j d\ln(m)$ and having defined a mean unsteady-lights mass diffusion coefficient

$$\mathcal{D}_i^a \equiv \frac{1}{X_u} \sum_j \mathcal{D}_{ij} X_j. \tag{28}$$

Writing eq. 27 consistent with the kinetic reduction model[1,2] in which variables X_q, X_H and C_{ave} are obtained from the reduced model as functions of the temperature, so that, for example $dX_H/dx = (\delta X_H/\delta T)(dT/dx)$, leads to

$$J_i = -n \left[\sum_j (\mathcal{D}_{ij} - \mathcal{D}_i^a) \frac{m}{m_j} \frac{dY_j}{dx} + B_{T,i}^e \frac{dT}{dx} \right] \tag{29}$$

where

$$B_{T,i}^e \equiv X_i \frac{D_{T,i}}{T} + \sum_q (\mathcal{D}_{iq} - \mathcal{D}_i^a) \frac{\delta X_q}{\delta T} + X_H \mathcal{D}_{iH} \frac{\delta \ln C_{ave}}{\delta T} - \mathcal{D}_i^a \frac{\delta X_H}{\delta T} \tag{30}$$

acts as an effective Soret coefficient for the reduced model.

Denoting the total reaction rate of species i by $\mathcal{R}_i$, the governing equation for species of mass fraction Y_i is

$$\frac{dY_i}{dx} = \frac{A}{\dot{M}} m_i \mathcal{R}_i - \frac{d}{dx} \left(\frac{A}{\dot{M}} m_i J_i \right). \tag{31}$$

In accordance with the reduced kinetic model

$$\mathcal{R}_i = \mathcal{R}_i|_{lights} + \mathcal{R}_i|_{heavies} \tag{32}$$

where $\mathcal{R}_i|_{lights}$ is computed using CHEMKIN II in conjunction with the LLNL rate data, and $\mathcal{R}_i|_{heavies} = N_c K_{net,i}$ where $K_{net,i}$ is computed by interpolation from tables where it is listed as a function of T for fixed (T_0, p_0, ϕ) with ϕ being the equivalence ratio and subscript 0 denoting initial conditions.

2. Energy equation

We write the energy equation under the assumption that the Dufour effect has a negligible contribution to the heat flux. Additionally, since in our model the heavy species are combined into a single constituent, we approximate the molar enthalpy of all heavy species averaged over the molar fluxes by the enthalpy $h_H = (1/X_H)\sum_l X_l h_l$ which is the mean heavy-species enthalpy based on an average of heavy species molar enthalpies h_l. The result is

$$q \doteq -\lambda \frac{dT}{dx} - \sum_i \left(\frac{m_i}{m_H} h_H - h_i \right) J_i \tag{33}$$

where λ is the mixture thermal conductivity. The energy equation is thus

$$\frac{C_p}{m}\frac{dT}{dx} = \frac{d}{dx}\left(\frac{A}{\dot{M}} \lambda \frac{dT}{dx} \right) - \frac{A}{\dot{M}} \left\{ \frac{dT}{dx} \left[\sum_i \left(\frac{C_{p,i}}{m_i} - \frac{C_{p,H}}{m_H} \right) (m_i J_i) \right] + \sum_i h_i \mathcal{R}_i - R_u T_{ref} N_c K_H \right\} \tag{34}$$

where C_p is the heat capacity at constant pressure and K_H is computed by interpolation from tables[2] where it is listed as a function of T for fixed (T_0, p_0, ϕ).

C. Equation of state

The pressure is calculated from the Peng-Robinson (PR) EOS

$$p = \frac{R_u T}{(v_{PR} - b_{mix})} - \frac{a_{mix}}{(v_{PR}^2 + 2 b_{mix} v_{PR} - b_{mix}^2)}, \tag{35}$$

where v_{PR} is the molar volume and a_{mix} and b_{mix} are functions of T and X_i (see Appendix A).

D. Transport properties

To derive transport properties consistent with the kinetic model approach, we define an ensemble of all light species and one mole-averaged heavy species: $L \cup H$. Indices p, n and r refer to any species from this ensemble. The transport properties under consideration are the diffusion coefficients $\mathcal{D}_{pn}$, the thermal diffusion factors $D_{T,p}$, and the thermal conductivity; the viscosity does not enter the calculations, since an inviscid situation is assumed, however, because transport property calculations of thermal conductivity and viscosity are very much related, we borrow from methods to compute viscosity in order to compute the thermal conductivity.

For the diffusion coefficients, the first task is to compute the binary diffusion coefficients which are the building blocks of the pairwise diffusion coefficients. To this end, we adopt the method of Harstad and Bellan[5] which gives (in cgs units)

$$n D_{pn} = 2.81 \times 10^{-5} \frac{f_D(T)}{r_D v_{C,pn}^{2/3}} \left[\left(\frac{1}{m_p} + \frac{1}{m_n} \right) T \right]^{1/2}, \tag{36}$$

where the subscript C denotes the critical state, $f_D(T) \equiv (T_{red})^s$ with $\ln s = \sum_{\alpha=0}^{5} a_\alpha^s (\ln T_{red})^\alpha$ where the a^s vector has elements {-0.84211, -0.32643, -0.10053, 0.07747, 0.0127, -0.00995}, and r_D is a constant $O(1)$ which provides an empirical adjustment for the specifics of the collisional interactions of a selected pair of species. Values of r_D are listed in Harstad and Bellan[5] for species pairs relevant to combustion. The heavy species molar mass is part of the reduced model tables and decreases as the reaction proceeds.

From the D_{pn} 's, the pairwise diffusion coefficients[6] can now be computed using, as an approximation (a

truncated series proposed by Ern and Giovangigli[7]),

$$\mathcal{D}_{pr} \doteq X_p \sum_n \widetilde{D}_{pn}\alpha_{D,nr}, \tag{37}$$

$$\widetilde{D}_{pn} = \frac{(1+Y_p)}{X_p}\mathcal{D}^*_p\delta_{pn} + (1-\delta_{pn})\frac{\mathcal{D}^*_p\mathcal{D}^*_n}{D_{pn}} - (\sigma_p\mathcal{D}^*_p + \sigma_n\mathcal{D}^*_n) + \sum_{r=1}^{N}(Y_r\sigma_r\mathcal{D}^*_r), \tag{38}$$

$$\mathcal{D}^*_p \equiv (1-Y_p)\left(\sum_{n\neq p}\frac{X_n}{D_{pn}}\right)^{-1}, \tag{39}$$

$$\sigma_p = \frac{m_p}{m}(1+Y_p) + \sum_{n\neq p}^{N} Y_n\frac{\mathcal{D}^*_n}{D_{pn}}, \tag{40}$$

where the mass diffusion factors are computed as

$$\alpha_{D,pn} = \frac{\partial X_p}{\partial X_n} + X_p\frac{\partial \ln\gamma_p}{\partial X_n} \tag{41}$$

from the EOS, with $\gamma_p \equiv \varphi_p/\varphi^o_p$, where φ is the fugacity coefficient and the superscript o denotes the pure ($X_p = 1$) limit.

According to Harstad and Bellan[6]

$$D_{T,p} \equiv \sum_{n=1}^{N}\left(\sum_{\substack{r=1\\r\neq n}}^{N} X_r\zeta_{r\ n}(T_{red,r\ n})\frac{(m_r\omega^T_n - m_n\omega^T_r)}{(m_r+m_n)D_{r\ n}}\right)X_n\widetilde{D}_{np}, \tag{42}$$

$$\omega^T_p = \frac{\omega^Q_p\lambda_p}{R_u n}, \tag{43}$$

where λ_p is the species p thermal conductivity computed according to eq. 51 and ω^Q_p is a weighting factor given by eq. 46. Factors $\zeta_{r\ n}(T_{red,r\ n})$ are closely related to the temperature derivative of D_{pn} taken at constant pressure,[8] and they are computed from

$$\zeta_{r\ n}(T_{red,r\ n}) = \frac{1}{5} - \frac{2}{5}\left[s_{r\ n} + T_{red,r\ n}\ln(T_{red,r\ n})\frac{\partial s_{r\ n}}{\partial T_{red,r\ n}}\right], \tag{44}$$

where $T_{red,r\ n}$ is defined in Appendix A.

To compute λ, we use the Wassiljewa-Mason-Saxona method described in Reid et al.,[9]

$$\lambda = \sum_{n\in L\cup H} X_n\omega^Q_n\lambda_n \tag{45}$$

where the weighting factors ω^Q_n are computed as recommended in Reid et al.,[9]

$$(\omega^Q_n)^{-1} = \sum_j \phi_{pn}X_n, \tag{46}$$

$$\phi_{pn} = \frac{\left[1+\left(\frac{m_n}{m_p}\right)^{1/4}\left(\frac{\eta_p}{\eta_n}\right)^{1/2}\right]^2}{\sqrt{8\left(1+\frac{m_p}{m_n}\right)}}, \tag{47}$$

where η_p represents the viscosity of species p. To compute the individual species viscosities, we adopt a method explained in Reid et al.[9] whereby

$$\eta_p = \eta_{ref,p}\ f_{R-T}(T_{red,p}), \tag{48}$$

where the subscript $R-T$ stands for "Roy-Thodos" and

$$f_{R-T}(T_{red,p}) = 2.25(\exp(0.0464T_{red,p}) - \exp(-0.2412T_{red,p})), \quad (49)$$

$$\eta_{ref,p} = 1.08 \times 10^{-4}(m_p T_{C,p})^{1/2} \left(\frac{Z_{C,p}}{v_{C,p}}\right)^{2/3}. \quad (50)$$

The other ingredient entering the λ calculation is the expression for λ_p which is here computed (in cgs units) using the Stiel-Thodos method (Reid et al.[9]) as

$$\lambda_p = \lambda_{ref,p}\left(f_\lambda f_{R-T}(T_{red,p}) + \frac{1}{Z_{C,p}^5} f_{E,p}(\rho_{red,p})\right), \quad (51)$$

$$f_\lambda = 3.75 + \frac{\frac{C_p}{R_u} - \frac{5}{2}}{0.7862 - 0.7109\Omega + 1.3168\Omega^2} \quad (52)$$

where f_λ is a function of the acentric factor Ω given by the Chung at al. formula,[9] $f_{R-T}(T_{red,p})$ of eq. 51 accounts for the small ρ_{red} (i.e. kinetic theory) limit whereas $f_{E,p}$ is an excess function of importance for larger ρ_{red}. According to the Stiel-Thodos method,

$$\lambda_{ref,p} = 8.9775 \times 10^3 \left(\frac{T_{C,p}}{m_p}\right)^{1/2} \left(\frac{Z_{C,p}}{v_{C,p}}\right)^{2/3}, \quad (53)$$

$$f_{E,p}(\rho_{red,p}) = 1.223 \times 10^{-2}[\exp(0.535\rho_{red,p}) - 1]. \quad (54)$$

Properties used in these calculations are provided in Table 1 for n-heptane, iso-octane and all light species and in Table 2 for the quasi-steady radicals. For these latter, estimates of p_C and v_C are made using the group contribution method of Joback (Reid et al.[9]). Then, T_C is estimated assuming $Z_C = 0.28$; the same assumption is made to estimate the p_C, v_C and Ω values in parentheses in Table 1.

III. Numerical method

The equations are solved using a numerical method relying on three to four steps, as follows. In a first step, Based on profiles of T and Y_i's obtained from published experimental data and models available in the literature, an initial guess is made for these profiles as a function of x, for a specified grid. In the second step, a preliminary relaxation integration relative to the grid is made by combining the assumed profiles of the first step with that obtained using differences from the conservation equations. Results are examined to assess if this preliminary relaxation procedure gives reasonable-looking profiles; if not, the first step is revised. In a final step, further profile relaxations are made using a pseudo-unsteady time increment procedure. This procedure is meant to relax the numerical residues of the conservation equations. For variables Y_i and T, the increments are

$$\Delta Y_i = u\Delta t\left[\frac{m_i\mathcal{R}_i}{\rho u} - \frac{d}{dx}\left(\frac{m_i J_i}{\rho u}\right) - \frac{dY_i}{dx}\right] \quad (55)$$

$$\Delta T = u\Delta t\left\{\left[\frac{d}{dx}\left(\frac{\lambda}{\rho u}\frac{dT}{dx}\right) + \frac{\sum_i h_i\mathcal{R}_i}{\rho u}\right]\frac{m}{C_{pe}} - \frac{dT}{dx}\right\} \quad (56)$$

where

$$C_{pe} \equiv C_p + \frac{m}{\rho u}\sum_i\left(C_{pi} - \frac{m}{m_H}C_{pH}\right)J_i. \quad (57)$$

The axial coordinate is discretized in intervals $\Delta x = O(10^{-3})$ cm and the iteration pseudo steps are $\Delta t = O(0.1)$ μs. Since $u = O(10^2)$ cm/s, each time iteration pseudo step corresponds to an axial distance change of $O(10^{-5})$ cm, or approximately 1% of Δx. For high-p flows, a fourth step is necessary because of the very steep flame: we re-grid successively in the flame region in order to obtain good resolution.

IV. Results

Several sets of results are discussed here, some of which are comparable with published experimental data. Because experimental data is not usually accompanied by illustrations of initial condition profiles, and

because the computations tend to be sensitive on how close the initial profiles are to the quasi-steady flame ones, simulations are still challenging from the numerical viewpoint in terms of achieving profile convergence under the one-dimensional assumption.

A. Case 1

The first case is one for which experimental data exists.[10] Experiments were performed for a premixed n-heptane/air jet under the following conditions: $\phi = 1$, $p = 1$ bar, $T_0 = 350$ K, $L = 0.6$ cm, $(\rho u)_0 = 0.18$ g/cm^2-s.[10] Illustrated in Fig. 1 are computations using our reduced kinetics model (Fig. 1a) as well as experimental results (Fig. 1b) . Clearly, the flame location is reproduced with good accuracy, the velocity up to the location of $(du/dx) = 0$ is very well predicted but its computed value after the flame exceeds that of the experimental data; the temperature is also very well predicted up to past the flame, however, the value at which levelling-off occurs is higher than in the experiment. Given the compact reduced kinetics, some inaccuracies are unavoidable. Further, in Fig. 1c are the reactant's profiles. The mass fractions of the reactants are constant until the flame region where a reduction in Y_{o2} is observed concomitant with a small increase in the Y_H; the Y_{o2} reduction is attributed to the initiation of the reaction whereas the small increase in Y_H is attributed to diffusion promoted by the large temperature. The same diffusion process explains the further increase in Y_{o2} until the kinetic rates take over and both Y_H and Y_{o2} decrease precipitously. Noteworthy, the heavy species disappear before all oxygen is exhausted, and the remaining oxygen is used for the light species reactions, in particular to convert CO to CO_2.

B. Case 2

The simulations of Case 2 are devoted to an iso-octane/air mixture under the conditions of $\phi = 1$, $p = 10$ bar, $T_0 = 300$ K, $L = 0.4$ cm, $(\rho u)_0 = 3.0$ g/cm^2-s. Results are displayed in Fig. 2. A quantitative comparison with the n-heptane/air flame must take into account the combined effect of the lower initial temperature but larger initial pressure, shorter domain and larger flow rate. Both velocity and temperature are larger than in Case 1, and also the first decrease in Y_{o2} and increase in Y_H are muted.

C. Case 3

For Case 3, we are returning to n-heptane/air mixtures but at a different initial conditions than Case1. For Case 3, $\phi = 1$, $p = 1$ bar, $T_0 = 500$ K, $L = 0.6$ cm, $(\rho u)_0 = 0.10$ g/cm^2-s and the results are exhibited in Fig. 3. By comparison with Case 1, T_0 is here larger but $(\rho u)_0$ is smaller. Expectably, the temperature is larger, and it is conjectured that this larger temperature induces the larger velocity. The reactants' profiles are qualitatively similar to those of Case 1, and the persistence of oxygen farther downstream than in Case 1 is noted.

D. Case 4

To show the capabilities of the model for rich flames, in Case 4 we compute a flame similar but not identical to that which has been experimentally addressed by El Bakali et al.[11] The reason that the same flame could not be computed is that for the very small mass flow rate in the experiment, the code did not converge; moreover, the domain size used in the experiment is unclear except for the fact that $L \geq 0.4$ cm. Thus, the initial conditions of the computation are: $\phi = 1.9$, $p = 1$ bar, $T_0 = 300$ K, $L = 0.5$ cm, $(\rho u)_0 = 0.0147$ g/cm^2-s (the mass flow rate is here increased by a factor of approximately 2.5 from that in the experiment). Results are depicted in Fig. 4. Both the temperature and the velocity have smaller values than those of Case 1 where T_0 was slightly larger, the mass flow rate was larger by an order of magnitude than in Case 4, and the domain size was slightly larger, but the general shape of the profiles is qualitatively similar in all cases. Similar to the experiment,[11] the results of Fig. 4 show substantial $Y_{co} > Y_{co2}$ (the experimental data shows mole fractions, whereas we display mass fractions), and $Y_{h2o} > Y_{co2}$.

V. Summary and conclusions

A model has been developed for simulating quasi-steady one-dimensional laminar premixed flames in the configuration of a jet injected in air. The model has been derived in the framework consistent with it being

used in conjunction with a reduced chemical kinetic model based on constituents and species. As such, the formulation includes a complete mass-diffusion matrix, and a mixture thermal conductivity computed taking into account the global constituent and all species. Furthermore, a real-gas equation of state is used.

The equations are solved using a pseudo-unsteady time increment procedure with initial profiles that are a guess of the steady-state profiles. Results have been presented for both n-heptane/air and iso-octane/air premixed flames under a variety of initial conditions. Comparisons with experimental results showed good agreement. Further simulations are necessary to explore the full potential of the model.

Acknowledgements

This study was conducted at the Jet Propulsion Laboratory (JPL), California Institute of Technology (Caltech) and sponsored at Caltech by the Army Research Office under the program of Dr. Ralph Anthenien.

Appendix A

Miscellaneous relationships relevant to the EOS are

$$a_{mix} = \sum_p \sum_n X_p X_n a_{pn}(T), \quad b_{mix} = \sum_p X_p b_p, \tag{58}$$

where indices do not follow here the Einstein notation, and

$$a_{pn} = (1 - k^{'})\sqrt{\alpha_{pp}\alpha_{nn}}, \tag{59}$$

$$\alpha_{pp}(T) \equiv 0.457236(R_u T_{C,p})^2 \left[1 + c_p(1 - \sqrt{T_{red,p}})\right]^2 / p_{C,p}, \tag{60}$$

$$c_p = 0.37464 + 1.54226\Omega_p - 0.26992\Omega_p^2, \tag{61}$$

where $T_{red,p} \equiv T/T_{C,p}$, $T_{C,p}$ is the critical temperature and Ω_p is the acentric factor. Also,

$$b_p = 0.077796\frac{R_u T_{C,p}}{p_{C,p}}, \tag{62}$$

$$T_{C,pn} = (1 - k_{pn})\sqrt{T_{C,p}T_{C,n}} \text{ with } k_{pp} = 0, \tag{63}$$

$$v_{C,pn} = \frac{1}{8}\left(v_{C,p}^{1/3} + v_{C,n}^{1/3}\right)^3, \tag{64}$$

$$Z_{C,pn} = \frac{1}{2}(Z_{C,p} + Z_{C,n}), \tag{65}$$

$$p_{C,pn} = \frac{R_u T_{C,pn} Z_{C,pn}}{v_{C,pn}}, \tag{66}$$

with $T_{red,pn} \equiv T/T_{C,pn}, Z_{C,p}$ being the critical compression factor defined as $Z = p/(\rho T R_u/m)$, $v_{C,p}$ being the critical volume, and $p_{C,p}$ being the critical pressure. k_{pn} is an empirical mixing parameter. The relationship between the parameters k_{pn} and k'_{pn} is

$$(1 - k_{pn}) = (1 - k'_{pn})\frac{(v_{C,p}v_{C,n})^{1/2}}{v_{C,pn}}. \tag{67}$$

Values of k'_{pn} are listed in Table 3, where the values were obtained from Reid et al.[9] or Knapp et al.[12] Otherwise, for pairs involving O_2, N_2, CO, CO_2 or H_2O, $k'_{pn} \simeq 0$.

References

[1]K. G. Harstad, J. Bellan, Combustion and Flame 157 (2010) 1594-1609.
[2]K. G. Harstad, J. Bellan, Combustion and Flame 157 (2010) 2184-2197.
[3]S. W. Benson, Thermochemical Kinetics., John Wiley & Sons, Inc., 1968.
[4]N. A. Okong'o, J. Bellan, J. Fluid Mech. 464 (2002)1-34.
[5]K. Harstad and J. Bellan, Ind. & Eng. Chem. Res., 43(2) (2004) 645-654.
[6]K. G. Harstad and J. Bellan, Journal of Chemical Physics, 120(12) (2004) 5664-5673.
[7]A. Ern, V. Giovangigli, Combust. Theory Modelling 2 (1998) 349-372.

[8]J. O. Hirshfelder, C. F. Curtis, R. B. Bird, Molecular Theory of Gases and Liquids, John Wiley & Sons, Inc., 1954.
[9]R. C. Reid, J. M. Prausnitz, B. E. Poling, The Properties of Gases and Liquids, 4th edition, McGraw-Hill, NY, 1987.
[10]C, Ji, E. Dames, Y. L. Wang, H. Wang, F. N. Egolfopoulos, Combust. Flame, 157 (2010) 277-287.
[11]A. El Bakali, J-L Delafau, C. Vovelle, Combust. Flame, 118 (1999) 381-398.
[12]H. Knapp, R. Doring, L. Oellrich, U. Plocker, J. M. Prausnitz, DECHMA Chem. Data Series, 6 (1982) DECHMA, Frankfurt.

Species	m (g/mol)	T_C (K)	p_C (bar)	v_C (cm^3/mol)	Ω
C_7H_{16}	100.2	540.2	27.4	432	0.349
C_8H_{18}	114.23	568.8	24.9	492	0.396
N_2	28.013	126.26	33.4	89.8	0.039
H_2O	18.015	647.3	221	57.1	0.344
CO_2	44.01	304.1	73.8	93.9	0.225
O_2	32.0	154.6	50.43	73.4	0.025
H	1.008	33.15	(12)	64.2	(0.)
H_2	2.016	32.94	12.84	64.3	-0.216
CO	28.01	132.9	35	93.2	0.066
CH_4	16.04	190.6	45.94	99.2	0.0108
H_2O_2	34.015	728	220	(77)	(0.1)
C_2H_2	26.04	308.3	61.4	112.7	0.19
C_2H_4	28.054	282.4	50.4	130.4	0.089
CH_2O	30.026	408	65.9	(144)	0.253

Table 1. Fuel and unsteady light species properties.

Radicals	m (g/mol)	T_C (K)	p_C (bar)	v_C (cm^3/mol)	Ω
O	16.0	116	76	35	0.
CH	13.02	183	73	58	0.
CH_2	14.027	210	66	73	0.
CH_3	15.034	221	62	82	0.
OH	17.01	167	85	45	0.
HCO	29.02	299	70	99	0.25
OOH	33.01	226	83	63	0.
HC_2	25.03	291	67	100	0.2
C_2H_3	27.044	292	57	119	0.1

Table 2. Quasi-steady radicals properties.

p	n	k'
alkane	alkane	0.0
alkane	N_2, O_2	0.15
alkane	CO_2	0.11
alkane	H_2O	0.093-0.006n_c
alkane	H_2	0.099n_c-0.81
H_2	N_2, O_2	0.12
H_2	CO_2	-0.162
CO_2	H_2O	0.095
CO_2	N_2, O_2	-0.017
H_2O	N_2, O_2	0.17

Table 3. Values of $k^{'}$ for species pairs. n_c is the number of C atoms in the species.

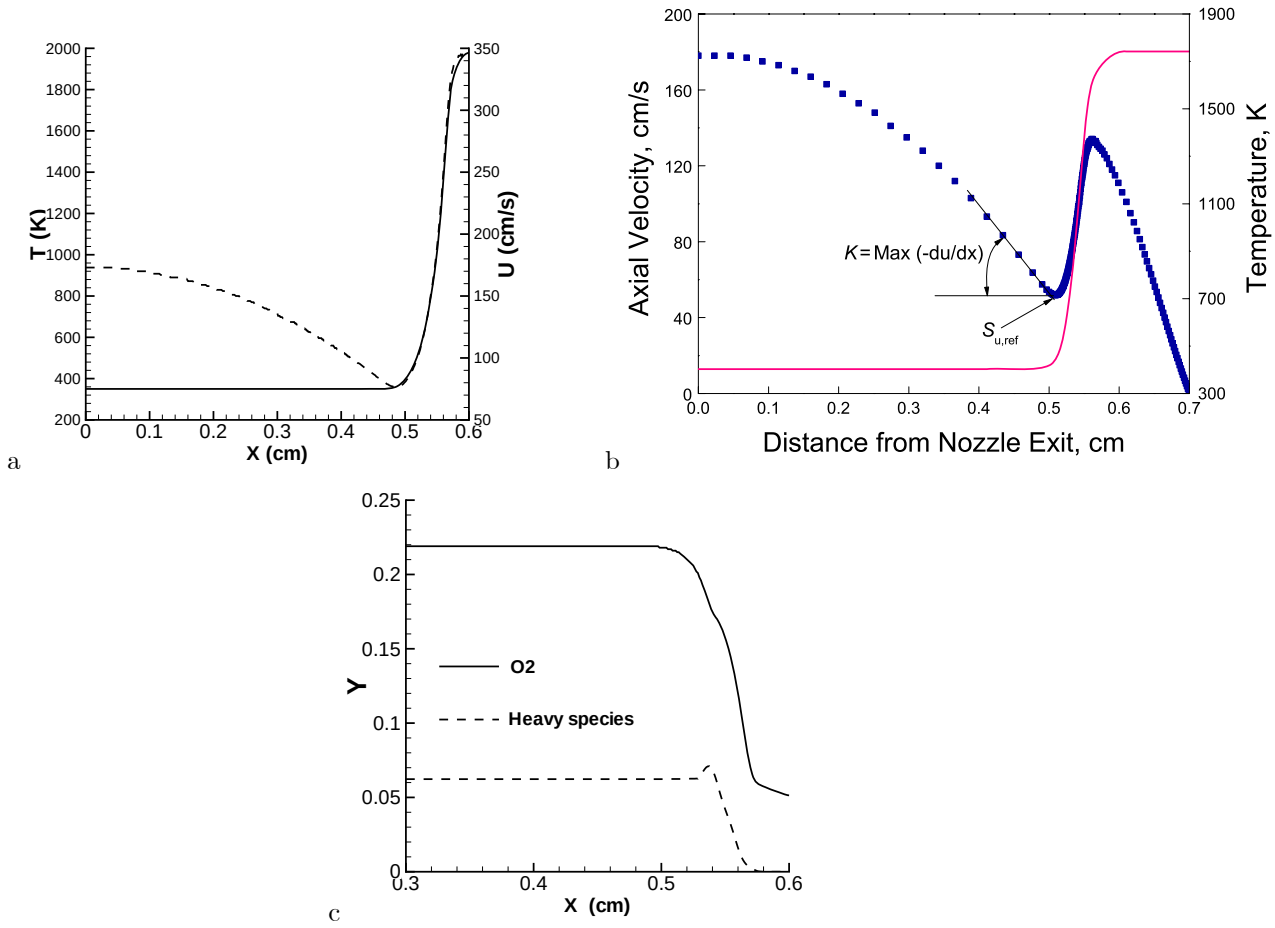

Figure 1. (a) Predictions of the reduced model for temperature and velocity, (b) corresponding experimental data, and (c) the reactants' mass fractions. Computations and experiments are for heptane/air with $\phi = 1$, $p_0 = 1$ bar, $T_0 = 350$ K, $L = 0.6$ cm and $(\rho u)_0 = 0.18$ g/cm^2-s. The temperature is represented by the solid line, and the velocity by the dashed line.

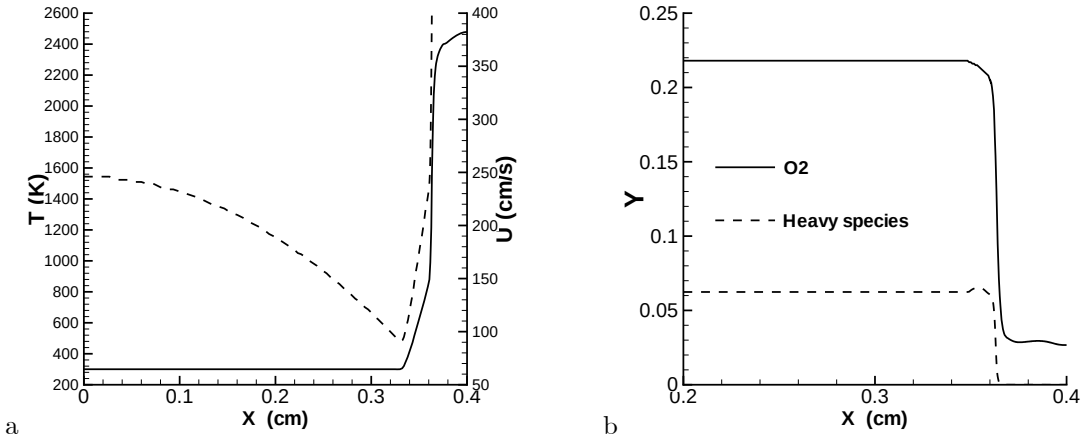

a b

Figure 2. Predictions of the reduced model for an iso-octane/air premixed flame under the following conditions: $\phi = 1$, $p = 10$ bar, $T_0 = 300$ K, $L = 0.4$ cm, $(\rho u)_0 = 3.0$ g/cm^2-s. (a) Temperature (solid line) and velocity (dashed line) and (b) reactants mass fractions.

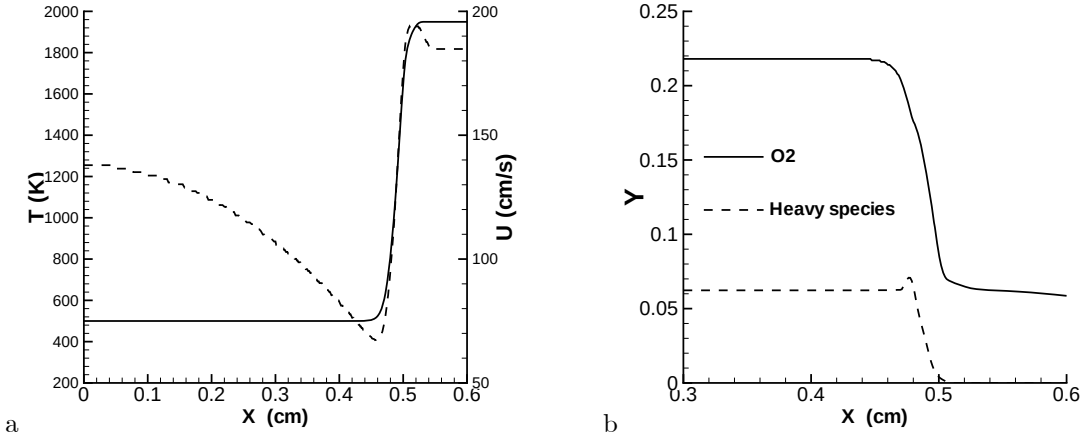

a b

Figure 3. Predictions of the reduced model for an heptane/air premixed flame under the following conditions: $\phi = 1$, $p = 10$ bar, $T_0 = 500$ K, $L = 0.4$ cm, $(\rho u)_0 = 0.10$ g/cm^2-s. (a) Temperature (solid line) and velocity (dashed line) and (b) reactants mass fractions.

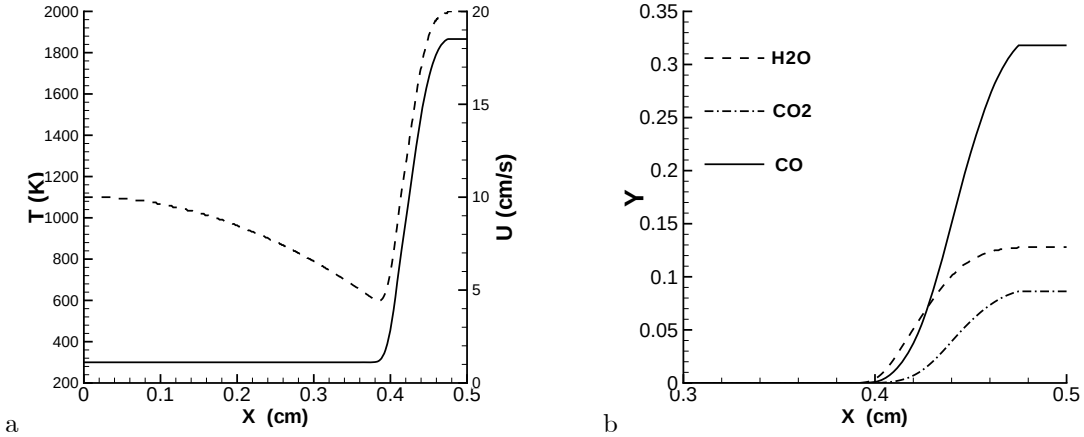

a b

Figure 4. Predictions of the reduced model for an heptane/air premixed flame under the following conditions: $\phi = 1.9$, $p = 1$ bar, $T_0 = 300$ K, $L = 0.5$ cm, $(\rho u)_0 = 0.0147$ g/cm^2-s. (a) Temperature (solid line) and velocity (dashed line) and (b) products mass fractions.